Effect of HVDC Polarity Reversal Stress on Life Expectancy of Insulation-Empirical Approach and Circuit Model

Doctoral Thesis

by

IYYAPPAN C 2017EEZ0010



DEPARTMENT OF ELECTRICAL ENGINEERING INDIAN INSTITUTE OF TECHNOLOGY ROPAR SEPTEMBER 2023

Effect of HVDC Polarity Reversal Stress on Life Expectancy of Insulation-Empirical Approach and Circuit Model

A Thesis Submitted

In Partial Fulfilment of the Requirements for the Degree of

DOCTOR OF PHILOSOPHY

by

IYYAPPAN C 2017EEZ0010



DEPARTMENT OF ELECTRICAL ENGINEERING INDIAN INSTITUTE OF TECHNOLOGY ROPAR SEPTEMBER 2023

IYYAPPAN	C: Effect of HVDC F	Polarity Reverse	al Stress on Life	e Expectancy o	f Insulation-
Empirical i	Approach and Circu	it Model			
Copyright All Rights	© 2023, Indian Inst Reserved	titute of Techn	ology Ropar		

DEDICATED TO FAMILY

I wish to dedicate all my knowledge owned through my degree to my parents. I am dedicating my thesis to them. Grateful to my parents for believing in me and for their prolonged support. I would like to appreciate my wife, daughter and in-laws for being a driving force in my Ph.D. Journey and expect the same to be continued in all my future endeavors.

Declaration of Originality

I hereby declare that the work which is being presented in the thesis entitled Effect of HVDC Polarity Reversal Stress on Life Expectancy of Insulation-Empirical Approach and Circuit Model has been solely authored by me. It presents the result of my own independent investigation/research conducted during the time period from January 2018 to September 2023 under the supervision of Prof. C.C. Reddy, IIT Ropar. To the best of my knowledge, it is an original work, both in terms of research content and narrative, and has not been submitted or accepted elsewhere, in part or in full, for the award of any degree, diploma, fellowship, associateship, or similar title of any university or institution. Further, due credit has been attributed to the relevant state-of-the-art and collaborations (if any) with appropriate citations and acknowledgments, in line with established ethical norms and practices. I also declare that any idea/data/fact/source stated in my thesis has not been fabricated/ falsified/ misrepresented. All the principles of academic honesty and integrity have been followed. I fully understand that if the thesis is found to be unoriginal, fabricated, or plagiarized, the Institute reserves the right to withdraw the thesis from its archive and revoke the associated Degree conferred. Additionally, the Institute also reserves the right to appraise all concerned sections of society of the matter for their information and necessary action (if any). If accepted, I hereby consent for my thesis to be available online in the Institute's Open Access repository, inter-library loan, and the title & abstract to be made available to outside organizations.

Signature

Name: IYYAPPAN C

Entry Number: 2017EEZ0010

Program: PhD.
Department: EED

Indian Institute of Technology Ropar

Rupnagar, Punjab 140001

Date: 20.09.2023

Acknowledgments

I wish to thank my supervisor Prof. C.C. Reddy for the continuous support and encouragement throughout my journey as a PhD candidate. I am inspired by his knowledge and problem solving skills. I wish to continue on his path to share my knowledge with others.

I am also immensely thankful to the IIT Ropar for giving me the opportunity to pursue my professional degree. I extend my gratitude to the Chairman Dr. Subramanya Murala for his valuable guidance and support. I am deeply appreciative to the doctoral committee members Dr. Sankar Raju, Dr. Ravi Mohan Prasad, and Dr. Ravi Teja for their constructive direction and timely support

Thanks to my respectful seniors Dr. Alam Pratap Singh, Dr. Ashish Gupta, and Dr. Avnish Kumar for sharing their knowledge, as well as thankful to my former colleagues Dr. Birender Singh, Dr. Ajith John Thomas, Dr. Sathyamoorthy and Himanshu for their valuable technical discussions. To my present colleagues - Priyesh, Purna, Pranav, Aritra, Harshith, Parimal, Ritesh, Adarsh, Manika, and Anas. I am grateful for your continuous support.

Finally, I extend my heartfelt thanks to Mr. Dilbag Singh and Mr. Jaspreet Singh for their continuous assistance throughout my research journey in laboratory experiments.

Certificate

This is to certify that the thesis entitled Effect of HVDC Polarity Reversal Stress on Life Expectancy of Insulation-Empirical Approach and Circuit Model, submitted by IYYAPPAN C (2017EEZ0010) for the award of the degree of Doctor of Philosophy of Indian Institute of Technology Ropar, is a record of bona fide research work carried out under my (our) guidance and supervision. To the best of my knowledge and belief, the work presented in this thesis is original and has not been submitted, either in part or full, for the award of any other degree, diploma, fellowship, associateship or similar title of any university or institution.

In my (our) opinion, the thesis has reached the standard fulfilling the requirements of the regulations relating to the Degree.

Signature of the Supervisor

Prof. C.C. Reddy

Electrical Engineering Department Indian Institute of Technology Ropar Rupnagar, Punjab 140001

Date: 12.09.2024

Lay Summary

Insulation is the heart of all the power equipment. The insulation material used in the power equipment varies depending on the application. E.g.: Kraft paper in transformer and polymer used in cables. The quality of the electrical equipment is graded based on the life and performance of insulation material. In higher voltage applications the life of insulation materials is decided based on unique testing procedures. The insulation design of the specific application is decided based on those test results. For instance, insulation material used in HVDC application is subjected to HVDC stress for evaluation. Henceforth the type of stress insulation experienced under operating conditions decides the testing procedure to measure the insulation performance and lifetime.

Similarly, polarity reversal (PR) stress is a typical stress experienced by the power cable insulation used in HVDC transmission links. The degradation of the material is accelerated as a consequence of the PR stress. However, a life model that incorporates the PR stress to evaluate the insulation reliability is still under examination. Consequently, a testing procedure including the actual PR stress following the existing testing technique is proposed in this thesis. The experimental results are concluded with a comprehensive life estimation model. Further, the degradation of a material due to PR stress is investigated with various characterization techniques.

The thesis proposes a life estimation technique so that the user can predict and optimize the life of the power cable insulation used in HVDC systems.

Abstract

Life estimation is an important aspect in the assessment of the reliability of power equipment. Life estimation under DC fields did not receive as much attention as that of AC, which has been dealt with for several ages. Further, polarity reversal is a distinct operating condition in conventional line-commutated converter-based high-voltage DC systems, complicating the life analysis. In literature, a few semi-empirical or phenomenological models have been proposed for life estimation with certain limitations. In the thesis, carefully designed experiments are reported, which indicate that, the change in frequency of PRs results in a change in the slope of V-t characteristics on a log-log scale (known as inverse power law). The power law parameters are shown to be systematic functions of frequency of PRs. Based on these results, the authors have proposed a comprehensive inverse power law that is valid for both DC and PRs stress application, in place of conventional inverse power law. The proposed modification is examined with experimental data of authors apart from that available in literature and found to be working well. The model provides the minimum duration (maximum frequency) of a reversal for maximizing the life of power equipment which may pave the way for deciding frequency of the 'planned reversals'.

Further the mechanism that leads to insulation degradation under DC and PR is investigated with conduction current measurement. In the early phase of current measurement for investigating LDPE conductivity, an anomalous current profile was detected specifically peaks were observed at different time instants for different voltages and temperatures. These anomalous current profile characteristics are reproduced by replicating the commercial electrometer. LDPE thin films are subjected to different electric fields and temperatures and the experimental results are matched with analytical calculations based on an LDPE equivalent circuit model, and the values are tabulated. The erroneous interpretation of actual current characteristics caused by the conventional electrometer is identified, and a solution to eliminate the error in the interpretation of current was provided based on proposed dielectric model. The peak current characteristics are distinguished from the total current and its characteristics under electro-thermal stress are derived. It is considered very important to correct this erroneous interpretation and arrive at a proper interpretation of the conduction current, due to the reason that the current profile is considered important for understanding space charge phenomenon. Further, the experiments are performed under PR conditions. The continuously measured current of each reversal interval is sequentially split into three sections and compared. A significant difference in instantaneous polarization and relaxation current is observed. Also, dissimilar current trend with different time intervals (different frequency of reversal) is observed. These results were correlated with the charge dynamics in LDPE to explain the difference in times to break down with different frequencies of PR.

Keywords: inverse power law, life estimation, reliability of power equipment, polarity reversal, planned reversals, unplanned polarity reversals, damage, HVDC, V-t characteristics, combined stresses, dielectric equivalent circuit, conduction current, leakage current measurement, anomalous peak current profile, LDPE model

List of Publications

Journals

- C. Iyyappan and C. C. Reddy, "Inverse Power Law based Inclusive Life Model for DC Polarity Reversal Stresses," in IEEE Transactions on Dielectrics and Electrical Insulation, vol. 28, no. 2, pp. 586-593, April 2021.
- C. Iyyappan and C. C. Reddy, "Understanding the Volumetric Current Dynamics of Low-Density Polyethylene", in IEEE Transactions on Dielectrics and Electrical Insulation. (Under review).
- C. Iyyappan and C. C. Reddy, "Peak current characteristics and its equivalent space charge dynamics in Low-Density Polyethylene", in IEEE Transactions on Dielectrics and Electrical Insulation. (Under preparation).

Other Contributions

- A. J. Thomas, **Iyyappan.** C and C. C. Reddy, "A Method for Surface Voltage Measurement of an Overhead Insulated Conductor," in IEEE Transactions on Instrumentation and Measurement, vol. 70, pp. 1-8, 2021.
- A. J. Thomas, **Iyyappan.** C and C. C. Reddy, "On the Measurement of Surface Voltage of Insulators and Bushings," in IEEE Transactions on Power Delivery, vol. 37, no. 1, pp. 464-471, Feb. 2022.

Conferences

- I. C and C. C. Reddy, "Effect of Electrometer Internal Circuit Parameters in Interpretation of Conduction Current Transient Characteristics," 2023 International Symposium on Electrical Insulating Materials (ISEIM), Shimane, Japan, 2023, pp. 01-04, doi: 10.23919/ISEIM60444.2023.10329161.
- C. Iyyappan and C. C. Reddy, "Leakage Current Measurement in LDPE under DC Polarity Reversal Stress," 2022 IEEE 6th International Conference on Condition Assessment Techniques in Electrical Systems (CATCON), Durgapur, India, 2022, pp. 432-435, doi: 10.1109/CATCON56237.2022.10077644.
- C. Iyyappan, D. Sathyamoorthy, P. Pandey and C. C. Reddy, "Investigation on nanocomposite materials for power cable insulation," 2017 International Symposium on Electrical Insulating Materials (ISEIM), Toyohashi, Japan, 2017, pp. 421-424, doi: 10.23919/ISEIM.2017.8088774.
- G. N. Reddy, B. Singh, **Iyyappan**, A. P. S. Tiwana and C. C. Reddy, "Estimation of Endurance Coefficient of Oil Impregnated Kraft Papers using DEM," *2019 IEEE 4th International Conference on Condition Assessment Techniques in Electrical Systems* (*CATCON*), Chennai, India, 2019, pp. 1-3, doi: 10.1109/CATCON47128.2019.CN0008.

Table of Contents

Declaration of Originality	v
Acknowledgments	vi
Certificate	vii
Lay Summary	viii
Abstract	ix
List of Publications	xi
Table of Contents	xii
List of Figures	xv
List of Tables	xviii
Notations and Abbreviations	xix
Chapter 1 Introduction	1
1.1 A Brief Contextual Overview of Underground Power Cables.	1
1.2 DC Polarity Reversal Stress	3
1.2.1 A Typical HVDC system	3
1.2.2 Effect of PR stress on insulation	4
1.3 Overview of Life Estimation Techniques	5
1.3.1 Experiments and Statistical Analysis	5
1.3.2 $V-t$ Characteristics	6
1.4 Motivation for Comprehensive Life Model	8
1.5 Material Characterization with Dielectric Model	10
1.5.1. Background of the current characteristics	10
1.5.2. Motivation for dielectric model	11
1.6 Organization of Thesis	12
Chapter 2 Literature Survey	14
2.1 Existing Life Models for DC plus Polarity Reversal	14
2.1.1. Phenomenological Model	14
2.1.2. Physical Model	15
2.2 Approach to Comprehensive Life Estimation Model	16
2.3 Literature Survey on DC Current Characteristics	17
2.3.1 Insulation assessments with transient current characteris	tics18
2.3.2 Modified linear equivalent circuit model	18
2.4 Problem Statement	20
2.5 Methodology Proposed	21

Cr	apter 3	Life estimation Model Under DC PR stress	22
	3.1	Experimental Setup and Procedure	22
	3.2	Breakdown Test Data	23
	3.3	$m{V}-m{t}$ Characteristics	27
	3.4	Fitted Power Law Components $m{n}$ and $m{D}$	30
	3.5	Comprehensive Life Model	31
	3.6	Fitting Proposed Life Model to Experimental Results	33
	3.7	Significance of b and c :	35
	3.8	Significance of $m{r}$ and $m{s}$:	36
	3.9	Validation of the Life Model	37
Cł	napter 4	Measurement Issues with Conduction Current Setup	40
	4.1	Schematics of Current Measurement with Commercial Electrometer	40
	4.2	Commercial Electrometer Current	40
	4.3	Conduction Current Measurement with Replicated Electrometer	41
	4.3.1	. Electrometer Internal Circuit	41
	4.3.2	. Significance of r_m and c_m	42
	4.3.3	. Current measured with replicated electrometer	44
	4.3.4	. Measured current	45
	4.4	Circuit Simulation	46
	4.5	Recreating Transient Current with Proposed Dielectric Model	50
	4.5.1	. LDPE Model	50
	4.5.2	. Systematic Current Measurement under Different Electro Thermal Conditions	50
	4.5.3	. Proposed LDPE Model along with complete measurement setup	53
	4.6	Actual Current	57
	4.7	Anomalous Current Profile-Interaction of LDPE and Electrometer Internal Circuit	58
	4.8	Peak Current Characteristics	61
	4.9	Experimental Validation	64
Cł	napter 5	Conduction Current Measurement under HVDC PR	66
	5.1	Introduction	66
	5.2	Effect of Time Interval $m{T}$ on Life Time $m{t}$	66
	5.3	PR Leakage Current Measurement	67
	5.4	Results and Discussions	69
	5.4.1	. Difference in 1 and 10 minute current characteristics	69
	542	Correlation of breakdown and current characteristics	71

5.4.3.	Equivalent circuit based analysis	72
Chapter 6 Con	clusions	75
References		77
Annendix		80

List of Figures

Figure 1.1 (a) The core length of DC-XLPE cables installed and under construction in year 2018 (b) Future growth predicted length of cable [1]1
Figure 1.2 Hybrid HVDC system [3]
Figure 1.3 Voltage distributions at PR [4]
Figure 1.4 Typical electrode setup and broken sample6
Figure 1.5 (a)Constant stress test (b) Step stress test
Figure 1.6 V-t characteristics of AC and DC test in log-log scale[2]9
Figure 1.7 Current characteristics of XLPE from [11]
Figure 1.8 Linear dielectric model
Figure 2.1(a)Typical voltage PR profile. (b) dc component of voltage PR with impulses superimposed at the time of reversals [7].
Figure 2.2 The transient current characteristics in [11]
Figure 2.3 The linear and modified dielectric model
Figure 3.1 Automated instruments profile for PR experiment and experimental elements in controlled environment
Figure 3.2 Typical profile of the PR voltage used in the experiment with time interval between reversals (T), ramping time (tramping)and voltage level (V_0) kV
Figure 3.3 Samples used
Figure 3.4 Weibull plots of LDPE – Time to breakdown
Figure 3.5 Weibull plots of silicone rubber –Time to breakdown
Figure 3.6 Weibull plots of kraft paper – Time to breakdown
Figure 3.7 V-t curves of LDPE showing variation in slope with change in time interval between reversals.
Figure 3.8 V-t curves of silicone rubber samples showing variation in slope with change in time interval between reversals.
Figure 3.9 V-t curves of Kraft paper samples showing variation in slope with change in time interval between reversals.
Figure 3.10 Power law exponent or endurance coefficient obtained experimentally at different time interval between reversals
Figure 3.11 Damage or strength constant obtained from inverse power law experimentally at different time interval between reversals
Figure 3.12 Time to breakdown versus Time interval between reversals for different voltages fitted for experimental data
Figure 3.13 Time to breakdown versus Time interval between reversals for different voltages fitted for experimental data of silicone rubber

Figure 3.14 Time to breakdown versus Time interval between reversals for different volta fitted for experimental data of kraft paper.	_
Figure 3.15 Reduction in percentage of logarithmic life with reversal frequency with resp to life under DC	ect
Figure 3.16 The experimental data from [7] fitted with proposed life model	38
Figure 4.1 Schematic of current measurement	40
Figure 4.2 Conduction current measurement at 50°C	41
Figure 4.3 Circuit configuration (a) Shunt (b) Feedback [23] types	42
Figure 4.4 Cable conduction current measurement with measuring setup [24]	42
Figure 4.5 Measurement setup simplified circuit	43
Figure 4.6 Complete measuring setup with a replicated electrometer internal circuit	44
Figure 4.7 Electrometer internal circuit	45
Figure 4.8 Current I_{IN} of C_m (a) $1\mu f$ (b) $10\mu f$	45
Figure 4.9 Simplified circuit representation of measurement setup	46
Figure 4.10 The current characteristics of I_{IN} (a) $R = 1T\Omega$ (b) $R = 2T\Omega$	47
Figure 4.11 The current characteristics of I_{DC} (a) $R = 1T\Omega$ (b) $R = 2T\Omega$	48
Figure 4.12 The v_m characteristics of 1kV applied voltage (a) $R = 1T\Omega$ (b) $R = 2T\Omega$	48
Figure 4.13 Voltage across the sample V_d (a) $R = 1T\Omega$ (b) $R = 2T\Omega$	49
Figure 4.14 The transient current characteristics	49
Figure 4.15 Proposed LDPE model	50
Figure 4.16 Current I _{IN} at different temperatures 30°C	51
Figure 4.17 Current I _{IN} at different temperatures 40°C	52
Figure 4.18 Corresponding converted current at temperature 50°C	52
Figure 4.19 Actual measured voltage v_o at temperature 50°C	52
Figure 4.20 Equivalent circuit of complete measurement setup	
Figure 4.21 Flow of (a)instantaneous polarization current(b) steady state characteristics	
current	
Figure 4.22 Calculated voltage v_o with the model at temperatures (a)30°C (b)40°C (c)50°	
Figure 4.23 The current I_{DC} at (a)30°C (b)40°C (c)50°C and the current I_{IN} at (d)30°C (e)40°C (f)50°C	
Figure 4.24 Calculated voltage across the LDPE at (a)1kV (b)2kV (c)3kV	59
Figure 4.25 Voltage profile (a) 3kV 40°C and (b) 3kV 50°C	60
Figure 4.26 The proposed dielectric model circuit	61
Figure 4.27 The absorption current differentiated from conduction current	62

Figure 4.28 The modified branch circuit and its current dynamics	62
Figure 4.29 (a)Replicated electrometer current matched with commercial electrometer (b) Actual current	65
Figure 5.1 The complete automated measurement setup	67
Figure 5.2 Typical profile of the PR voltage used in the experiment with the time interval between reversals (T), ramping time ($t_{ramping}$) and voltage level (V_0) kV	68
Figure 5.3 The 1 minute time interval leakage current (a) continuous (b) different period compared.	68
Figure 5.4 The different time period comparison of 10 minute reversal leakage current(a) continuous (b) different period compared	69
Figure 5.5 The 10 minute current characteristics under (a) positive (b) negative voltage	70
Figure 5.6 The 1 minute current characteristics under (a) positive (b) negative voltage	70
Figure 5.7 The 10 minute leakage current characteristics limited to 60 seconds for comparison, (a) positive (b) negative voltage.	71
Figure 5.8 The dielectric equivalent circuit	72
Figure 5.9 The current characteristics integrated value for 10-minute time interval	73

List of Tables

Table 3. 1 Samples used in experiments	23
Table 3.2 Weibull scale parameters of LDPE	26
Table 3.3 Weibull scale parameters of silicone rubber	26
Table 3. 4 Weibull scale parameters of kraft paper	27
Table 3. 5 Parameters obtained by performing experiment on different stress using different values of T	
Table 3. 6 Comparison of power law exponent (N) and damage (D) for $T \rightarrow \infty$ in proposed model with n and D obtained under DC conditions in [8].	37
Table 3.7 Proposed life model parameters estimated for [7] experimental data	38
Table 3.8 Power law exponent calculated for specified time interval for the experimental data given in [7]	
Table 4. 1 Circuit parameter values used	46
Table 4.2 Fitted equivalent circuit parameters for different applied voltage and temperature 5	56
Table 4.3Fitted Parameters	64
Table 5. 1. Parameter estimated from fitting 10-minute experimental data	73

Notations and Abbreviations

E	Electric stress	PR	Polarity Reversal
V	Voltage	LDPE	Low Density Polyethylene
N , $n_{H,}$, $N_{L,}$	Power law exponent	XLPE	Cross Linked Density Polyethylene
D	Damage	HVAC	High Voltage Alternating Current
t	Life time/ time to failure	HVDC	High Voltage Direct Current
λ	Reversal frequency	OIP	Oil Impregnated Paper
τ	Single relaxation time	VSC	Voltage Source Converter
D	Damage	LCC	Line Commutated Converter
a, b, s, r	Life model Stress coefficient constants	PEA	Pulsed Electroacoustic
T	Time Interval between reversal	DEM	Damage Equalization Method
D_0	Damage under dc	BDV	Breakdown Voltage
R	Insulation Resistor	PVC	Poly Vinyl Chloride
C	Insulation Capacitor	PDC	Polarization Depolarization Currents
R_{d}	Fictitious resistor	UG	Underground Cables
C_d	Absorption capacitor		
α ,β	Nonlinear dielectric model constants		
Z, Z_m, Z_d	Circuit Impedance		
μ	micron		
V_m	Voltage across the measuring circuit		
V_d	Voltage across the sample		

1.1 A Brief Contextual Overview of Underground Power Cables

Multitudinous factors including increase in urbanisation, right of way issues, hike in energy infrastructure expenditure, demand for renewable energy power transmission systems (viz., off-shore and on-shore wind farms, solar panels, hydel power plants etc.) resulted in rapid increase of high voltage underground (UG) cable installations. This is evident from the current and projected core length trends of UG cables all over the world [1] shown in Figure 1.1.

Different insulating materials are used to make the UG cables including PVC, polyethylene, kraft paper, silicone rubber etc. Oil-impregnated paper (OIP) and cross-linked polyethylene (XLPE) are typically used in high voltage cable applications. Although OIP cables are more reliable than extruded polymeric cables (In cities like Mumbai, there are still several OIP cables in the distribution network operating since 1970s, whereas recently laid polymeric cables often experience premature failures), they were phased out by the latter because manufacturing OIP cables is extremely time consuming and expensive, unlike polymeric cables which can be extruded faster and conveniently manufactured to the designed length. In addition, polymeric cables have higher load current carrying (thermal) capacity, better mechanical properties and are light in weight.

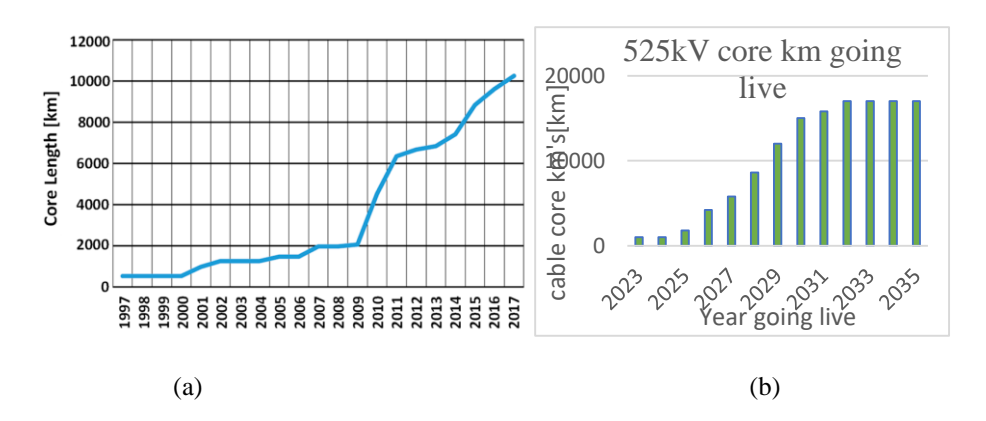


Figure 1.1 (a) The core length of DC-XLPE cables installed and under construction in the year 2018 (b) Future growth predicted length of cable [1]

XLPE is the most commonly used material among extruded polymers, since higher polymers require higher extrusion temperatures. Therefore, XLPE cables are the subject of

in-depth research, chiefly focused towards increasing their service life and power carrying capacity.

Rapid economic growth demands faster installation of energy infrastructure to meet the ever-rising power demands, which in turn leads to the tremendous growth of the UG power cables network, especially considering the right-of-way advantages that the UG cables have over overhead transmission lines. However, on the flip side, this also demands stringent reliability and performance criteria, to justify the huge expenditure involved. Hence, the enhancement of insulation strength of power cables is focused more on the dielectric and electric insulation society. Even while deciding the nominal voltage level of transmission lines, the reliability of insulating materials plays a major role. Numerous prequalification tests such as, tan delta, space charge, volume resistivity, and breakdown tests are part of the insulation design. Moreover, the insulation assessment criteria vary significantly based on its HVAC or HVDC applications.

The majority of the testing procedures created were based on the surges experienced by the insulation used in cables and accessories (such as joints, terminations etc.) in real time. The insulation design of UG cables for a specific nominal voltage is determined by the results of multiple tests, which follow an empirical approach. The phenomenological model derived from the breakdown test data is an instance of an empirical approach. Consequently, methods of testing play a role in determining the lifespan of cables. However, even after the rigorous analysis and careful design the extruded cables often fail to complete the estimated life. As per bath tub curve, failures are categorized into premature, normal and aged conditions caused by several factors including manufacturing defects, operating condition and temporary faults, and accordingly the time to failure of insulation varies.

The UG cables are operated either under HVAC or HVDC voltage stresses. Under HVAC, the degradation of insulation is quantified in terms of dielectric loss factor. In HVDC, the insulation degradation is related with the presence of space charge and with the changes in volume resistivity of insulation. In either of the cases, the electro thermal stress accelerates the insulation degradation. Normally the insulation under HVDC stress should withstand higher voltage compared to HVAC stress [2]. Hence, the life of a HVDC apparatus is expected to be more than that of HVAC.

However, in practice, insulation used in HVDC links failed drastically, way before its estimated life. The reason behind the failure were mainly attributed to polarity reversal (PR)

and consequently space charge enhanced field in HVDC links[6] and [7]. Thus, investigation under PR stress becomes necessary in order to make extruded cables more successful in HVDC-based systems.

1.2 DC Polarity Reversal Stress

1.2.1 A Typical HVDC system

A HVDC system is typically used to transmit power over long distances, or to interconnect two HVAC grids. A HVDC system broadly constitutes of converter station and an inverter station connected via overhead lines/UG power cables. There are several techniques used in HVDC transmission links, however, every technique is fundamentally based on LCC and VSC based operations. In LCC systems, the power reversal between interconnected HVAC grids is done by reversing the polarity of HVDC links. In VSC systems, the power reversal is done by changing the current direction. Together in hybrid mode the operation might differ. The cables used in LCC based HVDC system are subjected to frequent PRs in order to reverse the power flow.

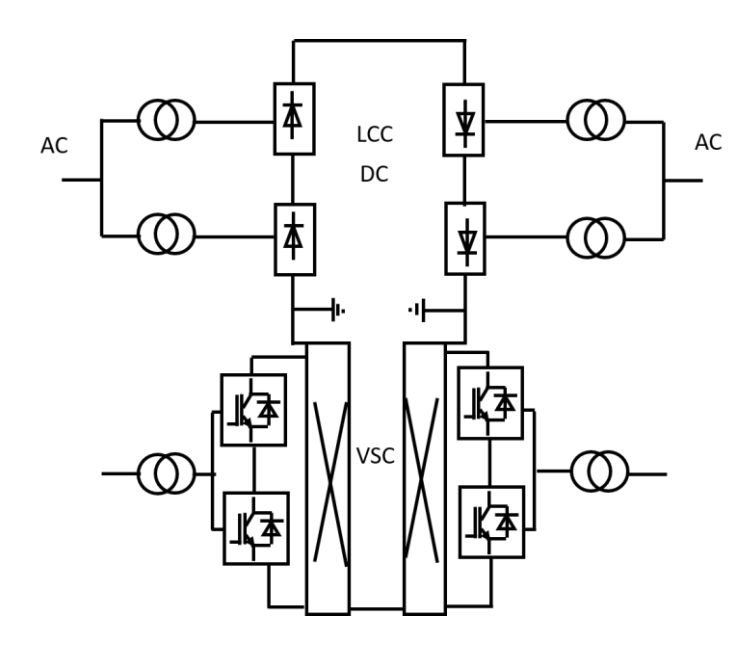


Figure 1.2 Hybrid HVDC system [3]

The converter converts AC to DC voltage and the inverter converts DC to AC voltage. After every power reversal the converter becomes inverter and the inverter becomes converter. This is done by controlling the firing angle of thyristor used in LCC based system.

Similarly, due to advancement in hybrid HVDC systems (where both LCC and VSC are used together) PR occurs even in VSC based HVDC links. The hybrid LCC and VSC system with UG cables used in transmission link from Japan [3] are shown in Figure 1.2.

Here in hybrid mode the PR in VSC is done manually by physically changing the polarity of the link with high-speed switches. Thus, the insulation and its accessories used in the overhead lines and cables in HVDC system undergoes PR [3] at the instant of power reversal. Approximately 1000 reversals are performed per year [3]. Subsequently there is a concern of service life of polymeric cables under PR stresses.

1.2.2 Effect of PR stress on insulation

The above discussion briefs that the PR is common in HVDC cable systems. Even the cables used in VSC based hybrid systems undergo PR. Unlike quasi static or steady state stresses, an electric field distribution in PR stress is determined by both permittivity and resistivity of material. In steady state, the electric field distribution is based on insulation resistivity and at the time of reversal it is based on insulation permittivity. Theoretically at the time of the PR, the insulation experiences enhanced transient electric field.

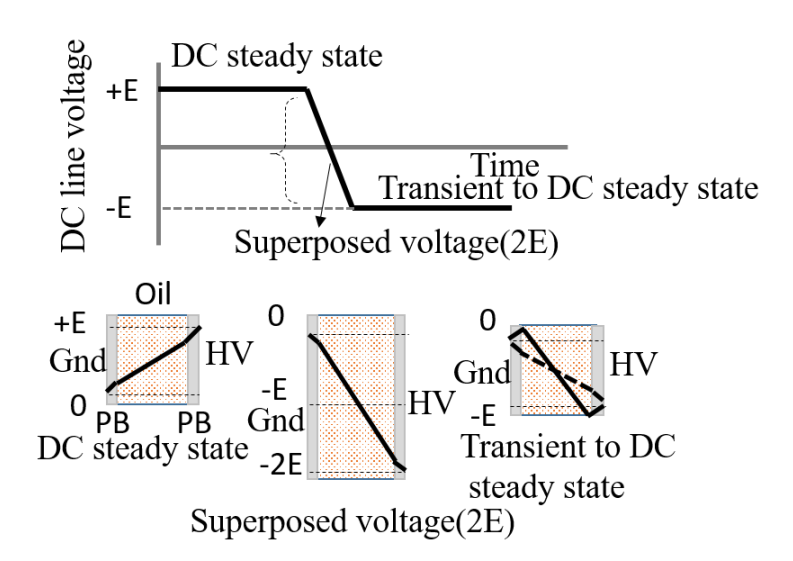


Figure 1.3 Voltage distributions at PR [4]

The steady state to transient voltage distribution and vice versa of converter transformer insulation is shown in Figure 1.3. Here the insulation is stacked with mineral oil and pressboard (PB). Since the permittivity of the oil is less compared to pressboard (PB), oil duct experiences high electric field, which is double at the time of PR. Even after the PR transient, the voltage distribution is not smooth in the interfaces for a while until steady state

is shown in Figure 1.3[4]. The test voltage waveform generated shows a smooth transition from positive to negative polarity. However, the voltage across the insulation does not mirror the applied voltage. Instead, it can rise to a peak that is double the applied voltage. This increase is attributed to stored charge within the insulation from the previous polarity, which hinders smooth reversal. Consequently, transient voltages persist even after the polarity is reversed. These prolonged transients complicate the dynamics of charge within the bulk of the insulation material.

Similarly, the UG cable insulation also undergoes momentary voltage and field spikes. The PR in an HVDC system is done in typically less than two minutes[12]. Thus, due to planned and unplanned PRs in an HVDC network, the abnormal field distribution (resistive to capacitive and vice versa [5]) experienced by power apparatus (cables and accessories) initiates insulating material degradation.

Few works of literature [6,7] incorporated these PR stresses into life estimation techniques to assess insulation degradation. The development of models and their limitations were discussed in detail in the second chapter. However, the models were proposed based on conventional life estimation techniques. The ideology behind it is keeping the life estimation technique simple and convenient for the user. This will be dealt with in a bit more detail in the subsequent sections.

1.3 Overview of Life Estimation Techniques

The insulation performance plays a major role in HVDC cable designs. There are established methods in practice to evaluate the insulation parameters. Primarily the insulation for HVDC cables is assessed with a DC voltage profile. Ideally, the intrinsic strength of the insulation material is expected to remain unaltered by external factors. However, the materials used for insulation are not without their imperfections. This is particularly true for polymers such as XLPE and LDPE, which are semi crystalline materials. Consequently, the failure of insulation is often attributed to the weak links within the material. As a result, the electrical breakdown strength of such materials tends to vary and is distributed over a range. Thus, a systematic procedure is needed to be followed to assess the insulation material.

1.3.1 Experiments and Statistical Analysis

The procedure encompasses the use of conventional testing methods and the application of statistical data analysis. The detailed information regarding breakdown test procedures

such as electrode geometry, testing procedures, and voltage profiles are followed from the standards of ASTM, IEEE and IEC. Specifically, ASTM D149 gives a detailed overview about the breakdown tests and are usually followed by the industries. A Typical electrode setup and a tested sample are shown in Figure 1.4.

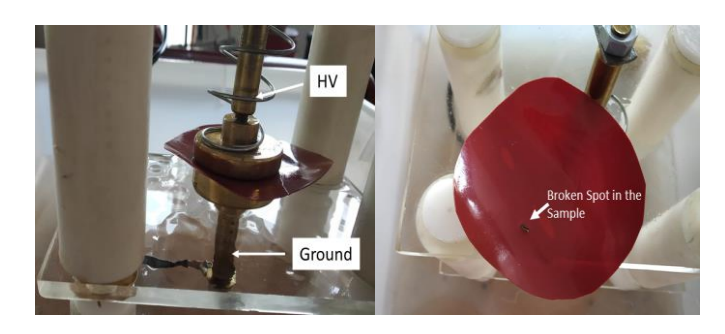


Figure 1.4 Typical electrode setup and punctured sample

To refine the distributed breakdown test data, probability analysis is used. Simply averaging the test data tends to underestimate the insulation performance. In this context, the Weibull probability distribution is particularly valuable as it provides a closer approximation to realistic values. The scale and shape parameters are calculated using the cumulative density function of two parameter Weibull expressions as in (1.1).

$$F(\alpha, V_{BD}, \beta) = 1 - \exp\left[-\left(\frac{V_{BD}}{\alpha}\right)^{\beta}\right]$$
 (1.1)

Where: F – cumulative density function, V_{BD} – breakdown voltage, α – scale parameter, (63.2% probability equivalent), β – shape parameter (decides the quality of data).

Here the V_{BD} denotes the breakdown voltage of the material, the maximum stress the insulation could withstand. However, designing the DC apparatus on the material's maximum stress strength is impractical because the time to failure is quite short. Moreover, there is no guarantee that the insulation does not fail below the maximum stress threshold estimated within a short timeframe.

1.3.2 V - t Characteristics

Therefore, the relationship between breakdown voltage and time to failure, referred to as the voltage-time graph or V-t characteristics is used. This graph plays a crucial role in estimating the insulation lifetime. Figure 1.5(a) displays typical V-t characteristics, illustrating that as the voltage level increases, the time to failure decreases, presented on a logarithmic scale. The V-t characteristics shown in Figure 1.5 (a) result from accelerated tests in which the voltage is maintained until the insulation sample breaks. The times to failure of repeated samples are subjected to probability analysis. These tests are repeated with

different voltage levels. The tests results govern an inverse relationship between voltage and time to failure.

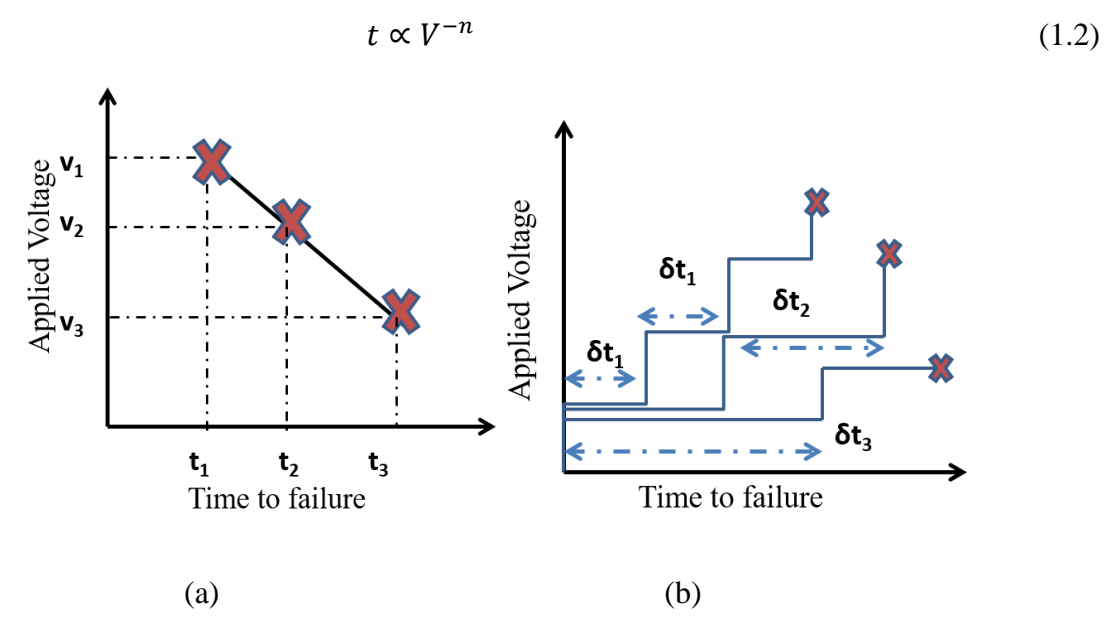


Figure 1.5 (a)Constant stress test (b) Step stress test

The V-t curves are well fitted into the "Inverse power law (IPM)" model shown in equation (1.3). The relationship between voltage and time to failure is formulated using power law.

$$t \times V^n = D \tag{1.3}$$

Here, t is life time, V is voltage level $\left(E = \frac{V}{thickness}\right)$, n is power law exponent or voltage endurance coefficient, D is a quantity known as strength constant or as the critical damage accumulated in the sample at failure.

The unknown coefficients are estimated from the experimental methods using least square methods. From the inverse power law and endurance coefficient, the life is estimated using the equation (1.4).

$$L(E) = L_H \left[\frac{E^{-n}}{E_H} \right] \tag{1.4}$$

Here, L(E) or $t = \text{Estimated life } L_H$ or $t_1 = \text{Life at higher fields } E_H$, (The E_H is the field applied across the sample during the stress test), E is the field at which the insulation life is to be estimated, n = voltage endurance coefficient.

Here *D* is the critical damage not the physical term but should be interpreted as a virtual term representing the same event/failure caused by the different stress level to a particular batch of

insulation material. The critical damage caused by V_1 and V_2 equated and interpretated as shown in equation (1.5).

$$t_1 V_1^n = t_2 V_2^n = D = t V^n (1.5)$$

Overall, life estimation techniques empirically relate the time to failure with the applied stress raised to the power of the voltage endurance coefficient n. Ideally, a negligible effect of voltage stress on the time to failure is anticipated for better reliability. However, in practice, this dependency exists and is well recognized in the voltage-time (v-t) characteristics of accelerated tests. Technically, a higher n value reduces the dependency of voltage stress on the time to failure, which corresponds to the ideal condition for better reliability. Thus, higher n values directly indicate better-performing insulating materials. Collectively, these are the concepts for conventional life estimation of insulation. The results are applied accordingly in simulations and cable designs. The constant stress test shown in Figure 1.5(a) is generally followed but it is time consuming process. Hence, new techniques were reported with step stress test [8]. Here the incremental voltage is maintained constant and increased at a fixed time interval δt_1 until breakdown. This process is then repeated with intervals $(\delta t_2, \delta t_3)$. Overall the experimental results used to estimate the voltage endurance coefficient are obtained more quickly as compared to traditional techniquesas shown in Figure 1.5(b). The damage accumulated in every step stress is incorporated in life estimation process. The results are concluded based on the IPM model.

$$D = \delta t_1 V_1^n + \delta t_1 V_2^n + \delta t_1 V_3^n \tag{1.6}$$

$$D = \delta t_2 V_1^n + \delta t_2 V_2^n \tag{1.7}$$

$$D = \delta t_3 V_1^n \tag{1.8}$$

It is reported in [6] using the proposed step-stress test based DEM, the D and n values could be estimated in short time. This shows that the upgradation of DC life estimation techniques is still under consideration.

1.4 Motivation for Comprehensive Life Model

Here the Figure 1.6 from [2] is displayed to illustrate the difference in voltage endurance coefficient n under different voltage profiles. However, the difference in n is used to compare similar types of material performance. The n is inversely proportional to the line

slope shown in Figure 1.6. Therefore higher the n value more the damage an insulation can withstand and that's how n reflects the material performance.

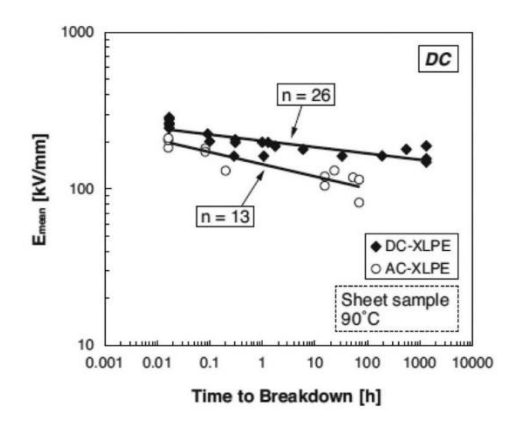


Figure 1.6 V-t characteristics of AC and DC test in log-log scale[2]

However, in [2] the voltage endurance coefficient *n* is reported to be high for HVDC as compared to the HVAC electric field. This shows that the voltage profile has a significant effect on performance of insulation. Similarly, it is to be understood PR stress has a significant effect on the estimated DC insulation life. The transformation of homo-charge to hetero-charge and vice-versa [4, 9 & 10] under *periodic* PR leads to space charge driven field enhancement, which demonstrates the enhanced damage/degradation due to reversals.

Even though literatures reported reduction in life due to PR, due to lack of reliable results the cable customers are forced to rely on last known best service cable properties. This becomes a burden on cable manufacturers to repeat/duplicate the performance of insulation. The PR reversal in the HVDC system is inevitable. Hence, understanding the degradation due to PR stress is important to improve the performance of material. Thus a better technique or comprehensive life model to evaluate and to effectively utilize the performance of insulation is looked essential. Additionally, understanding the degradation of insulation under PR, is considered important for enhancing the material performance. This paves way to efficiently utilize the power cables. It is to be noted number of PR in a HVDC network is also a variable. Therefore, very close experiments representing the PR stress are required for understanding its effect on the insulation life characteristics.

Hence, the scope of work started with the generation of PR voltage profile with different frequencies of reversal (i.e., Time interval between reversals) and further proceeded with the breakdown tests of insulation. The investigation rigorously followed the conventional statistical models, reliability models and testing procedures. The deliverables were more focused to optimize the working condition of insulation for its better performance. The work

is elaborated in Chapter 3.

1.5 Material Characterization with Dielectric Model

Furthermore, both the literature model [6] and experimental results presented in Chapter 3 indicate that LDPE degrades more rapidly under polarity reversal stress compared to other insulation materials. This is due to the more complex charge dynamics in LDPE, including phenomena such as trapping and detrapping. Therefore, understanding these dynamics is crucial. A comprehensive dielectric model is needed to fully comprehend the failure mechanisms in LDPE. This deeper understanding of LDPE will also facilitate the interpretation of non-destructive measurements related to polarity reversal.

1.5.1. Background of the current characteristics

The testing techniques of insulation materials were developed to predict their performance and degradation. The conduction current measurement is one of them that infers the change in volume resistivity of the insulation under different electro-thermal stresses.

Even the circuit simulation and FEM uses the field dependent conductivity equation obtained from the conduction measurement to estimate the electric field distribution in cable models for different load conditions. Generally, in DC application the degradation of polymers is assessed with the help of space charge and conduction current measurements. The space charge and leakage current characteristics are often correlated for better understanding of insulations. The space charge dynamics reflects in conduction current measurement.

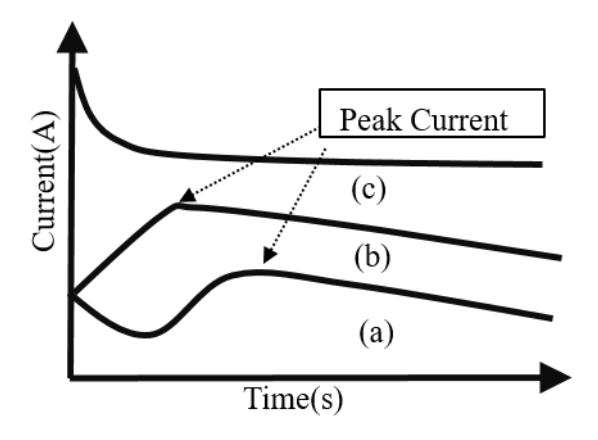


Figure 1.7 Current characteristics of XLPE from [11]

However, an anomalous transient conduction current often reported in literatures is shown in Figure 1.7 [11]. As per dielectric equivalent circuit shown in Figure 1.8 the expected current characteristic on an insulation is of Figure 1.7. curve (c) i.e., the current gradually

decreases to a steady state once polarized with a particular voltage in lossy dielectrics. The current characteristics shown in Figure 1.7 curve (c) are generally observed in OIP, and the differences in the current trend(exponential and steady state) is used to assess its ageing characteristics. Even in polypropylene PDC measurements were performed to find its degradation mechanism. Thus, the change in characteristics is found to be valuable and conveys useful information about insulation.

However in XLPE and LDPE the current characteristics as in Figure 1.7 of different types (a, b, c) are reported. i.e., the current decreases and increases dynamically based on the applied voltage and temperature[11]. It is often related to space charge dynamics inside the bulk of polymers.

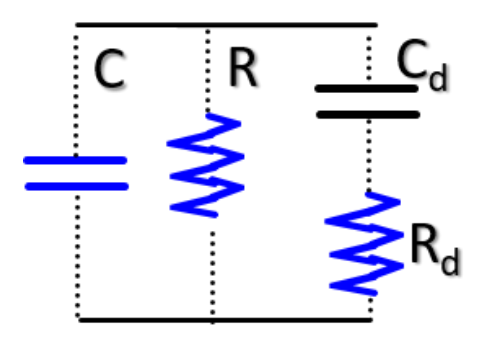


Figure 1.8 Linear dielectric model

These dynamic characteristics were not observed in OIP and polypropylene insulation materials. These characteristics relate to multiple aspects of insulation performance based on the results obtained from the simultaneous and separate measurement of space charge and conduction current. The conductivity equation was based on steady-state currents values obtained after a certain period. However the anomalies or transients were observed or reported in between the initial and steady state measurement of time. A better understanding of these transients is considered to be useful in interpreting DC and PR effects on insulation.

1.5.2. Motivation for dielectric model

The linear dielectric model shown in Figure 1.8 is insufficient to recreate the transient current characteristics shown in Figure 1.7. The literature [30] and [38] also discusses the need for complex dielectric model, especially for XLPE. Representation of current characteristics is more important that it is often related to space charge dynamics in polymers. In [22], the linear dielectric model equivalent circuit is modified according to the experimental results. Thus, the attempts to represent transient current characteristics in relation to equivalent circuit model give better understanding of the bulk of LDPE. These

current measurements involve electrometer/pico-ammeter, yet so far the transient currents have not investigated for experimental errors in any literature. In this case, the inadvertently missed scope was the possibility of instrumental error.

Consequently, a collaborative investigation of the transient current was undertaken, incorporating simulation, hardware setup, and a dielectric model. The details are in chapter 4. Furthermore, the currents were measured for two different frequencies of reversal and the results are presented in chapter 5.

1.6 Organization of the thesis

In the initial chapter, the focus lies on establishing the background briefly yet thoroughly. Several topics pertaining to the thesis including the origin of PR stresses, existing techniques and models used for evaluating insulation reliability, various life estimation models, dielectric models etc., are touched upon briefly. The chapter ends with the organization of the thesis.

The second chapter involves a detailed literature survey of existing life estimation models and their limitations. The need for investigation of the degradation of materials under the PR stress and a comprehensive life estimation model are enunciated, thus initiating the scope for one of the proposed objectives. A detailed literature survey on DC current characteristics, anomalous current characteristics and its pertaining modified dielectric circuit model is presented. A connection between the need for understanding the DC and PR current characteristics is established.

The third chapter explains the results and discussion of the PR life estimation model. It begins with the experimental setup and breakdown test results for three different materials at different PR time intervals. The V-t characteristics are plotted, power law components are evaluated and a comprehensive life model is proposed that is valid for both PR and DC fields. The percentage of life reduction among materials is compared. The reason behind the materials degradation is discussed. The safe PR time intervals were suggested for different materials.

The fourth chapter deals with conduction current measurement. The current characteristics are measured using commercial electrometer and with replicated electrometer internal circuit. The instrumental errors due to electrometer internal circuit are explained with the support of

an equivalent circuit. A new dielectric model is proposed based on Cole-Cole model. The actual current characteristics are identified and reported and are validated analytically and experimentally.

In the fifth chapter the experimental results of conduction current measurement under PR are presented. The differences in current characteristics are explored for two different time intervals. The results are related with deliverables obtained from the comprehensive life model.

The sixth chapter lists tangible conclusions drawn from the thesis that are of utmost significance to cable manufacturers and utilities, apart from a brief summary of the future scope of this work.

2.1 Existing Life Models for DC plus Polarity Reversal

A few models were proposed in the literatures [6,7] to study the life of an insulation material which attempt to describe the dependence of life of an insulation material on the frequency of PR. This section reviews the existing life model testing methodologies and their limitations.

2.1.1. Phenomenological Model

In [7] phenomenological approaches have been used to describe the life of insulation material under DC and PRs. Here the PR voltage has been considered as a superposition of pure DC and positive impulses as shown in Figure.2.1 (b) and the corresponding model is given in Equation (2.1). With PR voltage profile, the insulation losses and insulation degradation include polarization losses. In the case of the superimposed impulses on a DC bias voltage, the polarization processes will be different because there is no PR.

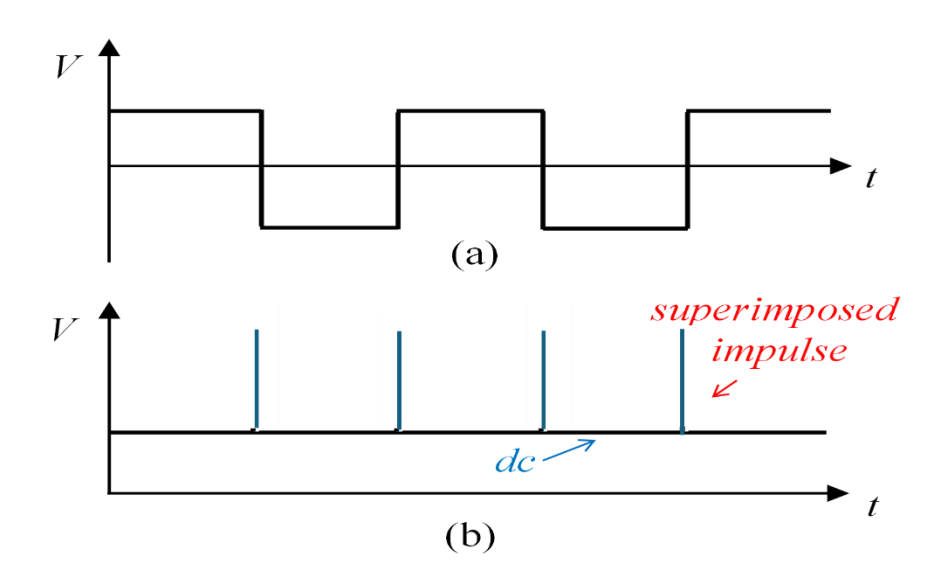


Figure 2.1(a)Typical voltage PR profile. (b) dc component of voltage PR with impulses superimposed at the time of reversals [7].

$$L(E,\lambda) = \frac{1}{\frac{1}{L_H} \left(\frac{E}{E_H}\right)^{N_L} + \frac{\lambda}{n_H} \left(\frac{E}{E_H}\right)^{N_R}}$$
(2.1)

 $L(E,\lambda)$ is the life of insulation under PR voltage and reversal frequency λ at field E. L_H is the life of material at highest test field E_H . N_L and N_n are the power law exponents in case of pure DC and in case of voltage inversion pulses respectively. n_H is the number of reversals till failure for applied pulse amplitude equal to E_H .

Model Limitation - Although equation (2.1) provides a mathematical description of insulation life, it comes with certain underlying assumptions. One key assumption is the representation of the PR voltage profile as a combination of pure DC and a series of positive impulses. This representation does not accurately reflect the actual pulsating electric field following each PR, as each PR opposes the existing field within the insulation material for that cycle. A positive DC with positive impulses is quite different from PR voltage as far as space charge formation is considered because the stressing will be only in one direction which is not true in case of PRs. The effects of impulse and DC part of voltage were assumed to be independent of each other and not in a cascaded manner one influencing the other. The ageing rate due to PR voltage was taken as a sum of the ageing rate due to DC and ageing rate due to impulses during reversals only, which may not be exactly true. The DC and impulses during reversals may have a synergic cascading effect on the ageing of material rather than just the addition of individual ageing rates.

2.1.2. Physical Model

Another physical model proposed in [6] relates the ratio of life of insulation under dc stress with PR to:

- 1. frequency of reversals,
- 2. space charge quantities such as, the absolute stored charge density after poling,
- 3. the maximum electric field in the specimen after PR, and
- 4. slope of the depolarization characteristic.

It is expressed by Equation (2.2).

$$\ln(L_{REL}) = \ln[(L/L_i) - 1] = A_1'' + A_2'' \ln(q_s'(E))$$
$$+ A_4'' \ln(s'(E)) + A_5'' \ln(f')$$
(2.2)

where L/L_i is the ratio of lives obtained from life tests at a given electric field without PR and with PR, $q'_s(E)$ is the normalized total absolute stored charge density after poling at a

given field E, s'(E) is the normalized slope of the depolarization characteristic at the same field and f' is the normalized frequency of PR. A multi-material approach i.e., life tests carried out in a given field, but on different materials of the same family, have been used to calculate the coefficients of the model. The model coefficients evaluated by the multi-material approach were assumed to be valid for all materials belonging to that insulation material family. The model proposed, is then recast to a simpler model relating the above mentioned ratio to the frequency of reversal and electric field given by Equation (2.3).

$$\frac{L}{L_i} = 1 + KE^{b_1} f'^{A_5} \tag{2.3}$$

Model Limitations-As per the model it has been stated in [6] that the reduction in a number of coefficients may decrease the accuracy of the model. The coefficients of Equation (2.3) were obtained by a multi-material approach and a single material approach (life tests on a single material with varying fields and frequencies). These coefficients showed good results for four variants of XLPE but were unable to explain the frequency dependence of the model in the case of HDPE, indicated differently by both approaches. Although space charge was considered one of the major contributing factors in ageing [6] there would be other phenomena such as partial discharges which could affect the rate of ageing, especially in the case of PRs.

Though, these models discuss the phenomena occurring in an insulation material, as far as accurate and practical application is concerned, empiricism dominates. Empiricism, in fact, is the basis for any life estimation as all phenomena occurring in insulation, including unpredicted phenomena, can also be accounted for in experimentation.

2.2 Approach to Comprehensive Life Estimation Model

Certain life models were suggested in the literature, with some limitations, which attempted to give a theoretical basis for the models based on observed theoretical phenomena [6,7]. However, in actual practice, the damage or degradation is believed to be a multiphysics phenomena, and an accurate empirical/practical estimation of life is needed for accurate predictions. As mentioned in the first chapter, one of the most widely used empirical models to study the life of power equipment is the *Inverse Power Law model (IPM)*. *Power-law exponent n* and *Damage D* (or strength constant) are the two important parameters which describe the inverse power law. These two quantities are assumed to be constant for a given

set of experimental conditions. The change in frequency of PRs can be considered as a change in an experimental condition. Hence, the aforementioned quantities (damage and power law exponent) are expected to show some variation. For the assessment of ageing and determination of the life of power equipment, it is important to study these inverse power law parameters and their variation with respect to the changing frequency of reversals. These variations in inverse power law parameters give scope for modifications and improvements in existing models to quantitatively explain the performance of equipment.

The model presented in this thesis to describe the life of an insulation material is based on inverse power law, after a careful observation of experiments on different materials. In literature, the use of the inverse power model has been validated [13-14] but very little emphasis has been given to the variation of power law parameters (power law exponent and damage) with respect to frequency of reversal i.e., the dependence of power law exponent and damage on frequency of reversals needs to be investigated. A comprehensive life model applicable to DC PR stresses is considered necessary to understand the effect of reversals and take adequate measures for life improvement.

2.3 Literature Survey on DC Current Characteristics

In LDPE volumetric current measurement, an anomalous current profile is typically observed in between the time interval of instantaneous polarization and steady state conduction for every different set of constant voltage and temperature[17][22]. The repetitively reported current characteristics in the literature are shown in Figure 2.2. This anomalous current profile varies with varying electric fields and temperatures. The current in Figure 2.2 (a) decreased initially after instantaneous polarization and then increased after a certain time interval. Whereas, in Figure 2.2 (b), the current increased first and later decreased.

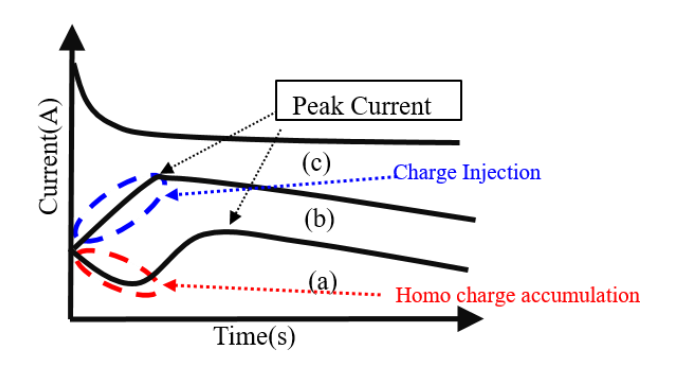


Figure 2.2 The transient current characteristics in [11]

This anomalous current profile is related to charge dynamics in LDPE and XLPE to assess material performance [11,16,17,18]. The initial dynamics i.e., decrease in current related with homo charge injection and increase in current relate to charge injection. The charge dynamics alter the electric field distribution in the bulk and interface of insulation.

2.3.1 Insulation assessments with transient current characteristics

A multiple approach based on the current characteristics was reported.

- In [11], the mini cables were subjected to the space charge and conduction current measurement separately. A distinct anomalous current profile was reported for every set of different electro thermal conditions. An attempt had been made in [11] to correlate the space charge and conduction current characteristics. Nevertheless, it was concluded that the occurrence of anomalous current profile peak did not match with the charge dynamics observed inside the cable.
- In [18] for simultaneous space charge and leakage current measurement of XLPE, the Figure.2.2 (a) type current was reported for different electrical fields. Since the charge dynamics inside the XLPE reflect the change in volumetric current measurements, an increase and decrease in volumetric current are related to charge injection and dipole relaxation respectively. Particularly the current trend was related to the injection of negative charges and their movement towards the anode.
- Likewise, in [16], instead of an anomalous current profile the occurrence of peak currents at specified electric field and temperature is identified as an electrical threshold marker to estimate the life of the insulation material.
- Additionally, the anomalous current profile at a higher field similar to Figure.2.2 (b)
 was explained with a double injection model in [17], related to bipolar charges
 transport.

Thus, the different perspectives on the measurement of anomalous current profile, such as life estimation techniques [16], charge transport model [17], and correlation with charge dynamics [18], highlight the important information about the insulation material under electro thermal stress.

2.3.2 Modified linear equivalent circuit model

Similar to the space charge profile, the DC current characteristics are associated with the linear dielectric model and it is often used in the assessment of insulation ageing

characteristics. The linear equivalent circuit of insulating material is modelled with resistor and capacitor (RC) parallel network shown in Figure.2.3 [19]. Where C, is the instantaneous polarization capacitance, R is insulation resistance, C_d and R_d represent absorption charge capacitance and the fictitious resistance respectively. The equivalent circuit current I(t) for an applied voltage U(t) is given in the Equation (2.4), the first term represents the conduction current and remaining two terms is of instantaneous and slow polarization currents.

$$I(t) = \frac{U(t)}{R} + \frac{d}{dt} \left\{ C U(t) + C_d \int_0^t U(\tau) f(t - \tau) dt \right\}$$
 (2.4)

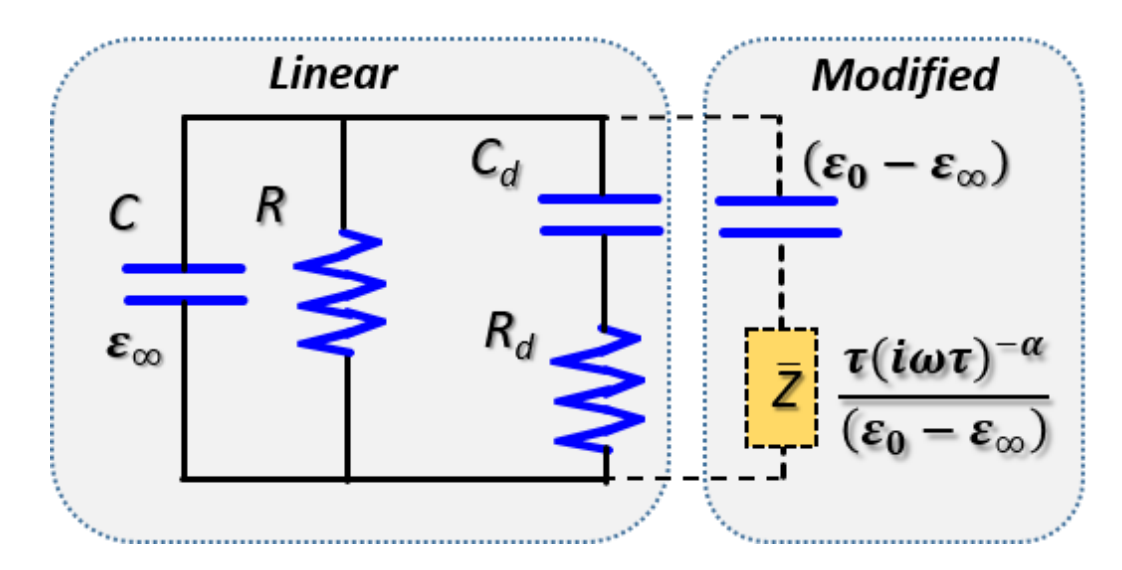


Figure 2.3 The linear and modified dielectric model

Modifications

• In [22] the linear equivalent circuit was modified with complex impedance \bar{z} is shown in Figure 2.3.

$$\bar{z} = \frac{\tau(i\omega\tau)^{-\alpha}}{(\varepsilon_0 - \varepsilon_m)} = R_d (sR_d C_d)^{-\alpha}$$
 (2.5)

The complex impedance \bar{z} given in equation (2.5) was used to represent the experimental non-linear current decay. Real and imaginary components of complex impedance \bar{z} did not have any conventional significance. However, it was used to closely fit the experimental data [22] with α termed as material dependent variable. For a unit potential difference, the current flowing through the complex impedance branch is derived as Equation (2.6) and Equation (2.7) by neglecting the initial polarization current.

$$I(t) = At^{-\alpha} \qquad t \ll \tau \tag{2.6}$$

$$I(t) = At^{-(2-\alpha)} \quad t \gg \tau \tag{2.7}$$

where $\tau = R_d C_d$.(detailed derivation solved in the appendix).

Here for two different time instants $\tau \gg t$ and $\tau \ll t$ the difference in monotonically decreasing complex impedance branch current trend was accounted by different slopes. Moreover, it does not account for any transient anomalous peak current profile peak characteristics.

• Similarly, in [25] the capacitor was modified with $\frac{1}{(s^n c)}$, to represent the diverse current flow with respect to time and given n close to one for low loss capacitors. Likewise, in [26] the time varying capacitor differentiated from a constant capacitor with a similar kind of modification. Similarly, in [37] and [38], the OIP and Polypropylene insulation current characteristics represented with equivalent circuits and the electrical field distribution were analyzed for DC and transient conditions.

These circuit modifications were done to differentiate the different kinds of insulation and their changes in properties. In some cases, the circuits are used to differentiate single insulation material ageing characteristics. Thus, the equivalent circuit quantifies the change in parameters accurately and is useful in understanding the material properties. Further the circuit model eases the simulation oriented analysis. Hence, the aforementioned modifications initiate the idea of modifying the linear equivalent circuit to fit the anomalous current profile in LDPE.

2.4 Problem Statement

Thus, it is understandable that the DC's current characteristics convey useful information about the bulk of the material. the modification with the dielectric model was more relevant in identifying the corresponding changes under different electrothermal conditions. It is also reported in [38] that a sophisticated model was required to represent the anomalies in LDPE/XLPE current characteristics. However, the multiple approaches highlighted in the literature have raised a concern about the possibility of error in the current measurement, especially considering the use of the electrometer in the current measurement. The insulation leakage current is typically in the range of pico (pA) to nano (nA) amperes and is measured using an electrometer or pico ammeter. However, nowhere the distinct anomalous current profile and the peaks were investigated for inherent error in the electrometer's internal

circuitry. Any error or inherent characteristic of the measuring instrument used in current measurement may lead to misleading information obtained on the insulation material.

2.5 Methodology Proposed

The literature survey stated a need for a dielectric model and an investigation for instrumental error. Typically, the electrometer's internal circuit is inaccessible to the user hence the investigation of instrumental error needs a hardware setup. Such a setup enables exploring variations in the current characteristics with changes in electrometer internal circuit parameters. However, the entire transient current characteristics could not be projected as an instrumental error unless it is proved. Hence, recreating the transient current as in an electrometer with a suitable dielectric model gives better clarification. For this a modification of the dielectric model is the best approach. By aligning the DC current characteristics with a circuit model, it is anticipated that a more comprehensive understanding of the material and the possibility of instrumental error can be verified.

.

The DC Polarity reversal breakdown test results for three different insulation materials are presented in this chapter. The obtained experimental data is statistically analysed. The effect of reversal frequency and its significant reduction in life has been experimentally demonstrated. Based on the fitted characteristics of inverse power law components, a comprehensive life model is proposed. To extend the life of insulation, an ideal safe time interval between subsequent polarity reversal is established.

3.1 Experimental Setup and Procedure

Rigorous experiments are planned to ascertain the nature of V-t characteristics under PRs. The experimental setup is arranged as shown in Figure 3.1. The experiments were performed using an HV amplifier (Matsusada-AMP-20B20) with +/-20kV amplitude range and slew rate of 700 V/ μ s, which is driven by a function generator (Keysight-33210A) with a10MHz frequency range. An oscilloscope (Tektronix-TBS1102B) with 100MHz bandwidth is used in the feedback loop to stop the test in the event of a breakdown.

All the samples are tested with planar brass electrodes of 50 mm diameter in an isolated thermal environment at 50°C. The PR voltage profile applied to the samples is shown in Figure 3.2.

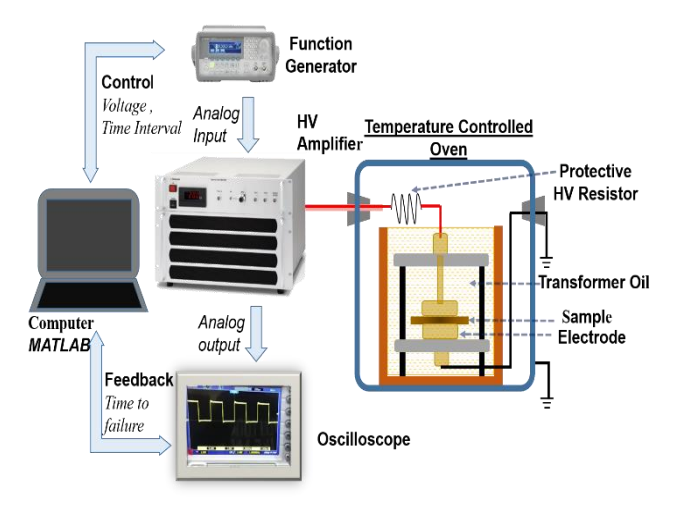


Figure 3.1 Automated instruments profile for PR experiment and experimental elements in a controlled environment

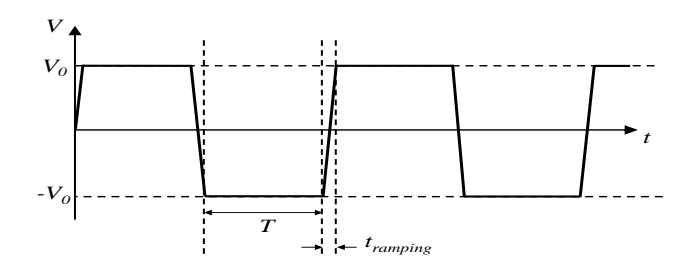


Figure 3.2 Typical profile of the PR voltage used in the experiment with a time interval between reversals (T), ramping time $(t_{ramping})$ and voltage level (V_0) kV



Figure 3.3 Samples used

Table 3. 1 Samples used in experiments

Materials	Thickness (µm)	Testing Electric Field (kV/mm)	Minimum number of samples at each Electric Field		
LDPE	100	200,180,160,150,130	10		
Silicone Rubber	100	80,75,70,60	10		
Kraft Paper	120	108.33,100,91.67	10		

The transition between reversals is done through ramping the voltage level with a fixed ramping time of 10 seconds for all levels of voltage. The duration is selected based on the constraints of high voltage source used in the experiments. In the experiments conducted, the time interval between PRs T is varied and the breakdown time was recorded. The materials subjected to the breakdown test included LDPE, silicon rubber and Kraft paper. The thin film samples used in the breakdown test are illustrated in Figure 3.3.The sample thicknesses and their corresponding test fields are detailed in Table 3.1.

3.2 Breakdown Test Data

The experimental results are critically analyzed in this section. Based on careful

observations, the proposed model has evolved. The model is then fitted to the experimental data. The significance of the model parameters is then put forth including a comparison of the performance of various materials used in power equipment under PR conditions.

It is well known that the times to failure at a constant stress (voltage) follow the Weibull probability distribution. Therefore, the times to failure at each voltage level for samples of each material are plotted using Weibull distribution and the corresponding scale parameter (63.2% time) is used as a representative time to failure at that voltage level for that material. The Weibull plots of LDPE, Silicon rubber and kraft paper breakdown time are shown in Figures 3.4, 3.5 and 3.6 respectively and their corresponding 63.2 % scale parameters are presented in Tables 3.2, 3.3 and 3.4 respectively.

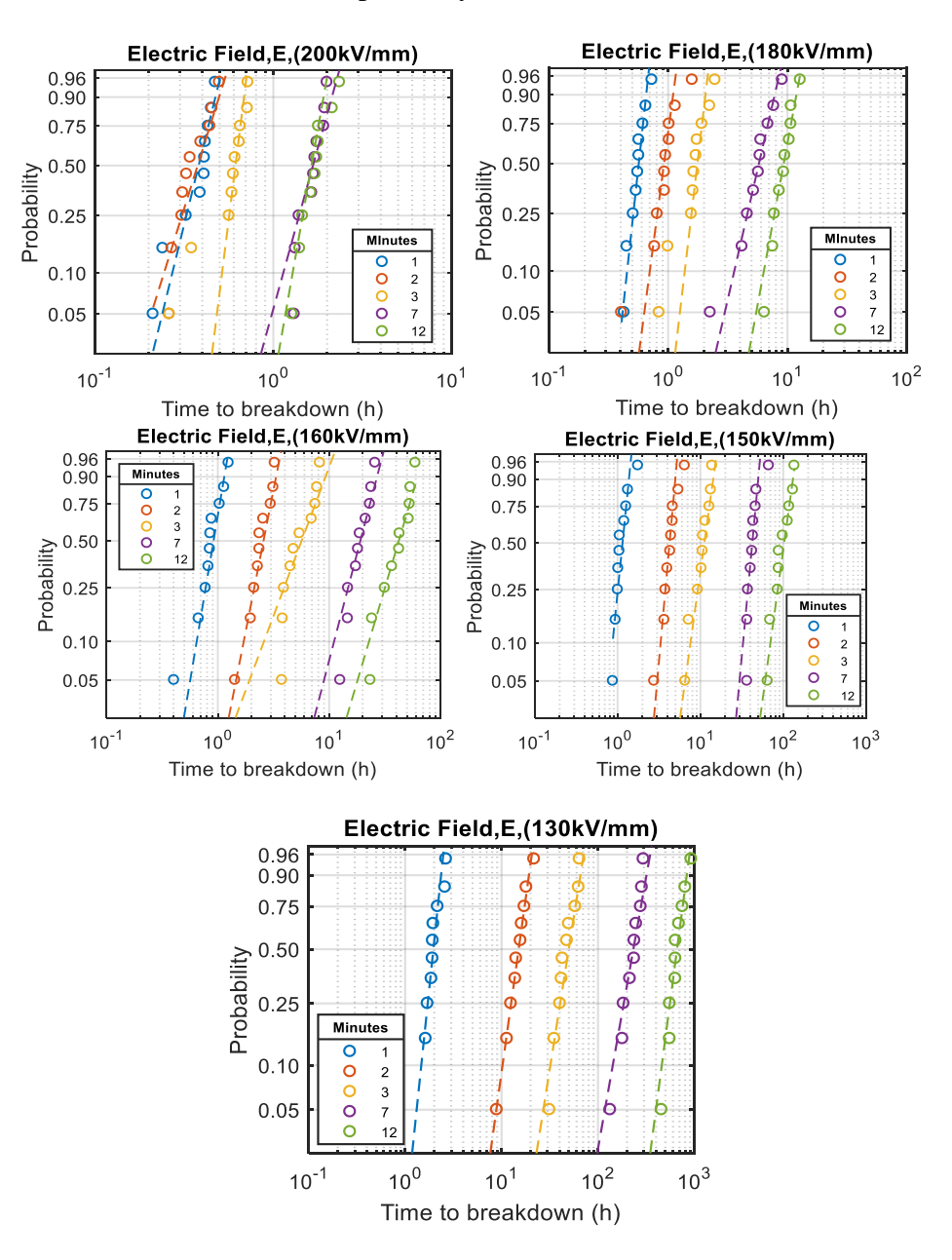


Figure 3.4 Weibull plots of LDPE - Time to breakdown

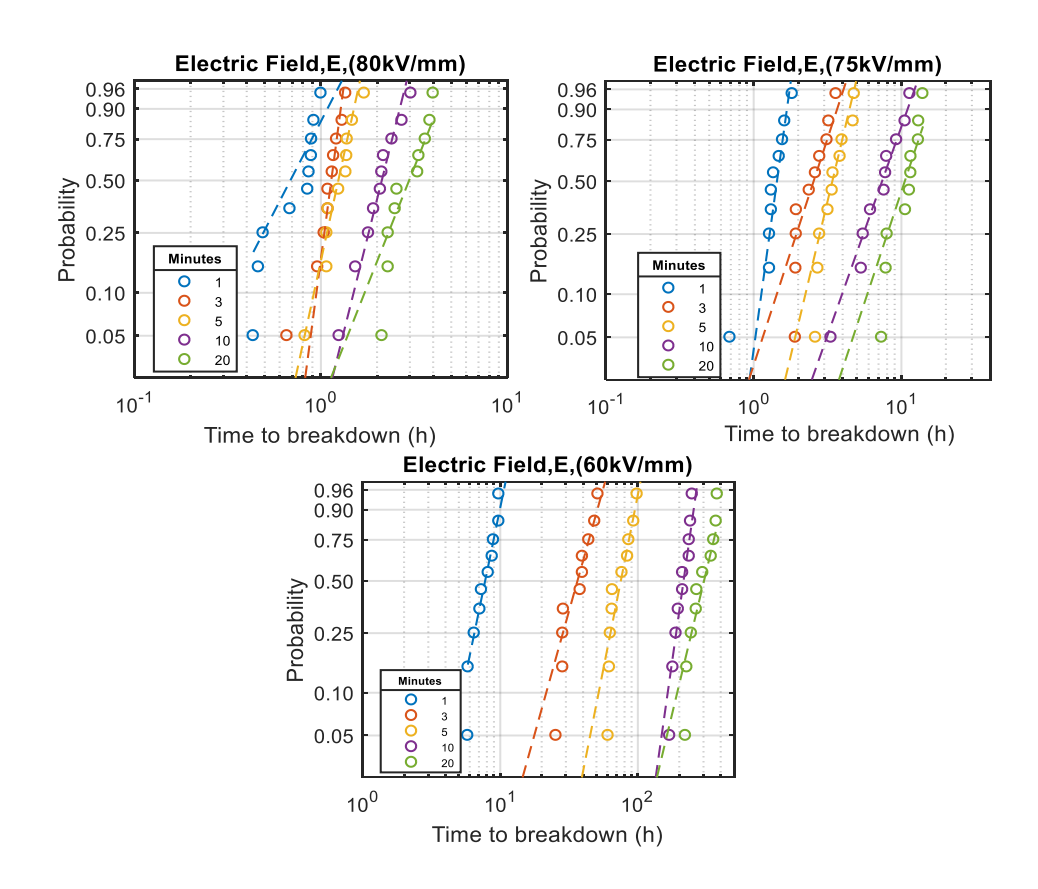
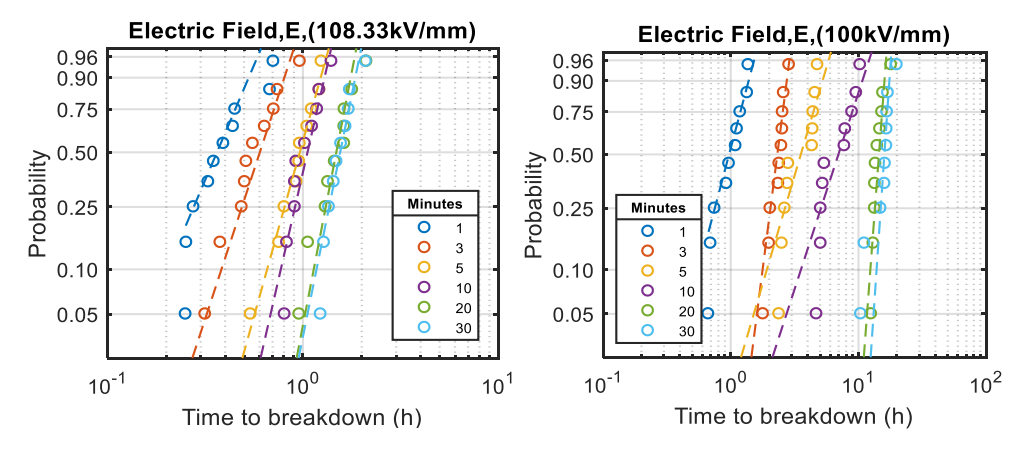


Figure 3.5 Weibull plots of silicone rubber -Time to breakdown



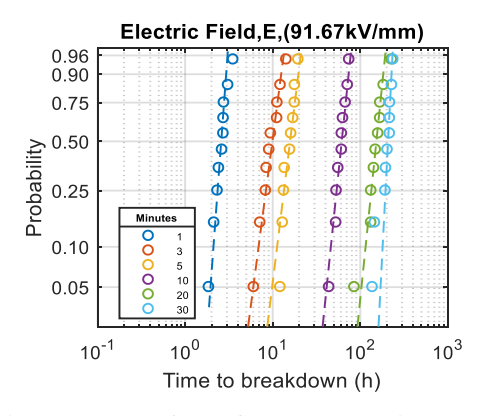


Figure 3.6 Weibull plots of kraft paper – Time to breakdown

Table 3.2 Weibull scale parameters of LDPE

Т	200kV/mm	180kV/mm	160kV/mm	150kV/mm	130kV/mm
(min)	α (h) (95% CI)	α (h) (95% CI)	α (h) (95% CI)	α (h) (95% CI)	α (h) (95% CI)
1	0.41 (0.37 - 0.45)	0.60 (0.55 - 0.66)	0.95 (0.82 - 1.11)	1.26 (1.09 - 1.46)	2.12 (1.84 - 2.43)
2	0.39 (0.34 - 0.45)	1.06 (0.89 - 1.28)	2.66 (2.35 - 3.02)	4.81 (4.19 - 5.52)	16.42 (14.3 - 18.86)
3	0.62 (0.55 - 0.7)	1.85 (1.58 - 2.17)	6.32 (5.3 - 7.53)	11.57 (10.28 - 13.02)	51.99 (45.47 - 59.51)
7	1.77 (1.64 - 1.92)	6.39 (5.32 - 7.67)	20.81 (18.32 - 23.65)	47.82 (41.58 - 55.01)	250.04 (222.83 - 80.64)
12	1.86 (1.66 - 2.09)	10.14 (9.04 - 11.37)	46.39(39.63 - 54.54)	108.93 (94.98 - 24.97)	721.94 (639.26 - 15.53)

Table 3.3 Weibull scale parameters of silicone rubber

Т	80kV/mm	75kV/mm	70kV/mm	60kV/mm
(:)				
(min)	α (h) (95% CI)	α (h) (95% CI)	α (h)(95% CI)	α (h) (95% CI)
1	0.82 (0.72 - 0.95)	1.49 (1.33 - 1.66)	2.4 (2.12 - 2.71)	8.4 (7.58 - 9.33)
3	1.18 (1.08 - 1.28)	2.79 (2.43 - 3.22)	6.11 (5.51 - 6.79)	41.53 (32.87 - 52.51)

5	1.36 (1.22 - 1.52)	3.86 (3.4 - 4.39)	8.99 (8.24 - 9.81)	81.48 (73.11 - 90.83)
10	2.31 (2.01 - 2.66)	8.37 (6.97 - 10.05)	18.99 (17.02 - 21.19)	224.31 (209.4 - 240.3)
20	3.27 (2.87 - 3.72)	11.77 (10.54 - 13.14)	27.29 (23.76 - 31.36)	321.54 (287.72 - 359.33)

Table 3. 4 Weibull scale parameters of kraft paper

Т	108.33kV/mm	100kV/mm	91.66kV/mm
(min)	α (h)(95% CI)	α (h)(95% CI)	α (h)(95% CI)
1	0.46(0.37 - 0.59)	1.11(0.97 - 1.27)	2.81(2.55 - 3.15)
3	0.65(0.53 - 0.78)	2.51(2.33 - 2.69)	10.76(9.30 - 12.44)
5	1.04(0.93 - 1.17)	3.94(3.40 - 4.58)	16.97(15.36 - 18.28)
10	1.11(0.99 - 1.24)	7.77(6.55 - 9.24)	65.32(59.61 - 70.41)
20	1.62(1.43 - 1.85)	15.13(14.03 - 16.34)	172(148.07 - 195.26)
30	1.66(1.50 - 1.85)	16.68(15.05 - 18.27)	213(197.82 - 229.66)

3.3 V - t Characteristics

Knowing the voltage and time to failure, the V-t characteristics are plotted on log-log scale, so that a line fitted to the data represents Equation (3.1). The V-t characteristics of LDPE, Silicone rubber and Kraft paper are plotted respectively in Figures 3.7, 3.8 and 3.9. In these figures, each marker point (or data point) represents a scale parameter of times to the breakdown of a minimum of ten samples. It may be seen that the time to breakdown is lesser for higher frequencies of reversals and follows inverse power law but for the differences in power law coefficients such as slope of line.

This is in agreement with the fact that the polarization-depolarization losses in a dielectric material increases with frequency of the applied voltage. The slope of V-t curves can also

be seen to change with frequency of reversals. The values of power law exponent n and damage D for different values of time intervals were obtained by fitting a straight line to the data points of each time interval, using Equation (3.1).

$$t \times V^n = D \tag{3.1}$$

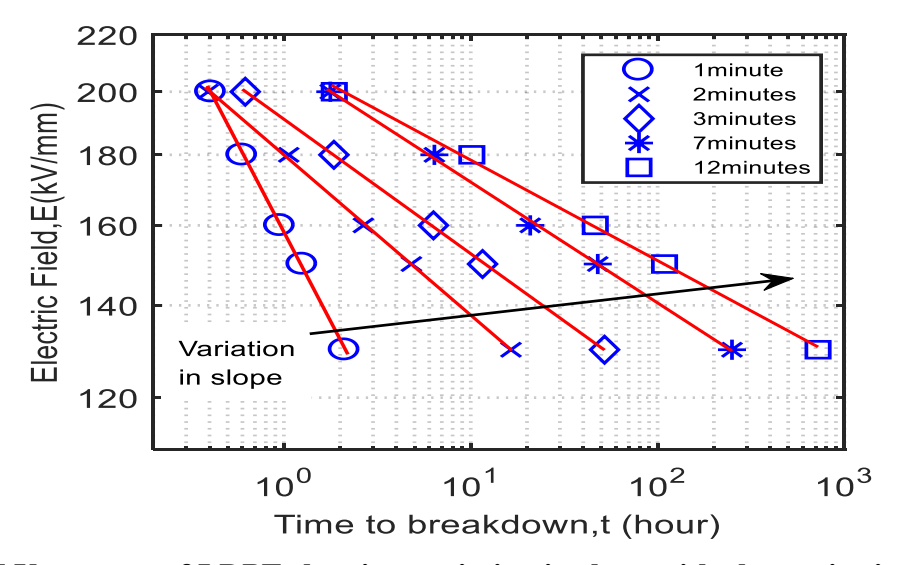


Figure 3.7 V-t curves of LDPE showing variation in slope with change in time interval between reversals.

The plots of power law exponent n and damage D with respect to time interval between reversals is as shown in Figures 3.10 and 3.11 respectively. The power law exponent and damage are found to increase with increase in the time interval between reversals. This behavior shows that the power law parameters change systematically with a change in the frequency of reversals.

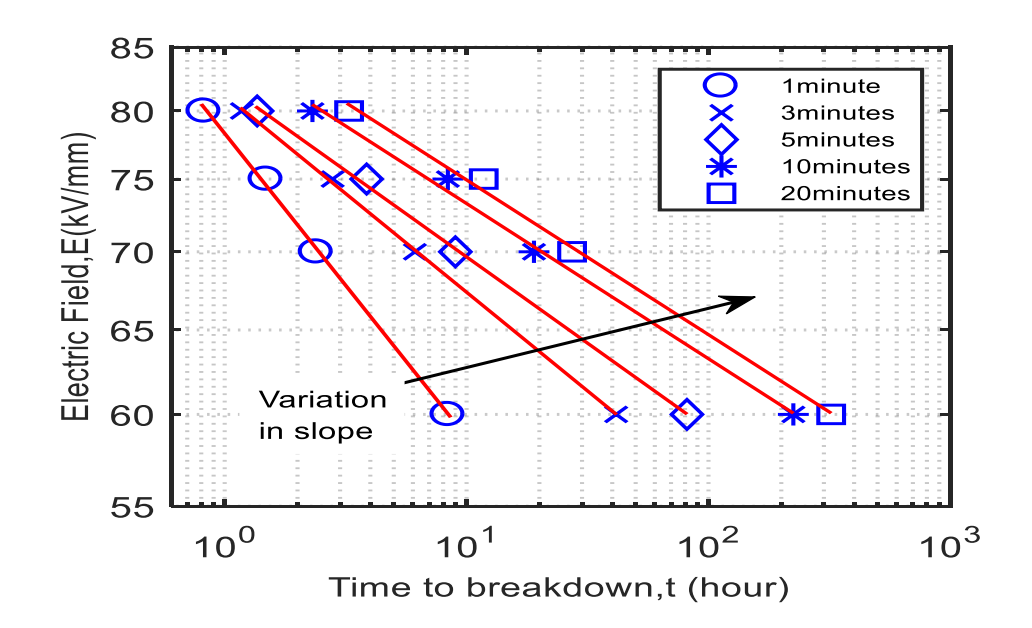


Figure 3.8 V-t curves of silicone rubber samples showing variation in slope with change in the time interval between reversals.

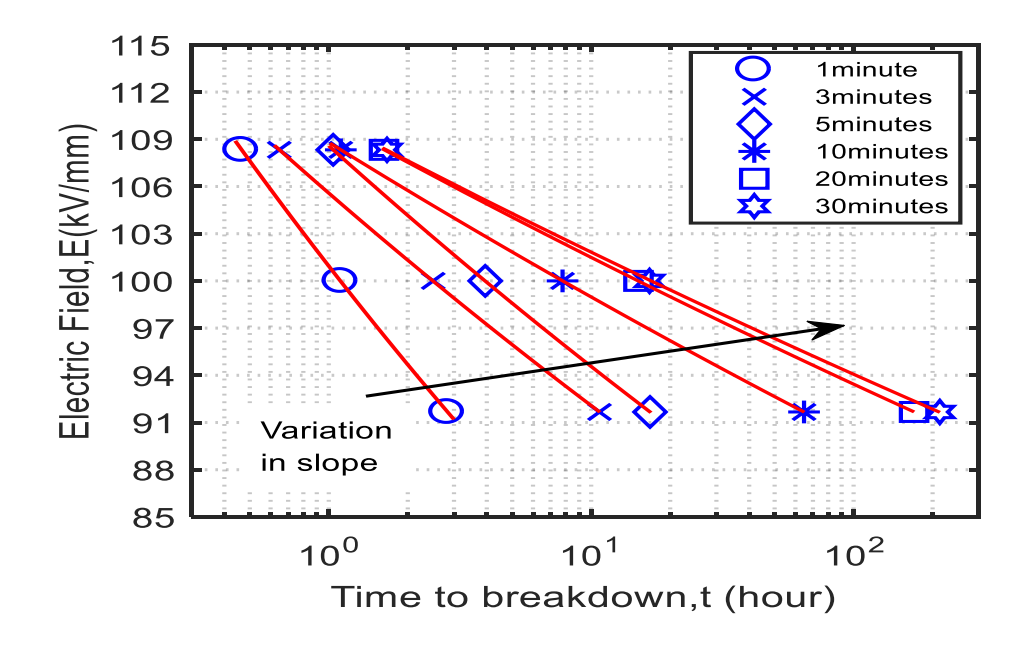


Figure 3.9 V-t curves of Kraft paper samples showing variation in slope with change in time interval between reversals.

With changing T, the ageing rate changes even at a fixed voltage level. The dependence of the quantity D on experimental parameters e.g., time interval between reversals T, strengthens the fact that the performance of the material under stress not only depends on its characteristic behavior but also the experimental or operating conditions. Hence, it becomes

inevitable to describe the power law parameters as a function of frequency to have a better insight into insulation behaviour. This eventually leads to a more vivid description of the dependence of time to breakdown on applied voltage and time interval between reversals, which is in fact the core of the model presented in this thesis.

3.4 Fitted Power Law Components n and D

From Figures 3.10 and 3.11, it can be said that although n and D are increasing but their values tend to saturate for higher values of time intervals.

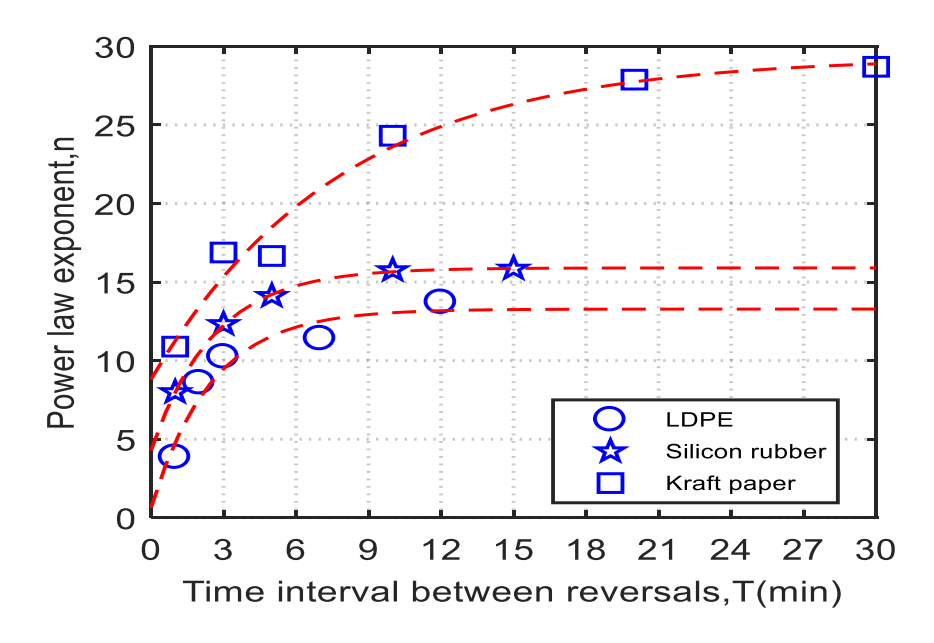


Figure 3.10 Power law exponent or endurance coefficient obtained experimentally at different time interval between reversals.

The limiting value of time interval between reversals i.e. $T \to \infty$ corresponds to the DC nature of applied voltage i.e. with zero frequency. Hence, the value of n can be expected to saturate at n_0 which is the power law exponent at pure dc application of voltage. Therefore,

$$\lim_{T \to \infty} (n) = n_0 \tag{3.2}$$

As per Equation (3.1), the critical damage D is a function of voltage applied V, power law exponent n and time to breakdown t. For pure dc application at a voltage level V, n and t have finite values. Hence the quantity D can also be expected to saturate at D_0 , where D_0 is the value of damage for very large values of T (ideally at pure dc).

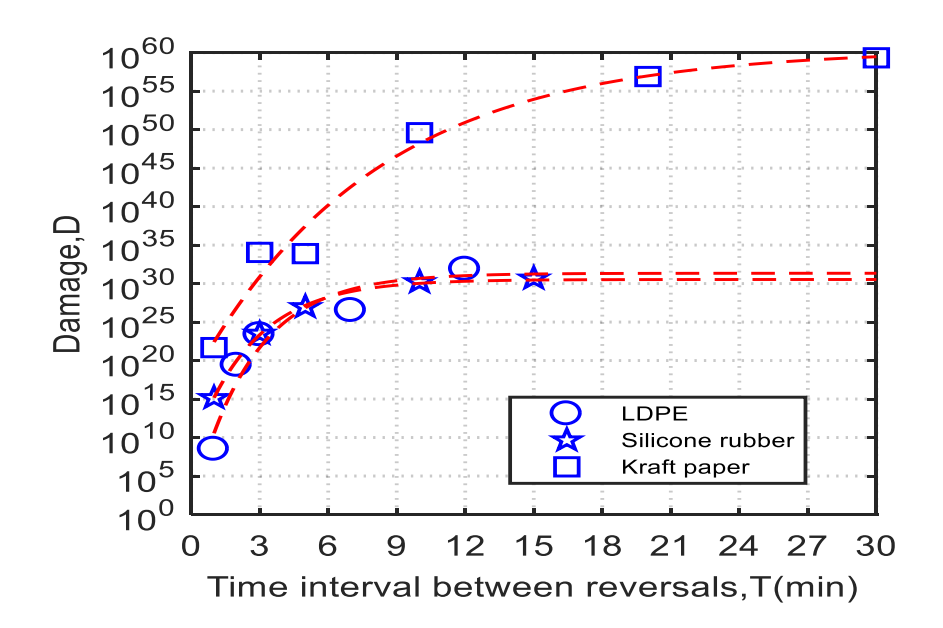


Figure 3.11 Damage or strength constant obtained from inverse power law experimentally at different time interval between reversals.

Therefore,

$$\lim_{T \to \infty} (D) = D_0 \tag{3.3}$$

The other limiting condition, $T \to 0$ is a mathematical singularity corresponding to $f \to \infty$, which is a physically not realizable condition. Therefore, the equations proposed in this chapter are for $0 < T \le \infty$, although, the limiting condition as T tends to zero might have some significance as discussed later.

3.5 Comprehensive Life Model

To quantitatively explain the dependence of n and D on T, based on experimental observations (Figure 3.10 and Figure 3.11), after careful analysis, the following mathematical models are proposed in this chapter, which accounts for the variation in n and D as expressed in Equation (3.4) and Equation (3.5) respectively.

$$n = n_o (1 - se^{-bT}) (3.4)$$

$$ln(D) = ln(D_0)(1 - re^{-cT})$$
 (3.5)

The models predict exponential variations in n and ln(D) with respect to T. Here b, c, s and r are constants for a given material.

From Equation (3.5)

$$D = D_0^{\left(1 - re^{-cT}\right)} \tag{3.6}$$

Therefore, the inverse power law can be modified as given in Equation (3.7).

$$V^{n_0(1-se^{-bT})}t = D_0^{(1-re^{-cT})}$$
(3.7)

From Equation (3.7), it can be observed that

$$t = D_0^{(1 - re^{-cT})} V^{-n_0(1 - se^{-bT})}$$
(3.8)

Equation (3.8) shows that time to breakdown under PRs is dependent on voltage level V and time interval between reversals T in a complicated manner. This could be due to a number of constants required to empirically account for multiple processes viz., partial discharge, space charge formation etc. occurring in the insulation material simultaneously. The effects of these simultaneously occurring processes may not be independent to each other i.e., one process may also affect the other in a way which may be difficult to quantify or express explicitly in a mathematical model, although the parameters do behave in a systematic manner for materials with certain phenomenon as discussed later.

To calculate the limiting value of time to breakdown t_{dc} i.e., for pure dc, we evaluate the limiting case of Equation (3.9) as $T \to \infty$, which yields:

$$t_{dc} = D_0 V^{-n_0} (3.9)$$

As verified from the experiments reported in previous sections, the time to breakdown in the case of PRs is much less as compared to the time to breakdown in the case of pure DC application. This clearly indicates that D_0 , which corresponds to the damage accumulated till breakdown, is attained quickly in case of PRs. Damage accumulation is faster in the case of smaller values of the time interval between reversals i.e., for high frequencies. This explains that dielectric degradation is higher for higher frequencies. To explicitly see the effect of PR, the proposed model in Equation (3.7) is rearranged as shown in Equation (3.10).

$$V^{n_0}t \left[D_0^{(re^{-cT})} V^{n_0(-se^{-bT})} \right] = D_0$$
 (3.10)

Equation (3.10) (or Equation (3.11)) may be considered as a generalized inverse power law

model which is applies to both DC and PRs.

The quantity $V^{n_0}t$ is the damage accumulated if only DC voltage would have been applied during the experiment for time t. Note that t is the time taken till breakdown in case of PR and it must not be confused with t_{dc} which is the time taken till breakdown in case of pure dc application at a given voltage. The multiplicative factor

$$D_0^{(re^{-cT})}V^{n_0(-se^{-bT})} (3.11)$$

represents the effect of PR on DC ageing. Equation (3.11) shows how the DC ageing is accelerated in case of PRs, accumulate the critical damage required to cause failure of the insulation material.

3.6 Fitting Proposed Life Model to Experimental Results

The least squares approach is used to find the parameters for the proposed model by fitting the data obtained from PR breakdown test at different frequencies. The common parameters obtained after simultaneous curve fitting for different voltage levels are summarized in Table 3.5 and the corresponding plots shown in Figure 3.11, 3.12 and 3.13 are seen to be fitting well.

It can be seen from Figures 3.11, 3.12 and 3.13 that the effect of increasing frequency of reversals on time to breakdown is dominant especially at higher values of frequencies (smaller values of time to breakdown). Whereas, the effect of voltage on time to breakdown is dominant at lower values of frequency of reversals (higher values of time to reversal).

Table 3. 5 Parameters obtained by performing experiment on different stress using different values of T

Samples	n_{\circ}	ln(D _o)	b (min ⁻¹)	c (min ⁻¹)	S	r
LDPE	13.43	72.2	0.4	0.383	0.965	0.973
Silicone Rubber	15.76	70.3	0.397	0.380	0.733	0.736
Kraft Paper	29.61	139.2	0.125	0.126	0.706	0.714

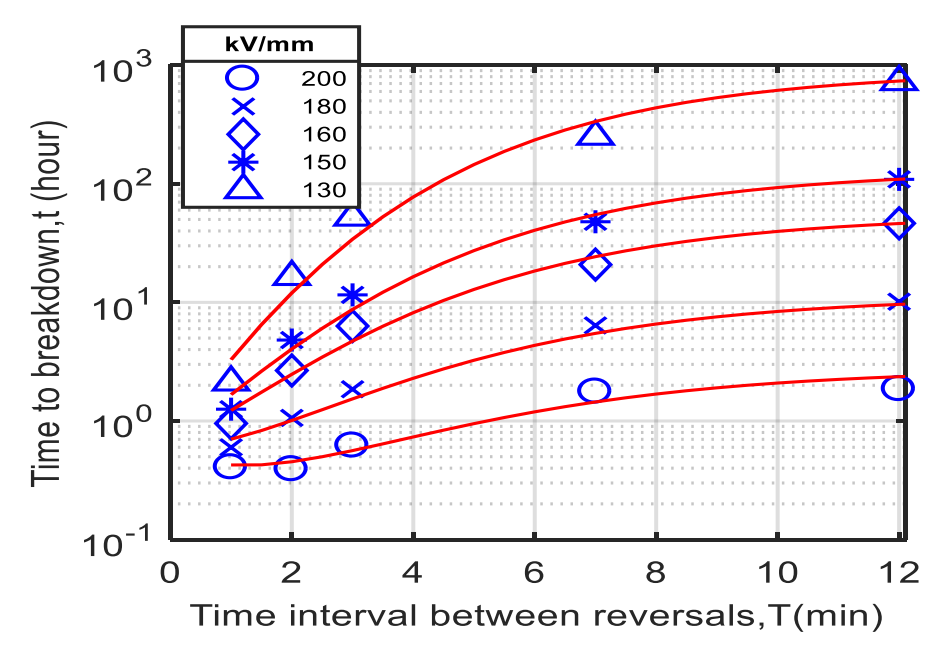


Figure 3.12 Time to breakdown versus Time interval between reversals for different voltages fitted for experimental data of LDPE.

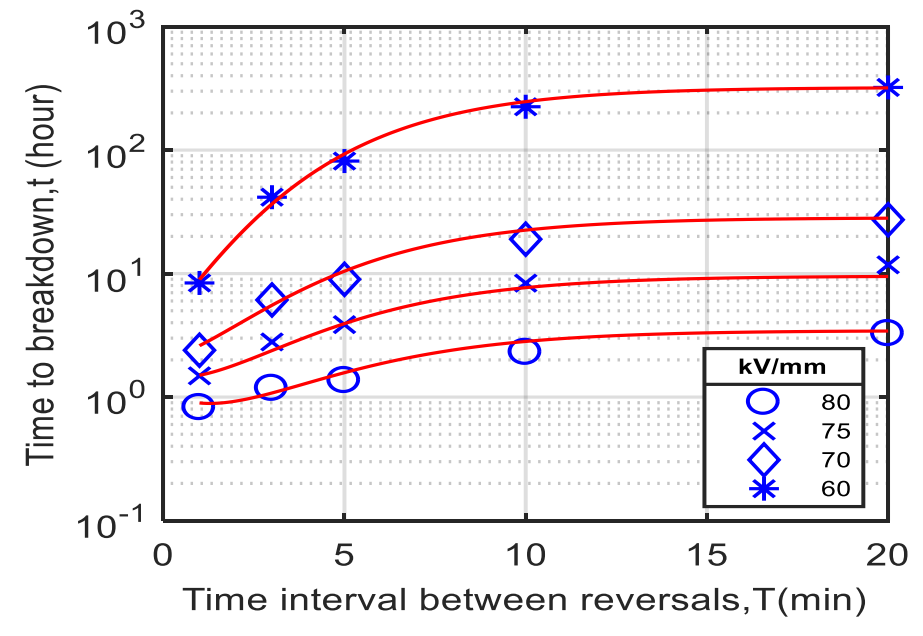


Figure 3.13 Time to breakdown versus Time interval between reversals for different voltages fitted for experimental data of silicone rubber.

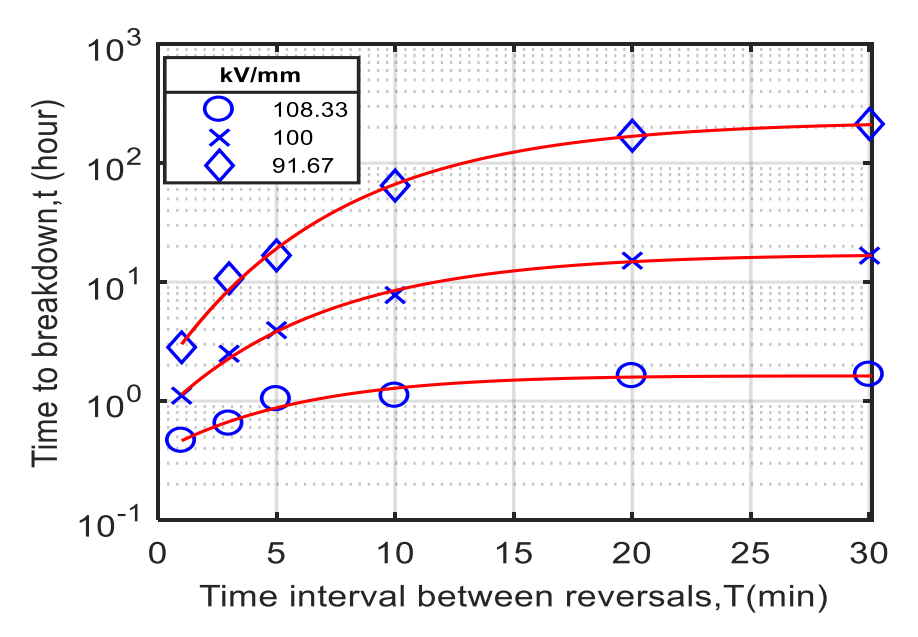


Figure 3.14 Time to breakdown versus Time interval between reversals for different voltages fitted for experimental data of kraft paper.

3.7 Significance of b and c:

The values of *b* and *c* are observed to be very close to each other. However, fitting error is observed to be more if the parameters are taken as same (i.e. It was observed when the b coefficient was fitted with c coefficient values, the goodness of fit percentage for LDPE decreased from 93% to 90%), indicating the presence of two different time constants, perhaps may be related to two distinct phenomena. For samples known for space charge, these values are observed to be relatively higher. Perhaps due to the settling time of the space charge these values become a little bit different from each other. The significance of these values lies in the fact that they indicate the minimum time duration for a reversal to have negligible effect on the equipment. For example, 95% of the logarithmic lifetime can be achieved with a minimum reversal time duration of (five times the time constant),

$$T_{min} \approx \frac{5}{b} \approx \frac{5}{c}$$
 (3.12)

Or, maximum frequency of operation, as,

$$f_{max} \approx \frac{b}{5} \approx \frac{c}{5} \tag{3.13}$$

where T_{min} is the minimum time duration for a reversal, above which the effect of reversal on life is negligible and f_{max} is the maximum frequency of reversals, up to which there will be negligible (maximum 5% on logarithmic life) impact on life. The minimum duration for safe

reversal turns out to be, 12.5 min for LDPE, 12.8 min for SR and 38.75 min for the Kraft paper. However, the effect (on life) of lesser time duration than this minimum is more significant in the case of LDPE.

3.8 Significance of r and s:

The r and s values are observed to be nearly the same and close to unity but slightly less than unity. These minute differences are important to obtain a minimum fitting error (i.e It is observed when the r and s coefficient fitted with one, the goodness of fit percentage of LDPE reduced to 92% from 93%.), again, perhaps for the same reasons as stated above.

Further, if the minor differences in r and s are ignored, mathematically,

$$\lim_{T \to 0} (t) = D_0^{(1-r)} V^{-n_0(1-s)} \approx t_{dc}^{(1-r)} \quad or \quad t_{dc}^{(1-s)}$$
(3.14)

This is the finite time to breakdown at very high frequency PRs. A high value of r and s indicates a very large drop in breakdown/lifetime with the frequency of PRs, which is observed in the case of LDPE that suffers from space charge accumulation. The percentage drop in the logarithmic time to breakdown from its dc life is given by $(100 \ r)$ or $(100 \ s)$. For the case of LDPE, it is 96.5 % to 97.3 %, for SR it is 73.3 % to 73.6 %, and for Kraft paper, it is 70.6 % to 71.4 %. Further, if the differences in b and c as well as r and s are neglected, the life characteristics Equation (3.8) may be approximated as,

$$t = t_{dc}^{(1-re^{-cT})} \approx t_{dc}^{(1-se^{-bT})}$$
(3.15)

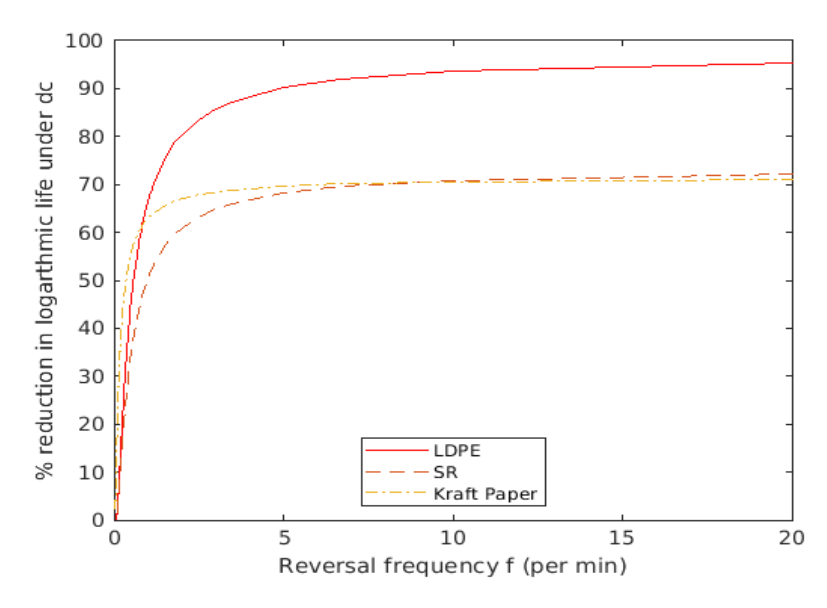


Figure 3.15 Reduction in percentage of logarithmic life with reversal frequency with respect to life under DC

Therefore, the general characteristics of percentage reduction of logarithmic life with respect to DC value is given by, $100re^{-cT}$ or $100se^{-bT}$. The characteristics are compared for various materials as shown in the Figure 3.15. The drastic reduction in life of LDPE at high frequencies explains the failure of extruded power cables during PRs. Often a reversal is accompanied by high frequency damped sinusoidal oscillations superimposed on the reversal waveform. Therefore, a drastic reduction in life at high frequencies is detrimental.

3.9 Validation of the Life Model

The life model parameters obtained using *PR breakdown* test are matching closely with the limiting case of DC under room temperature conditions [8] as given in Table 3.6.

Table 3. 6 Comparison of power law exponent (N) and damage (D) for $T \rightarrow \infty$ in proposed model with n and D obtained under DC conditions in [8].

n ₀	n [8]	$ln(D_0)$	ln(D) [8]
13.43	13.67	72.2	68.7

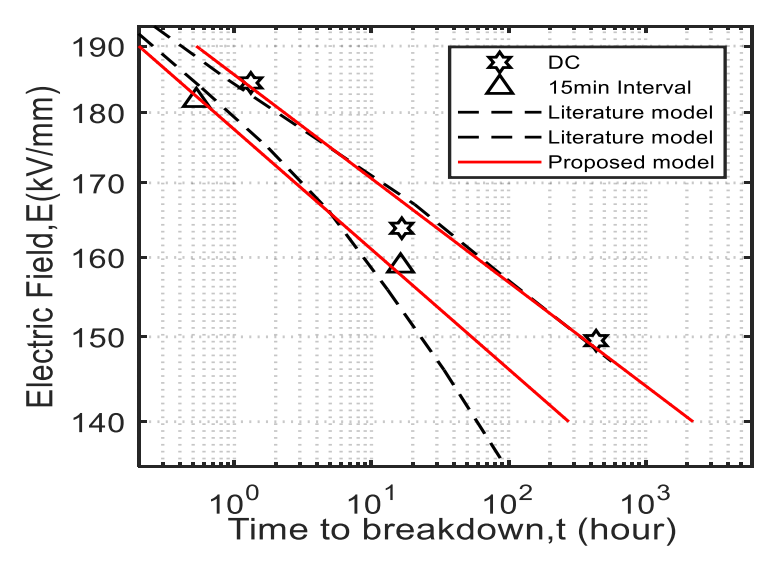


Figure 3.16 The experimental data from [7] fitted with proposed life model

Validation is also done using the experimental data available in the literature. The experimental data with minimum two data sets for each time interval in [7] are compared by fitting with proposed life model shown in Figure 3.16. It can be seen that the proposed model fits closely compared to the model available in the literature. The estimated parameters are shown in Table 3.7, while Table 3.8 shows the DC and 15-min endurance coefficient estimated using the model. From the results, it may be observed that the model works well and fits well to the experimental data and useful information can be obtained from the model parameters.

Table 3.7 Proposed life model parameters estimated for [7] experimental data

Sample	n	ln(D _o)	b	С	c	r
	n _°	III(D _o)	(min ⁻¹)	(min ⁻¹)	S	1
Film [7]	27.33	142	0.1245	0.1235	0.871	0.905

Table 3.8 Power law exponent calculated for specified time interval for the experimental data given in [7]

	n_{\circ}		
Sample	dc	15-minute Interval	
Film [7]	27.33	23.65	

Measurement Issues with Conduction Current Setup

In this chapter, the internal circuit of the electrometer is discussed in detail. The possibilities of inadvertently ignored instrumental errors in literature are subjected to investigation. The analytical solution combining the dielectric model and the internal circuit is obtained to study the impact of internal circuit parameters in the measurements. The experimental current characteristics are reconstructed with a new dielectric circuit model. The model is validated by reconstructing the current characteristics and the actual current characteristics are identified. The reason behind the anomalies is identified and explained with the backing of the proposed dielectric model.

4.1 Schematics of Current Measurement with Commercial Electrometer

In the measurement system, the commercial electrometer is used to measure the LDPE volumetric current with a three-electrode setup as shown in Figure 4.1.

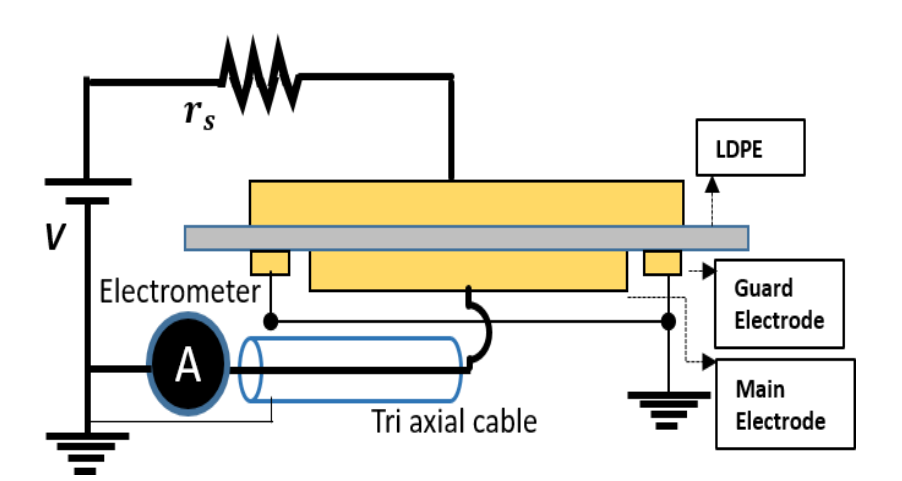


Figure 4.1 Schematic of current measurement

4.2 Commercial Electrometer Current

The current characteristics measured using a commercial electrometer in our lab are shown in Figure 4.2. The currents are measured under 1kV ,2kV and 3kV respectively at 50°C. The transient current characteristics as reported in literature [11] is observed. These anomalies illustrated are also a motivation behind the following investigation.

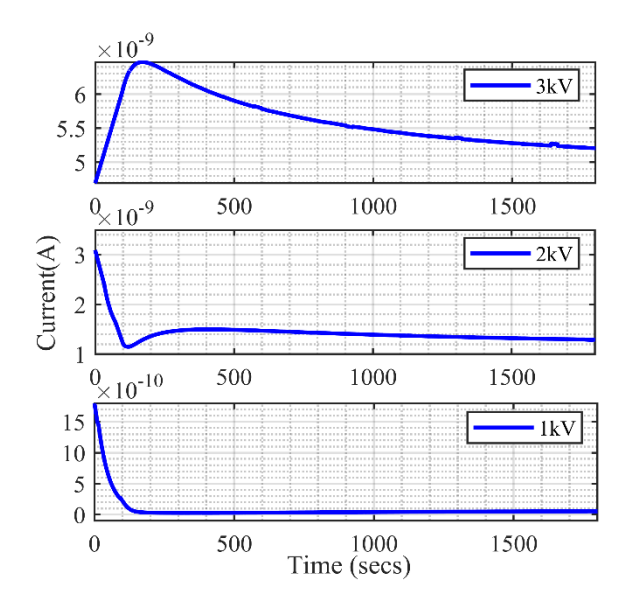


Figure 4.2 Conduction current measurement at 50°C

4.3 Conduction Current Measurement with Replicated Electrometer Internal Circuit

The commercial electrometer internal circuit was inaccessible to user. Hence, an analytical and simulation study performed to replicate the electrometer internal circuit, which is elaborated in the section below.

4.3.1. Electrometer Internal Circuit

Figure 4.3 illustrates the shunt and feedback types configuration of the actual internal circuit of conventional electrometer, which is described in Keithley's Low Level Measurement Handbook [23]. The feedback type configuration is used for pA range current measurement and for higher than pA range shunt type configuration used. Here, r_m is the measuring resistance, and c_m is total capacitance parallel to r_m . The current I_{IN} from the dielectric under test (DUT) is very low, so it is amplified with an op-amp.

$$I_{IN} = \frac{v_o}{r_m \left(1 + \frac{R_A}{R_B}\right)} \tag{4.1}$$

$$I_{IN} = \frac{v_m}{r_m} \tag{4.2}$$

The current I_{IN} converted from v_o is given in Equation (4.1). The r_m is designed with multi range of $1M\Omega$ to $10G\Omega$ to measure all range of currents and the c_m values was not disclosed in manual.

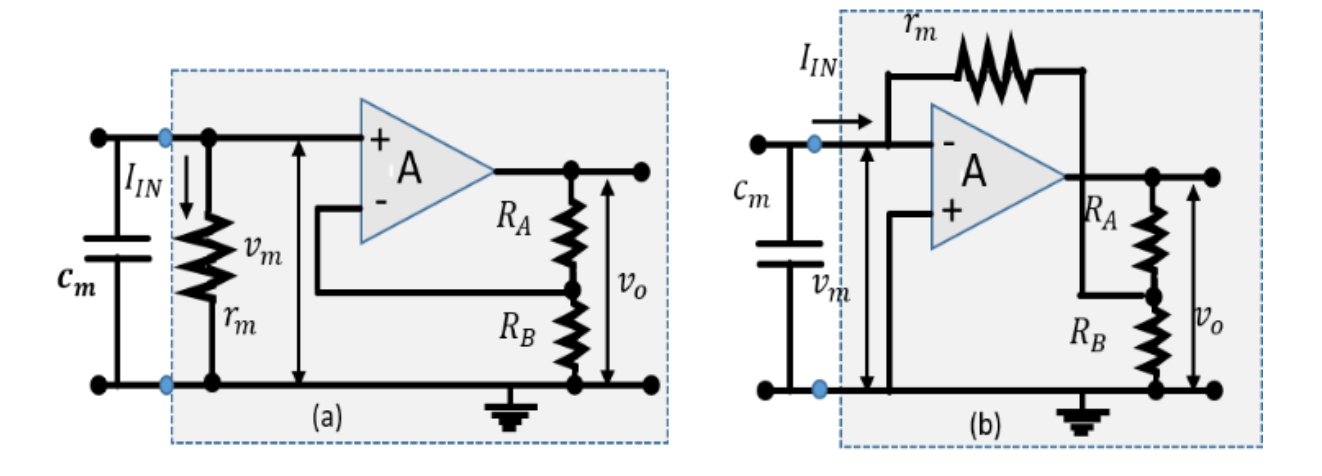


Figure 4.3 Circuit configuration (a) Shunt (b) Feedback [23] types

But in [24], the c_m of $10\mu F$ is used and referred as an oscillatory circuit component, as shown in Figure 4.4, and it is also mentioned that c_m has no significant effect under steady-state conditions

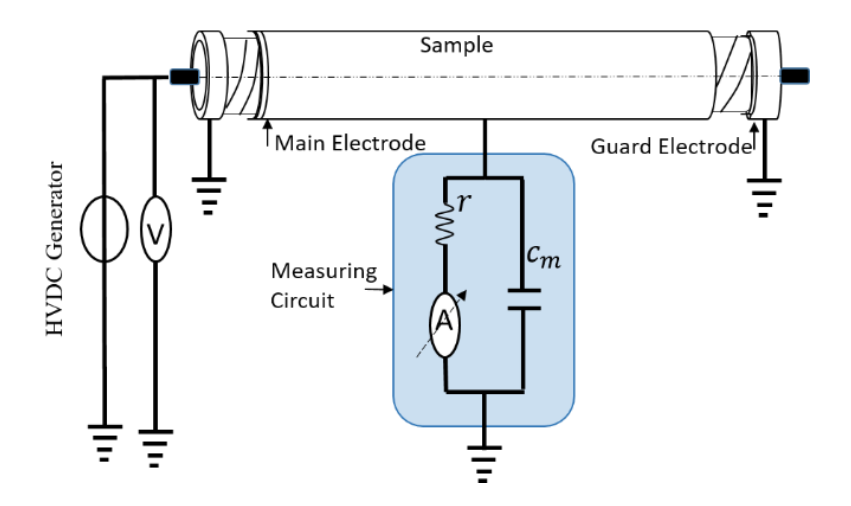


Figure 4.4 Cable conduction current measurement with measuring setup [24].

4.3.2. Significance of r_m and c_m

The internal circuit adds a parallel combination of r_m and c_m in series with the insulating material. With the simplified dielectric model, the complete measurement setup equivalent circuit is shown in Figure 4.5. The linear dielectric model restricted alone with the R and C combination to simplify the analysis.

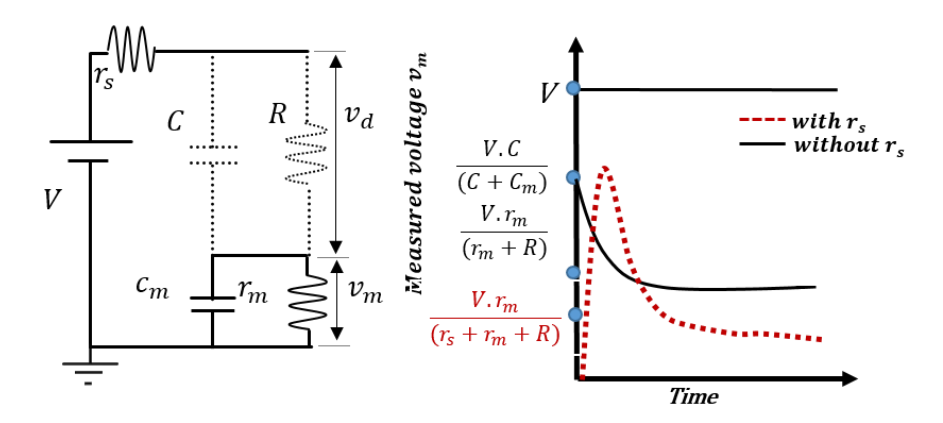


Figure 4.5 Measurement setup simplified circuit

As the electrometer measures and converts the current as in Equations (4.1) and (4.2), the analytical solution is solved in terms of voltage across the measuring circuit v_m . By applying the voltage division rule, the voltage v_m across the measuring device, which is amplified into v_o to compute the current, is determined for an applied voltage V, simplified without r_s .

$$v_{m} = \frac{V\left(r_{m} + \frac{(RC - r_{m}c_{m})e^{-\frac{(R + r_{m})t}{Rr_{m}(C + c_{m})}}}{(C + c_{m})}\right)}{(R + r_{m})}$$
(4.3)

To select appropriate values and to find the effect of r_m and c_m on the measurement results, the equation (4.3) is solved for two extremes, viz. initial and steady state time conditions,

Thus at $t \to 0^+$,

$$v_m = \frac{V\left(r_m + \frac{(RC - r_m c_m)e^0}{(C + c_m)}\right)}{(R + r_m)} = \frac{VC}{(C + c_m)}$$
(4.4)

at $t \to \infty$,

$$v_m = \frac{Vr_m}{(R+r_m)} \tag{4.5}$$

Here, equation (4.4) and (4.5) represent the initial and steady state values of v_m . From the equations (4.4) and (4.5) it was also understood that $r_m \ll R$ and $c_m \gg C$ should be maintained to keep the measuring voltage as minimum as possible. Additionally, the analytical calculation for Figure 4.5 is performed without c_m to explore the importance of the same.

Thus, in the absence of c_m at $t \to 0^+$, v_m is equal to the applied voltage as in equation (4.7).

$$v_m = \frac{V\left(r_m + Re^{-\frac{(R+r_m)t}{CRr_m}}\right)}{(R+r_m)} \tag{4.6}$$

$$v_m = \frac{V(r_m + Re^0)}{(R + r_m)} = V ; t \to 0^+$$
 (4.7)

Hence, it is uncertain whether c_m indirectly protects r_m from high voltage stress. With all the understanding from analytical calculation and literature [24], a range of values of r_m and r_m selected for the hardware setup and is used in the measurement.

4.3.3. Current measured with replicated electrometer internal circuit

The replicated electrometer circuit with shunt configuration is incorporated in the measurement setup is shown in Figure 4.6. The complete measurement setup consists of DC source (Make-Matsusada), function generator (Keysight 33210A), oscilloscope (Keysight 2024A) and the replicated electrometer internal circuit. The replicated/developed electrometer internal circuit hardware is shown in Figure 4.7, and is designed with an operational amplifier (TL084CN) of gain 58.

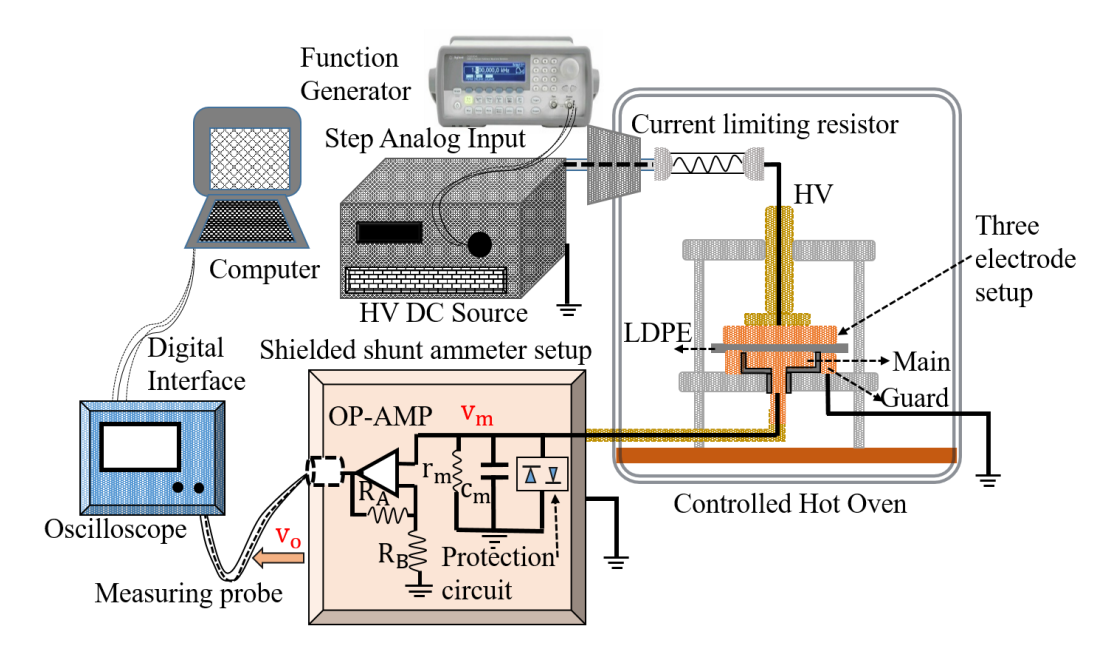


Figure 4.6 Complete measuring setup with a replicated electrometer internal circuit

The LDPE film and electrode setup were kept inside hot air oven and the current is measured at 40°C. The low magnitude current is amplified and measured in terms of voltage v_o using the oscilloscope. The measured voltage v_o from the oscilloscope is recorded w.r.t

time using MATLAB data logging.

$$v_o = v_m \left(1 + \frac{R_A}{R_B} \right) \tag{4.8}$$

$$I_{IN} = \frac{v_o}{r_m \left(1 + \frac{R_A}{R_B}\right)} = \frac{v_m}{r_m} \tag{4.9}$$

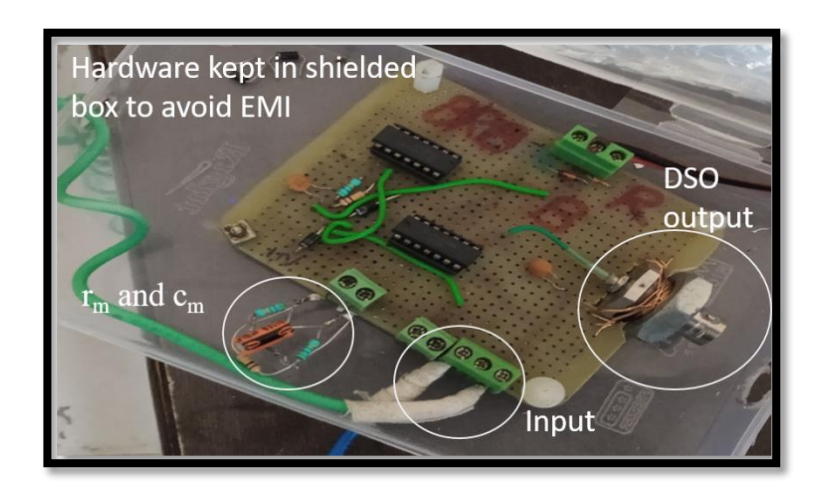


Figure 4.7 Electrometer internal circuit

4.3.4. Measured current

The corresponding current I_{IN} converted from voltage v_o using equation (4.9) for an applied voltage of 1, 2 and 3kV are shown in Figures 4.8 (a) and (b). Initially the setup is explored with r_m fixed to 11.2M Ω and the c_m varied for 1 and 10 μ f. It was recognized for the similar applied voltage V the current dynamics were different.

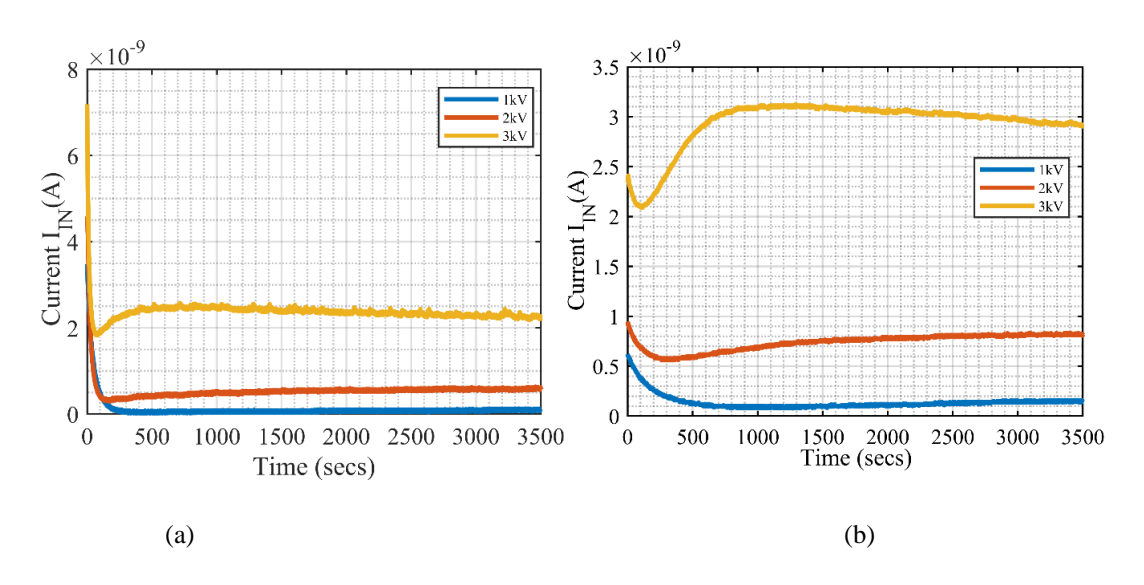


Figure 4.8 Current I_{IN} of C_m (a) $1\mu f$ (b) $10\mu f$

Preliminary investigation shows that the change in the ammeter passive component value

alters the current characteristics. Hence, using the PSICE simulation, the experimental current characteristics is subjected to further analysis.

4.4 Circuit Simulation

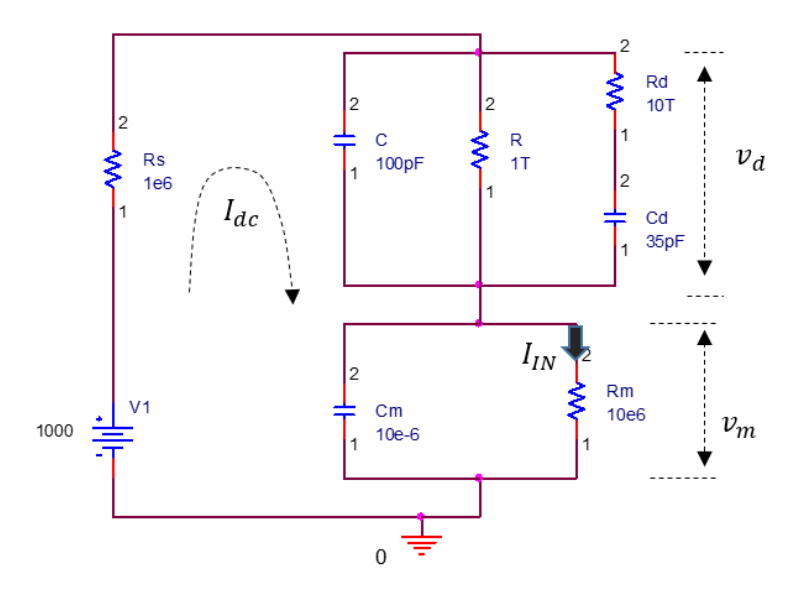


Figure 4.9 Simplified circuit representation of measurement setup

The linear dielectric model circuit used as an equivalent to LDPE in simulation. The equivalent circuit of complete measurement setup embedded with material and electrometer internal circuit as shown in Figure 4.9. Here the R is insulation resistance, C is instantaneous polarized capacitor and R_d and C_d are absorption capacitance and resistance of LDPE material. In simulation the absorption branch considered as it has no significant effect on initial and steady state conditions. The r_m and c_m correspond to electrometer's internal circuit. The amplifying circuit shown in Figure 4.3 is omitted to simplify the analysis.

Table 4. 1 Circuit parameter values used

	R	1ΤΩ,2ΤΩ		$r_{ m m}$	10MΩ
Material	С	100pF	Internal Circuit	-111	
Parameters	C_d	35pF	Parameters C _m	10μF	
	R _d	10ΤΩ		- III	•

The insulation resistance (R) and the instantaneous polarized capacitance (C) of the LDPE sample were determined using experimental results and sample dimensions. The capacitance C calculated using the formula $C = \varepsilon^A/_d$, where ε is the relative permittivity, A is the area of the sample and d is the thickness of the sample. The resistance of material are calculated using the formula $R = E d/_I$, were E is the electric field, d is the thickness of the sample and I is the conduction current flow through the material. Experimental measurements of leakage current and spectroscopy were used as references to determine these parameters accurately. The calculated circuit parameters values used in the simulation were given in Table 4.1. Correspondingly the values of R_d and C_d were configured with the support of literatures [27]. The r_m and c_m values were chosen based on conditions derived in equations (4.4) and (4.5). Here the simulation is performed for two different insulation resistances, $R = 1T\Omega \& 2T\Omega$, without changing the remaining circuit parameters. The two different conditions represent change in insulation resistance at two different temperatures. The simulated current I_{IN} is shown in Figure 4.10. This is equivalent to the current calculated in electrometer from v_m using equation (4.1).

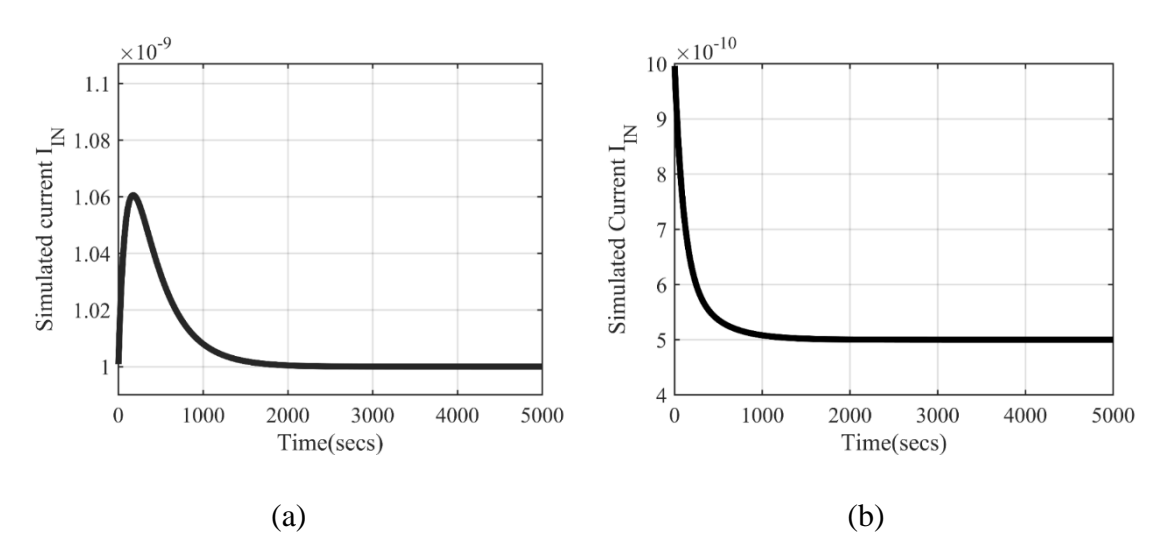


Figure 4.10 The current characteristics of I_{IN} (a) $R = 1T\Omega$ (b) $R = 2T\Omega$

Here the I_{IN} characteristics shown in Figure 4.10 (a) and (b) are different. A kink is observed around 200 seconds for R of $1T\Omega$ whereas in $2T\Omega$, the current is exponentially decayed. The overall current I_{dc} drawn by the circuit from the DC source is shown in Figures 4.11(a) and(b). Here in both cases, kink did not appear, the current decayed exponentially and settled at a steady state value.

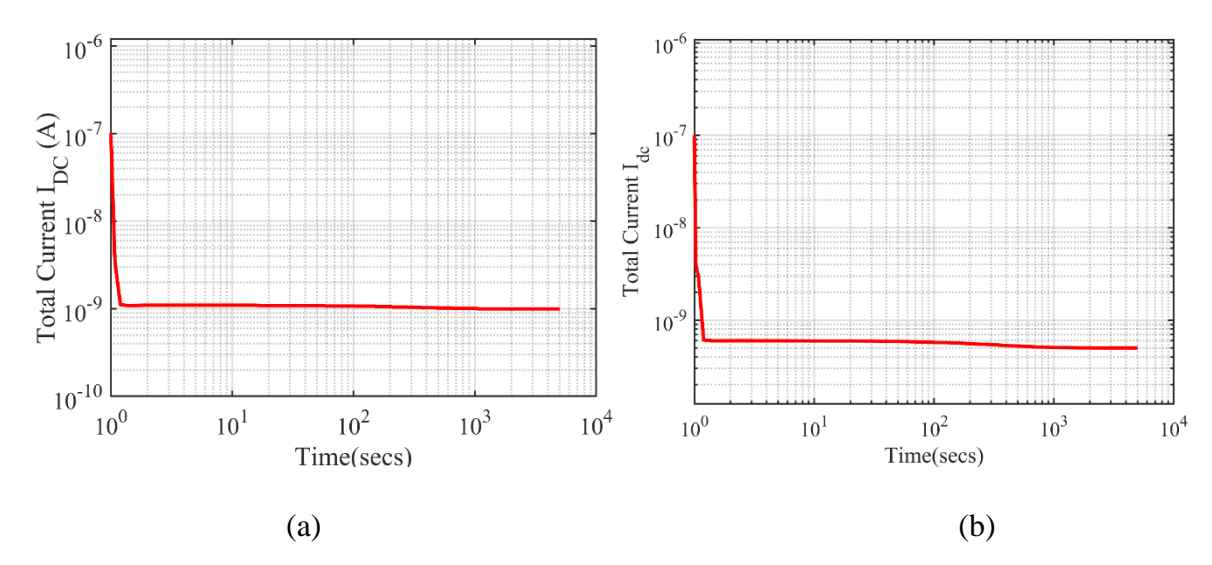


Figure 4.11 The current characteristics of I_{DC} (a) $R=1T\Omega$ (b) $R=2T\Omega$

This variation in current characteristics between I_{dc} and I_{IN} were explored in relation to voltage characteristics. Because internally in the electrometer, the current is calculated from voltage (refer equation (4.1)). The v_m voltage characteristics is shown in Figure 4.12. The v_m trend w.r.t to time looks similar to I_{IN} .

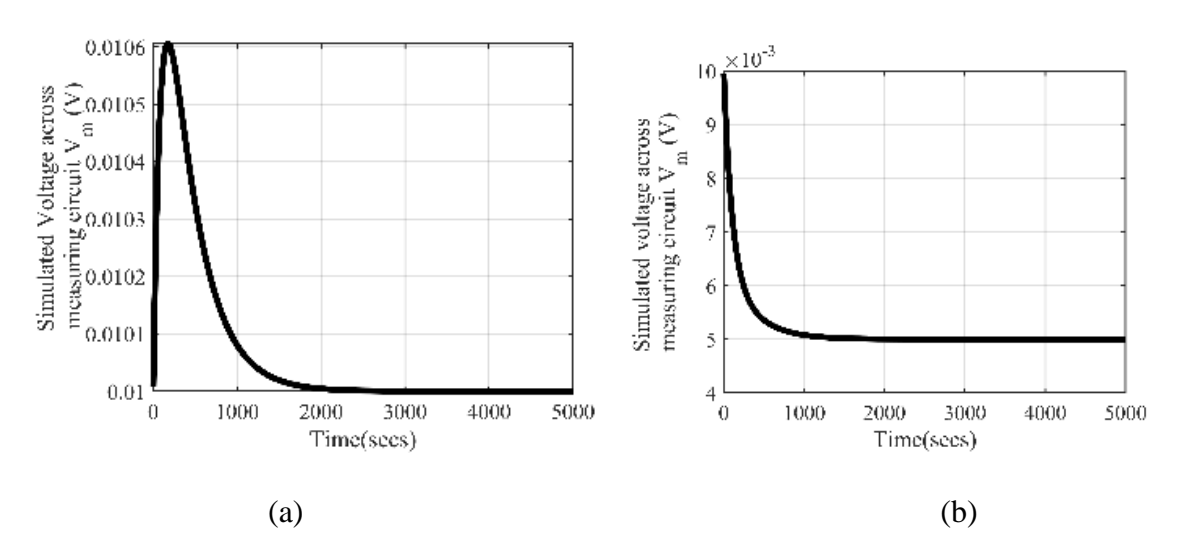


Figure 4.12 The v_m characteristics of 1kV applied voltage (a) $R=1T\Omega$ (b) $R=2T\Omega$ Similarly the corresponding voltage across the sample v_d is also plotted from the

simulation results as shown in Figures 4.13 (a) and (b).

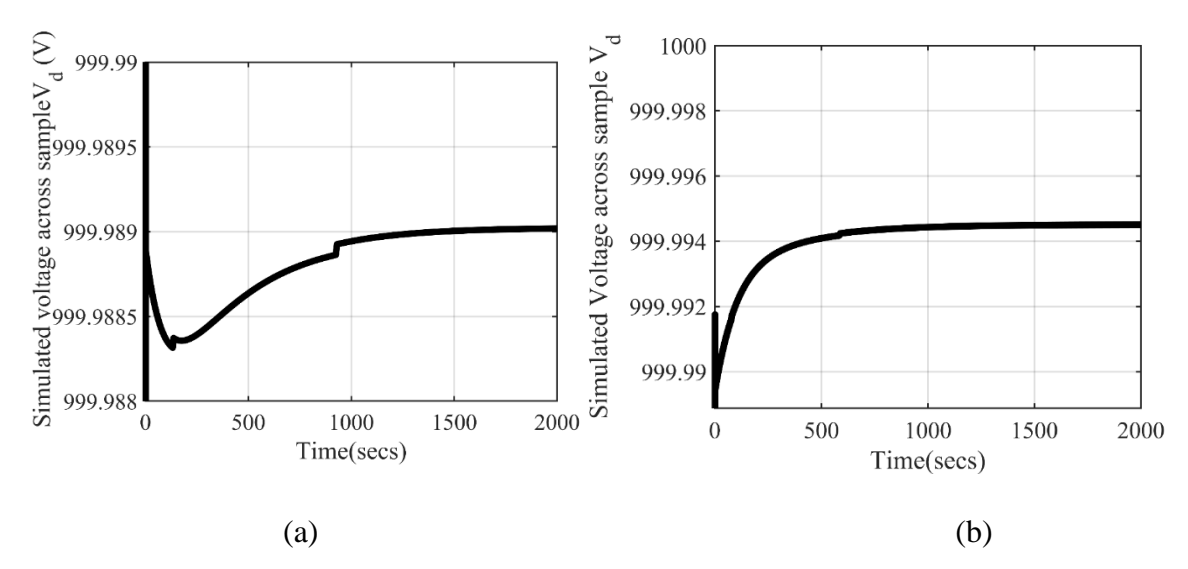


Figure 4.13 Voltage across the sample V_d (a) $R = 1T\Omega$ (b) $R = 2T\Omega$

The v_d in Figure 4.13 (a) shows inverse to trend of v_m in Figure 4.11(a). The same inverse trend for Figure 4.13 (b) and Figure 4.11(b) is observed. Generally, the voltage across sample is anticipated to be constant throughout the measurement. But in Figure 4.13 the voltage across the sample was not constant and it is inverse to the measuring circuit voltage. Hence, it is anticipated from the simulation results, the actual insulation current characteristics I_{dc} is misinterpreted as I_{IN} , as it is representing the voltage characteristics. However, the linear dielectric model used in simulation failed to create the exact experimental current characteristics as in Figure 4.8. Specifically, the current characteristics observed in Figure 4.14 type (a) are not recreated by linear dielectric model.

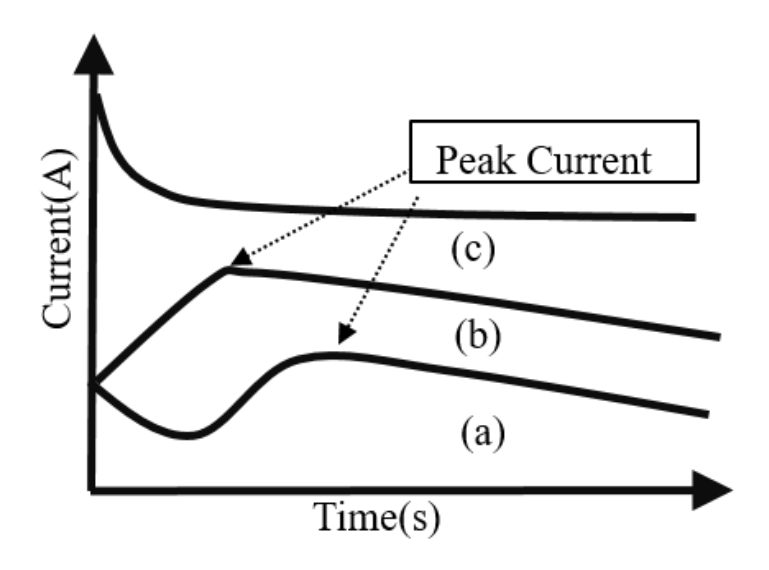


Figure 4.14 The transient current characteristics

As the simulation with linear dielectric model failed to create exact current dynamics as observed in experimental results, it is believed a sophisticated dielectric model is required to get into more in-depth understanding of the topic.

4.5 Recreating Transient Current with Proposed Dielectric Model

4.5.1. LDPE Model

As already discussed in Chapter 2 the existing dielectric model current monotonically declines with time, it is necessary to modify the circuit to visualize the anomalous current observed in LDPE. Accounting with all the considerations from linear and modified circuit shown in Figure 2.3 (Chapter 2) the equivalent capacitor $\frac{1}{(s^1C)}$ of the dielectric model was modified with β constant as $\frac{1}{(s^\beta C_d)}$. In addition, the complex impedance is also modified as $R_d(sR_ds^\beta C_d)^\alpha$ with positive constant to fit the time varying anomalous current profile in LDPE. These modifications were done to fit the experimental data followed as similar to [22]. The proposed LDPE model is shown in Figure 4.15 in Laplace domain. By substituting $\alpha = 0$ and $\beta = 1$ the LDPE model is simplified to linear dielectric model shown in Figure 2.3.

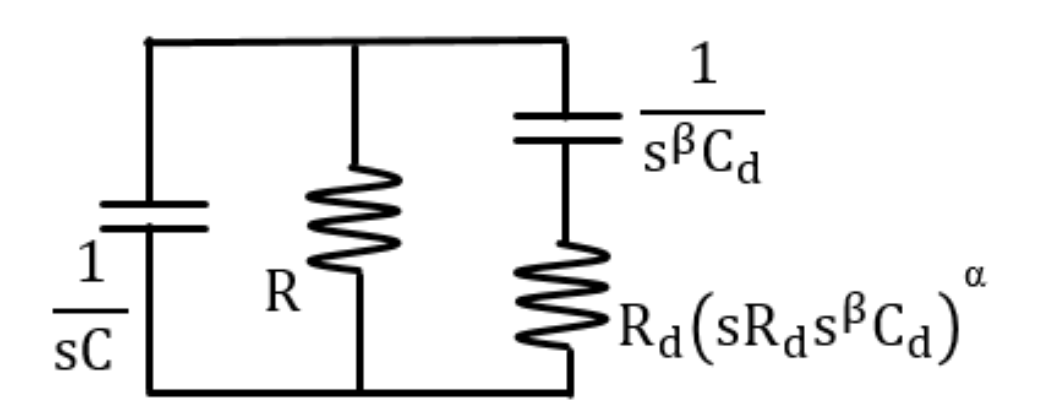


Figure 4.15 Proposed LDPE model

4.5.2. Systematic Current Measurement under Different Electro Thermal Conditions

To validate the dielectric model a systematic current characteristic is required Hence, the further investigation is carried out with replicated electrometer with known internal circuit parameters. The measurement setup is shown in Figure 4.6 with the c_m of $10\mu f$ and r_m of $11.2M\Omega$. The currents measured for different ranges of temperature 30, 40 and 50°C at

applied voltages of 1, 2 and 3kV, and the corresponding trends are shown in Figures 4.16, 4.17 and 4.18 respectively.

The measured voltage v_m is shown in Figure 4.19 and its corresponding converted current I_{IN} at 30,40 and 50°C is shown in Figure 4.16, 4.17 and 4.18. The I_{IN} converted from v_o w.r.t time using the Equation (4.12) and (4.13) with the known amplifier gain (58) and $r_m(11.2\text{M}\Omega)$ value. As the current I_{IN} is converted from voltage v_o , it is obvious that both the waveforms w.r.t time are similar and differ only in terms of magnitude. The procedures are same as followed earlier, the low magnitude current is amplified and measured in terms of voltage v_o using the oscilloscope as in Equation (4.12). The measured voltage v_o from the oscilloscope is recorded w.r.t time using MATLAB.

$$v_o = v_m \left(1 + \frac{R_A}{R_B} \right) \tag{4.12}$$

$$I_{IN} = \frac{v_0}{r_m \left(1 + \frac{R_A}{R_B}\right)} = \frac{v_m}{r_m} \tag{4.13}$$

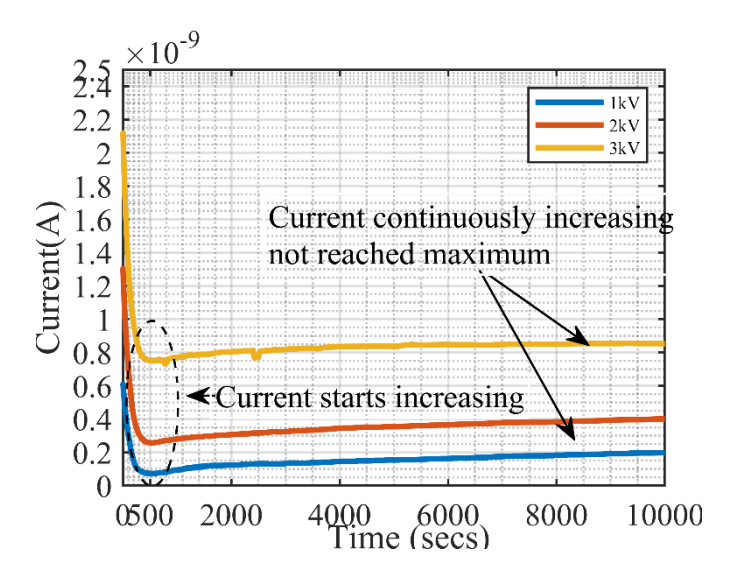


Figure 4.16 Current I_{IN} at different temperatures 30°C

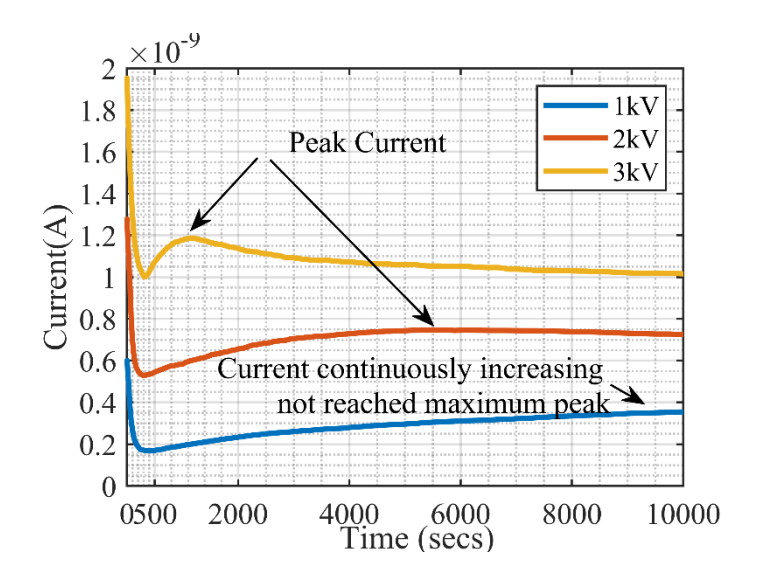


Figure 4.17 Current I_{IN} at different temperatures 40°C

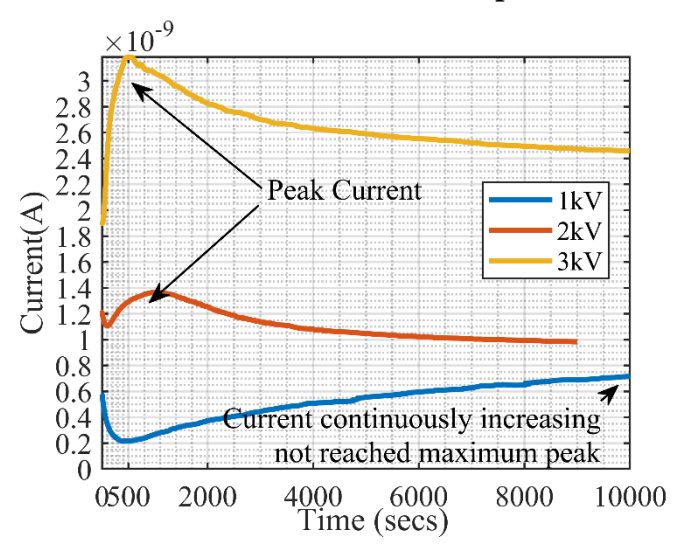


Figure 4.18 Corresponding converted current at temperature 50°C

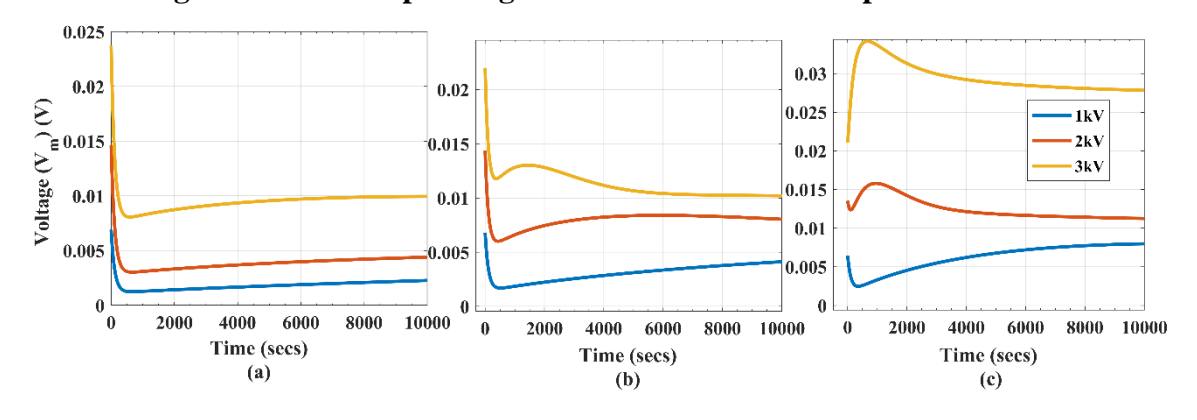


Figure 4.19 The measured voltage v_m at temperatures (a)30°C (b)40°C (c)50°C

The anomalous current profile as in [11] is observed and the peak variation with time highlighted. So, a similar kind of anomalous current profile with change in voltage and

temperature is observed as in [11] using a replicated electrometer internal circuit. Also, the shift in current peak as function of electric field and temperature is observed as in [11,29]. Now the measuring circuit and the corresponding leakage current profile of certain voltage and temperature were known. With measurement results a circuit-based approach is presented including measuring system internal circuit and LDPE model to recreate the obtained anomalous current profiles.

4.5.3. Proposed LDPE Model along with complete measurement setup

Figure 4.20 shows the complete measurement circuit with proposed LDPE model.

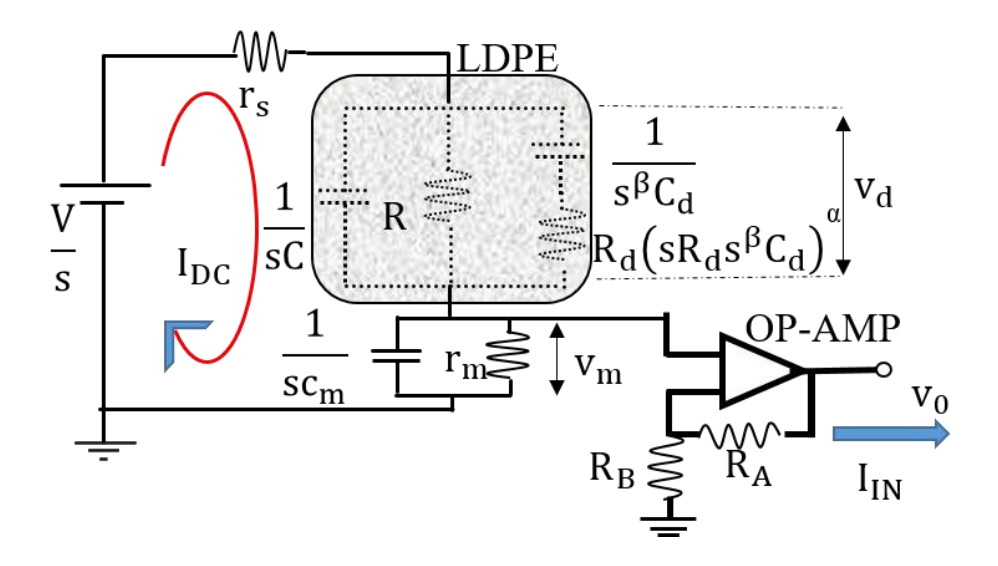


Figure 4.20 Equivalent circuit of complete measurement setup.

The total LDPE complex impedance $Z_d(s)$ and the measuring circuit impedance $Z_m(s)$ were calculated as given in equations (4.14) and (4.16).

$$\frac{1}{Z_d(s)} = \frac{1}{\frac{1}{C*s}} + \frac{1}{R} + \frac{1}{\left(\frac{R_d}{(s*R_d*s\beta*C_d)^{-(\alpha)}} + \frac{1}{(s\beta*C_d)}\right)}$$
(4.14)

$$Z_{d}(s) = \frac{R\left(\frac{R_{d}}{\left(s^{(1+\beta)}*R_{d}C_{d}\right)^{-\alpha}} + \frac{1}{s^{\beta}C_{d}}\right)}{Cs\left(\frac{R}{Cs}\right) + \frac{\frac{R_{d}}{\left(s^{(1+\beta)}R_{d}C_{d}\right)^{-\alpha}} + \frac{1}{\left(s^{\beta}C_{d}\right)}}{(Cs)} + R\left(\frac{R_{d}}{\left(s^{(1+\beta)}R_{d}C_{d}\right)^{-\alpha}} + \frac{1}{\left(s^{\beta}C_{d}\right)}\right)}$$
(4.15)

$$Z_m(s) = \frac{r_m}{\left(c_m s \left(\frac{1}{(c_m s)} + r_m\right)\right)} \tag{4.16}$$

The current I_{Dc} of the complete circuit as shown in Figure 4.20 is calculated as in equation (4.17).

$$I_{Dc}(s) = \frac{V}{s*(Z_d(s) + Z_m(s) + r)}$$
(4.17)

The voltage v_m across Z_m due to current I_{Dc} is given in equation (4.18).

$$v_m(s) = I_{DC}(s)Z_m(s) \tag{4.18}$$

By substituting equation (4.17) in equation (4.18) the v_m is calculated as in Equation (4.19).

$$v_m(s) = \frac{v}{s * (Z_d(s) + Z_m(s) + r)} * Z_m(s)$$
(4.19)

The amplified voltage v_o from v_m is given in Equation (4.20).

$$v_o = \left(1 + \frac{R_A}{R_B}\right) v_m = A v_m \tag{4.20}$$

By substituting (4.19) in (4.20), the measured voltage v_o is identified as Equation (4.21).

$$v_o(s) = A * \frac{v}{s * (Z_d(s) + Z_m(s) + r)} * Z_m(s)$$
(4.21)

The voltage v_o is the actual measured voltage by both conventional and the replicated electrometers circuit. The current I_{IN} is converted from v_o using Equation (4.13). Hence, the fitting of experimental data is done in terms of v_o .

The fitting is done by matching known experimentally measured (v_o-t) voltage time characteristics (i.e., Figure 4.19) of particular applied voltage (i.e., 1, 2 and 3kV) and temperature with the analytically calculated v_o-t characteristics using Equation (4.21). The unknown LDPE parameters R_d , C_d , R, C, α and β are estimated and adjusted accordingly.

Here the R, C values are estimated by considering two instants of measurement: $t=0^+$ and $t\to\infty$. At $t=0^+$ under applied DC voltage V the series combination of C and c_m in the circuit of Figure 4.20 gets instantaneously polarized with initial charging current as shown in Figure 4.21(a). Hence, the voltage v_m at $t=0^+$ is decided according to the capacitance ratio C and c_m as given in equation (4.22) [20].

$$v_m = \frac{vc}{(c+c_m)} \Rightarrow v_0 = A * \frac{vc}{(c+c_m)}$$

$$\tag{4.22}$$

Hence, with already known v_0 at $t = 0^+$ from experimental data, the C can be estimated.

At $t \to \infty$, the v_m of Figure 4.20 settles as in Figure 4.21(b) with the ratio of R and r_m given in equation (4.23). Similarly, R also can be estimated by using known v_o for corresponding applied voltage V.

$$v_m = \frac{Vr_m}{(R+r_m+r_s)} \Rightarrow v_0 = A * \frac{Vr_m}{(R+r_m+r_s)}$$
 (4.23)

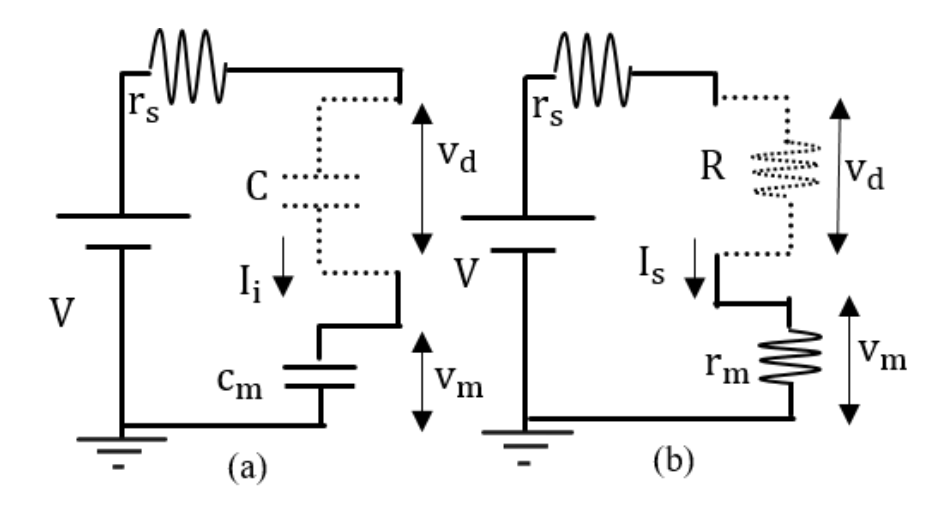


Figure 4.21 Flow of (a)instantaneous polarization current(b) steady state characteristics current

Hence, by implementing equations (4.22) and (4.23), LDPE C and R at voltages 1, 2 and 3kV of temperature 30,40, and 50°C were determined, that both correspond to initial and steady state circumstances. The remaining unknown values of Z_d were taken from literatures. Thus the C_d in between 10% to 50% of C [27], polyethylene α of 0.6 [22] and β in between 0 and 1 [25] were assumed and used to fit the experimental data. Figure 4.22 shows the analytically fitted $v_o - t$ characteristics plots.

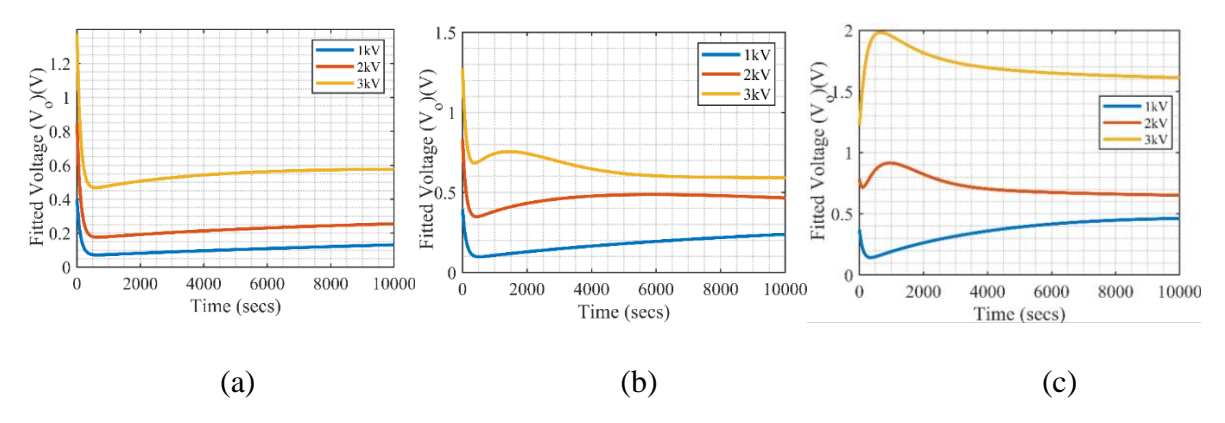


Figure 4.22 Calculated voltage v_o with the model at temperatures (a)30°C (b)40°C (c)50°C .

The estimated values for LDPE model are given in Table.4.2.

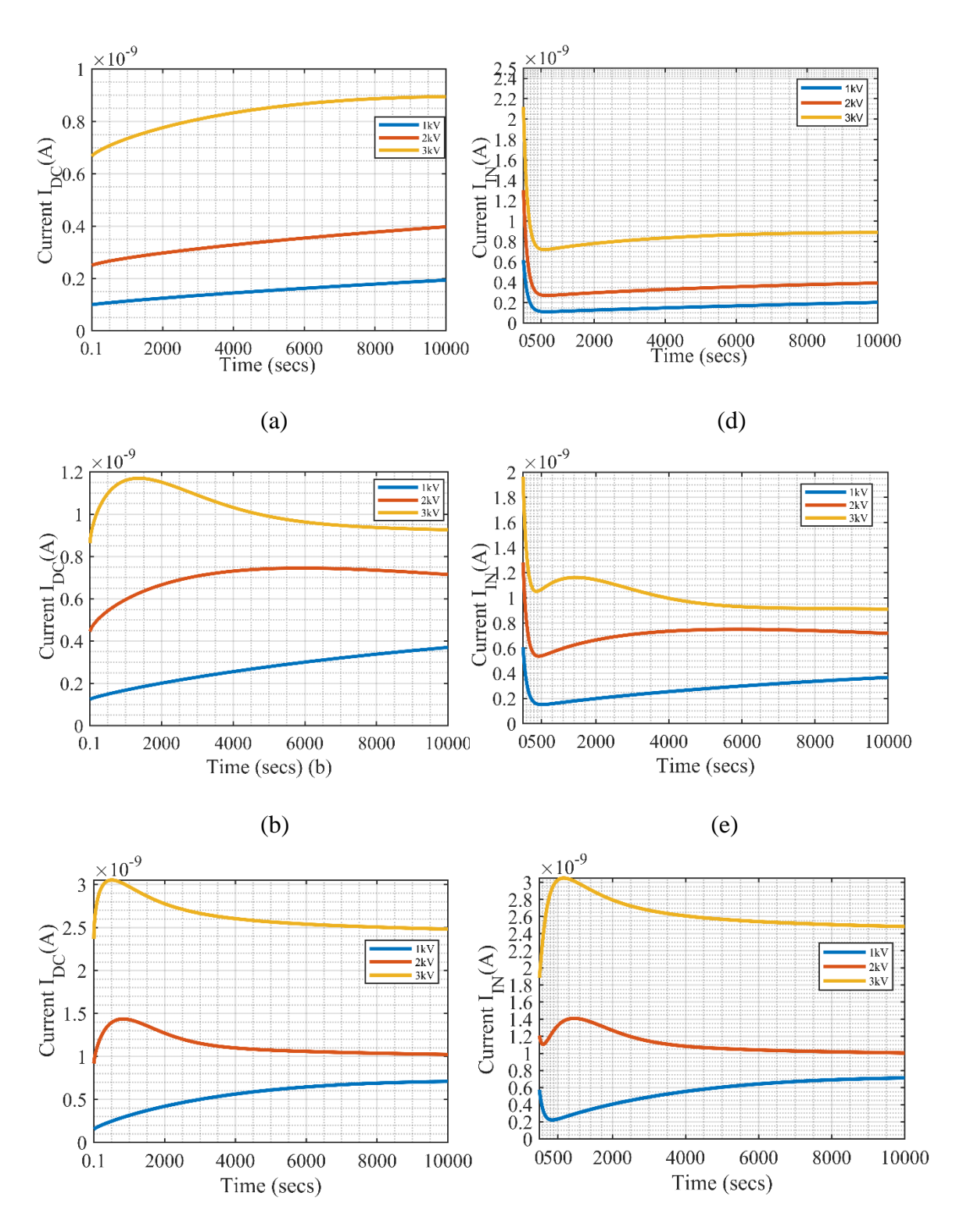
Table 4.2 Fitted equivalent circuit parameters for different applied voltage and temperature

temper ature							
Volt,V	т,° <i>С</i>	C, pF	Cd, pFs- β	R Ω	$egin{array}{c} R_d \ \Omega \end{array}$	α	β
1000	30	70	8	1e13	2e14	0.67	0.28
	40	69	8	8e12	1e14	0.66	0.28
	50	65	8	6.5e12	4.3e13	0.66	0.27
2000	30	74	10	8e12	2e14	0.56	0.35
	40	72.5	10	4.5e12	7e13	0.48	0.45
	50	68	10	2.2e12	2.1e13	0.47	0.5
3000	30	78	10	4.5e12	1.9e14	0.5	0.5
	40	74	10	3.5e12	5e13	0.4	0.58
	50	70	10	1.3e12	1.2e13	0.33	0.5

Thus the proposed dielectric model is validated by fitting the transient current characteristics as observed in experimental measurements under different electro thermal conditions.

4.6 Actual Current

The corresponding current characteristics I_{DC} and I_{IN} w.r.t time were shown in Figure 4.23.



$$(c) (f)$$

Figure 4.23 The current I_{DC} at (a)30°C (b)40°C (c)50°C and the current I_{IN} at (d)30°C (e)40°C (f)50°C

From the $v_o - t$ characteristics plots shown in Figure 4.22 the current I_{IN} is converted using Equation (4.24) as calculated in commercial electrometer (i.e., divide the v_o by r_m and amplified gain).

$$I_{IN} = \frac{v_0}{r_m \left(1 + \frac{R_A}{R_B}\right)} \tag{4.24}$$

Similarly, instead of converting the current I_{IN} as in Equation (4.24), a circuit-based solution as in equation (4.25) with all known values of LDPE from Table.4.2 is shown.

$$I_{DC}(s) = \frac{V}{s*(Z_d(s) + Z_m(s) + r)}$$
(4.25)

It is identified from Figure 4.23 that the I_{DC} and I_{IN} trend was different.

4.7 Anomalous Current Profile-Interaction of LDPE and Electrometer Internal Circuit

The I_{IN} is mere conversion of voltage across the measuring system. This is verified in reference with the voltage across the LDPE. It is quite impractical (Or is it unfeasible?) to measure v_d . But now with proposed LDPE model v_d can be calculated from the circuit given in Figure 4.20 by using similar procedure followed in calculating v_m .

$$v_d(s) = \frac{V}{s} * \left(\frac{Z_d(s)}{Z_d(s) + Z_m(s) + r}\right)$$
 (4.26)

The calculated v_d using equation (4.26) and its corresponding characteristics w.r.t to time is shown in Figure 4.24. By comparing the v_o with the v_d it is comprehended that v_d and v_o transients shapes were inverse to each other.

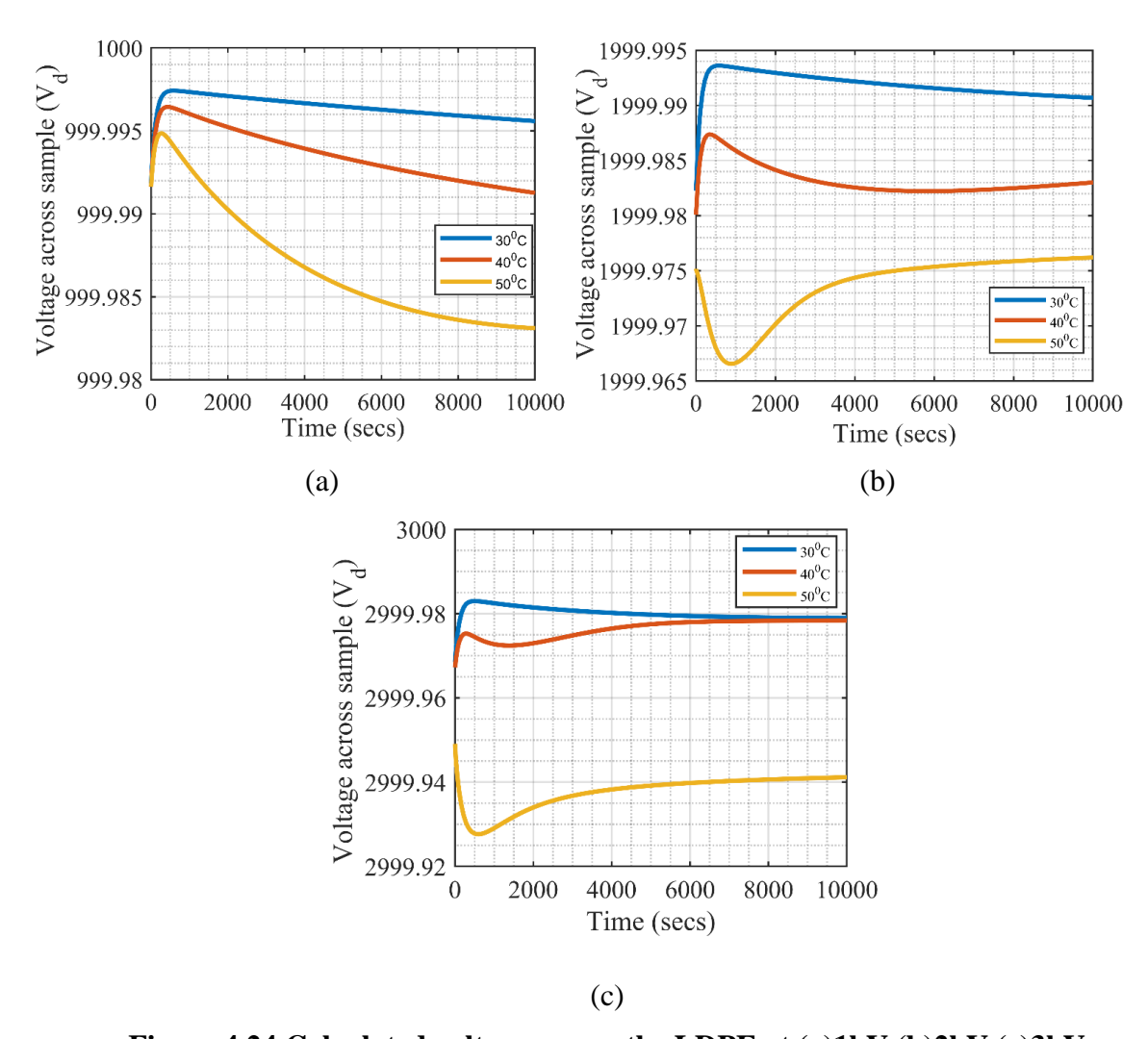


Figure 4.24 Calculated voltage across the LDPE at (a)1kV (b)2kV (c)3kV

The primary reason for the inversion is explored with the typical voltage trend observed in the overall measurements. Specifically, two different anomalous profiles are selected for investigation (that are repeatedly observed in experiments). All the three voltages (i.e., applied voltage V, voltage across the LDPE v_d and the voltage $v_m(\sim v_d)$) are compared together as shown in Figure 4.25 (drawn with normalized scale to avoid the magnitude differences among V, v_m and v_d).

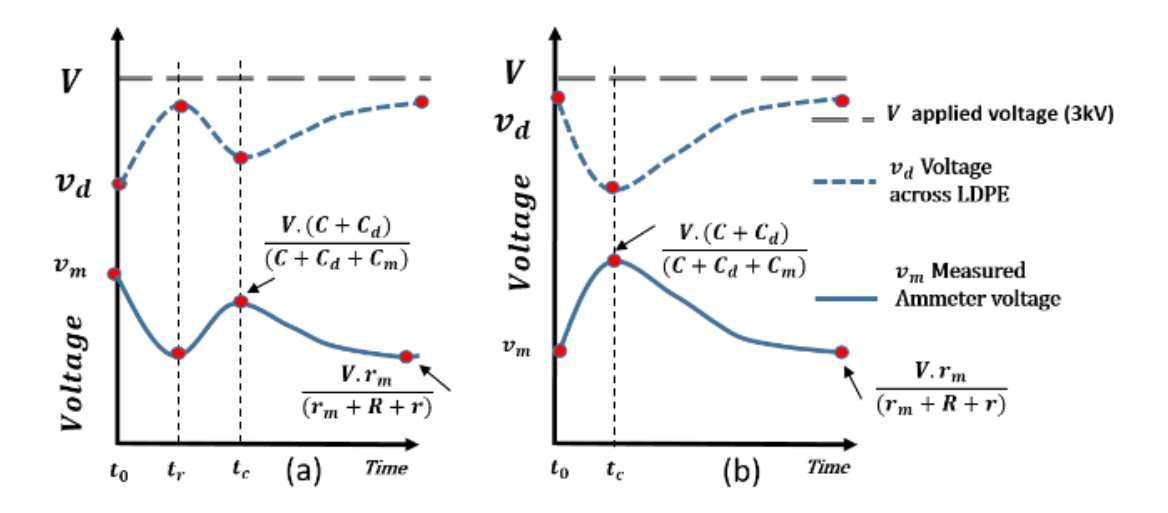


Figure 4.25 Voltage profile (a) 3kV 40°C and (b) 3kV 50°C

• 3kV voltage profile under $40^{\circ}C$ – Figure 4.25(a)

The estimated LDPE resistance R and R_d at 40°C is higher when compared to 50°C. (i.e., as temperature increases resistance of material decreases).

At time t_0 - the v_d and v_m are decided based on the ratio of C and C_m . The rate of charging depends on external resistance.

Between times t_0 to t_r - two phenomenon occur here following instantaneous polarization

- \triangleright The high R_d increases $R_d C_d$ time constant and cause slow polarisation of C_d
- \triangleright At the same time high R approaches normal relaxation (steady state condition)

Thus the voltage shape tends to shift from capacitance to resistance division temporarily. Hence, the v_m decreases and v_d increases.

At time t_r - meeting point of partially charged C_d and the temporary steady state condition

Between time t_r to t_c - the C_d approaches full polarisation so the voltage ratio is shifted from resistance to capacitance division with increased capacitance $(C + C_d)$. Subsequently the v_m increases and v_d decreases.

At time t_c - C_d is fully charged

Beyond time t_c - the actual relaxation trend tends to flow reaching the steady state condition and the v_d and v_m is decided based on the ratio of R and r_m .

• 3kV voltage profile under $50^{\circ}C$ – Figure 4.25 (b)

At higher voltages and temperatures, the rate of flow of absorption charge is fast, thus increase in total capacitance of LDPE dominates the conduction current and only one kink is observed as in Figure 4.25(b). The observed anomalous profile in voltages v_m is reflected in current I_{IN} . Hence, it is proven that the current I_{IN} converted from v_o is mere representation of voltage across the measuring system whereas the I_{Dc} is the actual LDPE current characteristics. Therefore, it is incorrect to interpret or associate the LDPE with the current trends I_{IN} obtained using conventional electrometers.

The I_{Dc} solved using the LDPE model is the actual LDPE current characteristics. The I_{Dc} trend was similar as explained in TSLC theory [28], that in lower electro thermal stress no or slow trapping occurs causing delay in reaching the peak current (i.e., 1kV 30°C,40°C and 50°C I_{Dc} current characteristics) and as stress increases it is approaching a fast trap leading to shorter time peaks (i.e., 2 and 3kV, 40°C and 50°C I_{Dc} current characteristics).

4.8 Peak Current Characteristics

In comparison with LDPE impedance Z_d the measuring impedance Z_m is negligible hence the LDPE model alone considered as in Figure 4.26 to derive peak current characteristics.

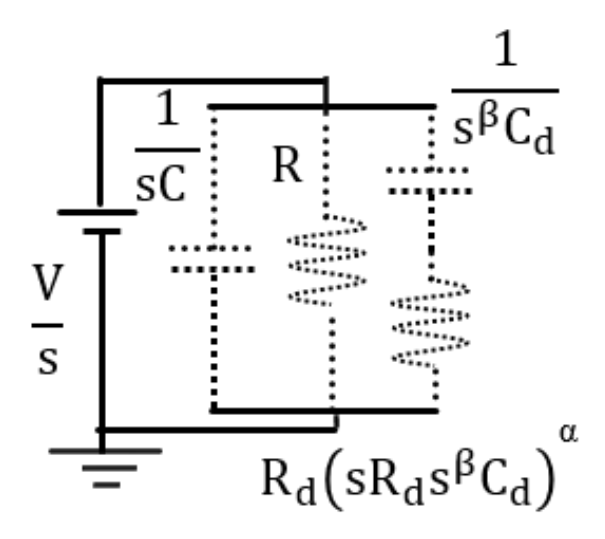


Figure 4.26 The proposed dielectric model circuit

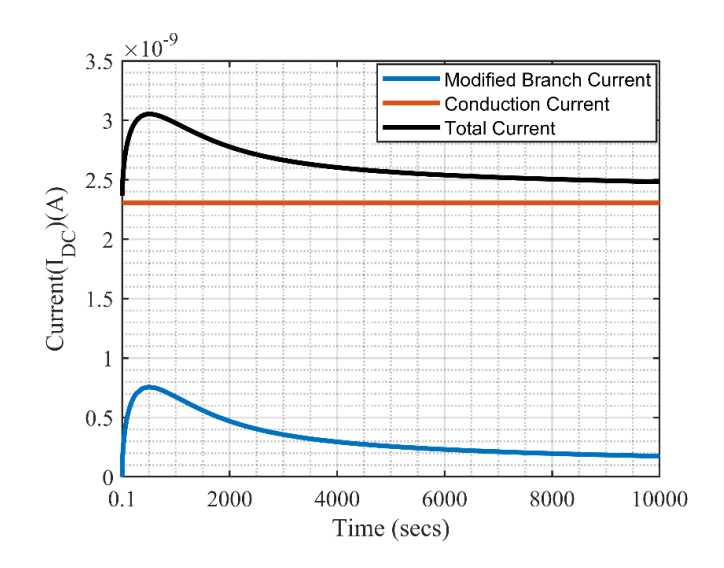


Figure 4.27 The absorption current differentiated from conduction current

Here the instantaneous polarization current flow across the C w.r.t rate of change of applied voltage is huge and become negligible after t > 0. Therefore, the current after t > 0 in the LDPE model is the summation of modified branch and conduction currents. It was known the LDPE conduction current is temperature and field dependent, but is constant at a certain voltage and temperature. Hence, the peak shape is obviously due to the modified branch current. By disregarding constant conduction, the modified branch current seen initially increases and then drops, as shown in Figure 4.27.

All the current peak occurs in between initial polarization and steady state conduction hence a theoretical study was conducted by considering current in the modified branch alone. The current is derived as similar to the analysis performed in [22], the Equation (4.27) represents the current in the branch given in Laplace domain.

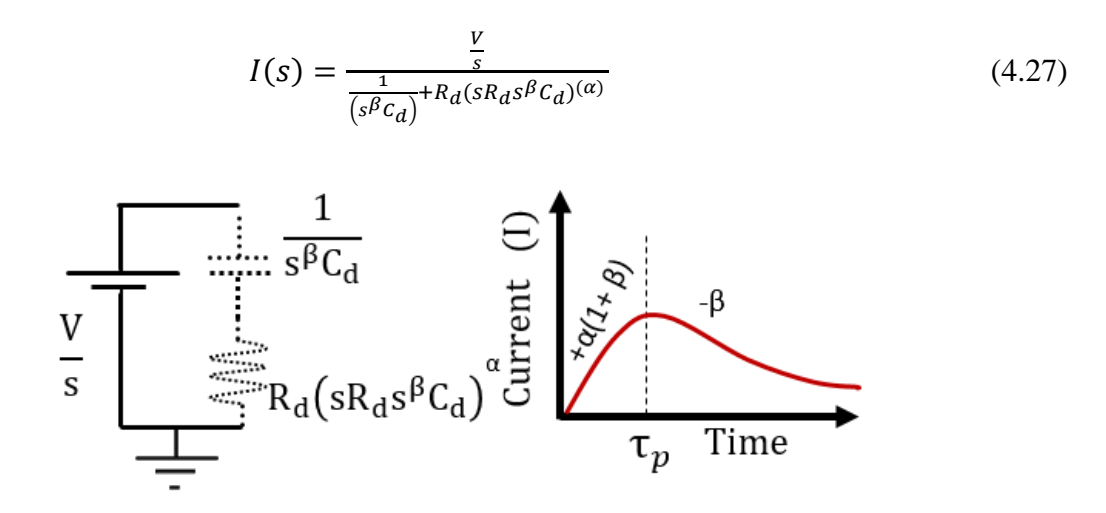


Figure 4.28 The modified branch circuit and its current dynamics

The modified branch resultant current shape is given in Figure 4.28. The current is analysed w.r.t peak time τ_p . For $t \ll \tau_p$, the current solved and shown in Equation (4.28),

$$I(s) = \frac{V * k}{s^{1+\alpha(1+\beta)}} \frac{C_d}{\left[1 + \frac{k}{s\alpha(1+\beta)+\beta}\right]}; \quad k = (R_d C_d)^{-(1+\alpha)}$$
(4.28)

and the series is expanded (refer to Appendix) and its inverse Laplace solution is given in Equation (4.29).

$$I(t) = V * C_d \sum_{m=1}^{\infty} \frac{(-1)^{m-1} (k)^m * t^{m\alpha(1+\beta) + (m-1)\beta}}{\Gamma(m\alpha(1+\beta) + (m-1)\beta + 1)}$$
(4.29)

By considering the dominant factors alone, the positive $\alpha(1+\beta)$ to the power time in Equation (4.30) explains the increase in current initially.

$$I(t) = At^{\alpha(1+\beta)} \tag{4.30}$$

For $t \gg \tau_p$ the current decreases gradually with the time similar to time varying capacitor [26],

$$I(s) = \frac{V}{s^{1-\beta}} \frac{C_d}{\left[1 + \frac{s^{\alpha(1+\beta)+\beta}}{k}\right]}$$
(4.31)

$$I(t) = V * C_d \sum_{m=1}^{\infty} \frac{(-1)^{(1-m)} (k)^{1-m} t^{-((m-1)\alpha(1+\beta)+m\beta)}}{\Gamma(1-(m-1)\alpha(1+\beta)-m\beta)}$$
(4.32)

$$I(t) = VC_d \left[\frac{t^{-\beta}}{\Gamma(1-\beta)} \right] = At^{-\beta}$$
 (4.33)

Thus, Equations (4.30) and (4.33) indicate the modified branch current peak with respect to time. Table 4.1 shows that estimated α approaches zero and β approaches one with an increase in electro thermal stress. Hence, by substituting the above ($\alpha \rightarrow zero$ and $\beta \rightarrow one$), the LDPE modified impedance model resembles the linear equivalent circuit as shown in Equation (4.36).

$$Z_{drc} = \frac{R_d}{(s * R_d * S^{\beta} C_d)^{-(\alpha)}} + \frac{1}{(s^{\beta} * C_d)}$$
(4.34)

$$Z_{drc} = \frac{R_d}{(s*R_d*s^1C_d)^{-(0)}} + \frac{1}{(s^1*C_d)}$$
(4.35)

$$Z_{drc} = R_d + \frac{1}{(s * C_d)} \tag{4.36}$$

Thus, the peaks current was due to the inherent semi crystalline and amorphous properties of LDPE material [29]. The change in LDPE properties at different applied voltage and temperature alters the rate of charging of the modified branch which causes the shift in peaks.

4.9 Experimental Validation

The commercial electrometer current shown in Figure 4.2 is matched with replicated electrometer internal circuit components for r_m and c_m of $1\text{M}\Omega$ and $40\mu\text{F}$ as shown in Figure 4.29(a). And the fitted parameters are given in Table.4.3.

Table 4.3Fitted Parameters

V KV	C pF	C _d pFs ⁻¹	R Ω	R_d Ω	α	β
1	65	8	2.0E+13	4E+14	0.65	0.25
2	68	10	2.0E+12	2E+14	0.45	0.55
3	70	10	6.00E+11	3E+14	0.3	0.5

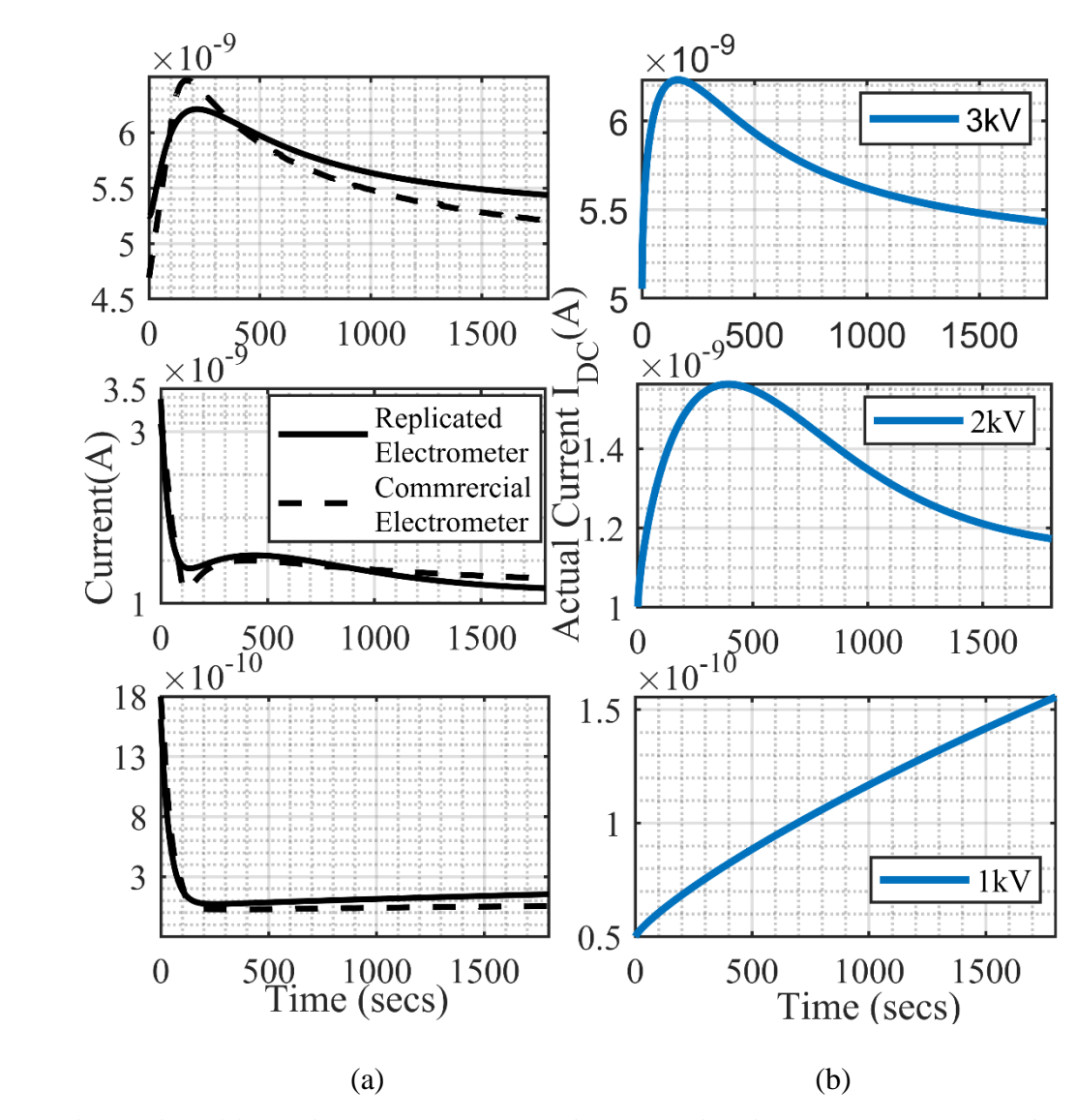


Figure 4.29 (a)Replicated electrometer internal circuit current matched with commercial electrometer (b) Actual current.

Chapter 5

Conduction Current Measurement under HVDC PR

5.1 Introduction

Insulation material performance is severely impacted by HVDC PR. The life estimation models demonstrate that LDPE under short reversal time interval fails quickly as compared to higher intervals. This difference in breakdown time is explored in relation with LDPE current characteristics. The experiments were performed in a 30µm sample under 200 kV/mm electric field of 1 minute and 10-minute reversals. An ammeter hardware setup is used to measure the current until breakdown. The continuously measured current of each reversal interval was sequentially split into three sections and compared. Significant differences in instantaneous, polarization and relaxation currents are observed. Also, dissimilar leakage current trends in 1-minute and 10-minute tests are observed, and these results were correlated with the charge dynamics in LDPE to explain the variations in the breakdown.

5.2 Effect of Time Interval T on Life Time t

A life estimation model including PR stress proposed in Chapter 3 is given in Equation (5.1)

$$t = D_0^{(1 - re^{-cT})} V^{-n_0(1 - se^{-bT})}$$
(5.1)

Here t is the lifetime estimated for particular voltage V and time interval T. b, c, s and r are the fitted coefficients for a given material. The life estimation experimental procedure is detailed in Chapter 3. In that, among the other materials tested, LDPE shows drastic life reduction under PR. Also, it is observed under similar electric fields the samples break earlier at a shorter time interval PR compared to a longer time interval. Under PR tests, irrespective of reversal time interval, the insulation is exposed to a series of voltage transients and alternating polarities. Subsequently, the breakdown and its occurrence had the sequential effect of applied voltage transients and their polarities. However, the dominant phenomenon (transient or polarities) causing the major damage to insulation and the difference in breakdown times is still under examination. The space charge and leakage current measurements have often been reported in the literature for only a few PR cycles with fixed reversal frequency, which share considerable changes in material properties. In [31] the leakage current characteristics were recorded under one fixed time interval PR and reported

that the current initially increases and then decreases after significant reversals. Therefore, above mentioned experimental analysis until a breakdown in different PR profiles is necessary to give a better understanding of the difference in the times of occurrences of breakdown.

5.3 PR Leakage Current Measurement

The leakage current is measured using a replicated electrometer circuit shown below.

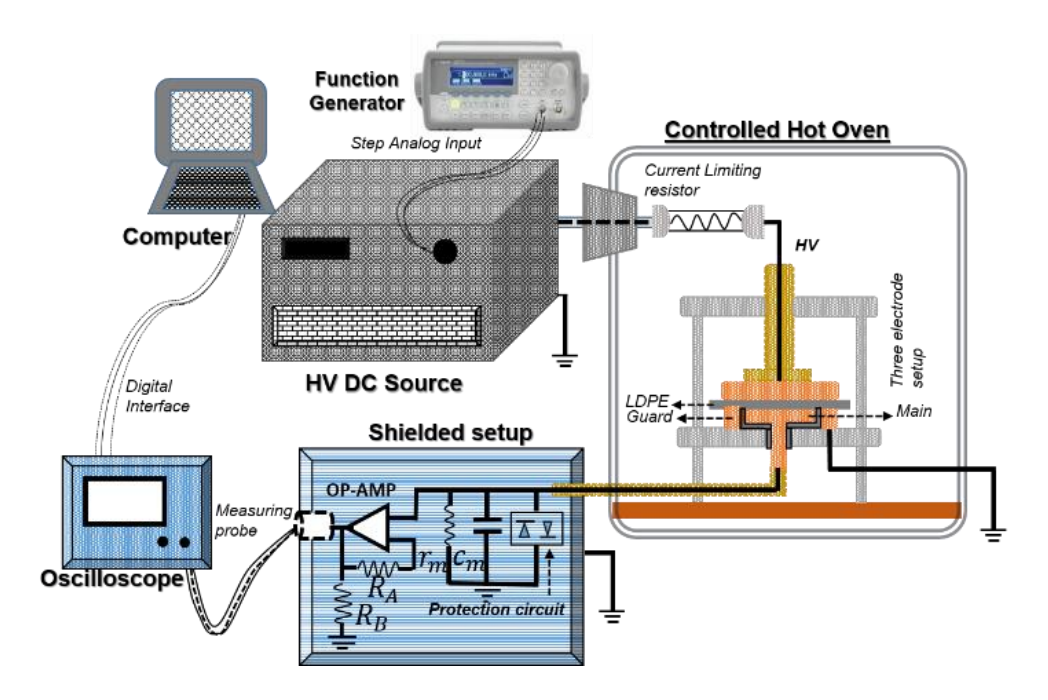


Figure 5.1 The complete automated measurement setup

The current through the thin film LDPE is recorded using an oscilloscope and the actual current (proportional to v_d) was measured. Figure 5.2 shows the voltage profile used. Measurement is conducted for two different time intervals (1 minute and 10 minutes). The ramping time is fixed to 10 seconds for PR. The experiment was conducted at a constant electric field of 200 kV/mm for both time intervals.

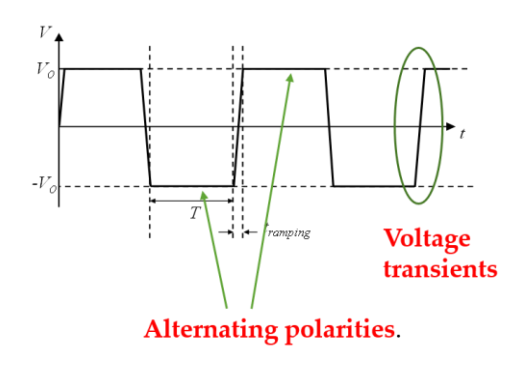


Figure 5.2 Typical profile of the PR voltage used in the experiment with the time interval between reversals (T), ramping time $(t_{ramping})$ and voltage level (V_{θ}) kV

Figure 5.3 (a) shows the continuous current measured over a 1-minute interval PR. The current is measured till breakdown (occurred at $\sim 40^{th}$ minute). The continuously measured current is split into three sub-sections i.e., around 1 minute, 15 minutes and 30 minutes and compared among themselves as shown in Figure 5.3 (b). A significant difference in the current magnitudes related to both instantaneous polarization and relaxation is observed.

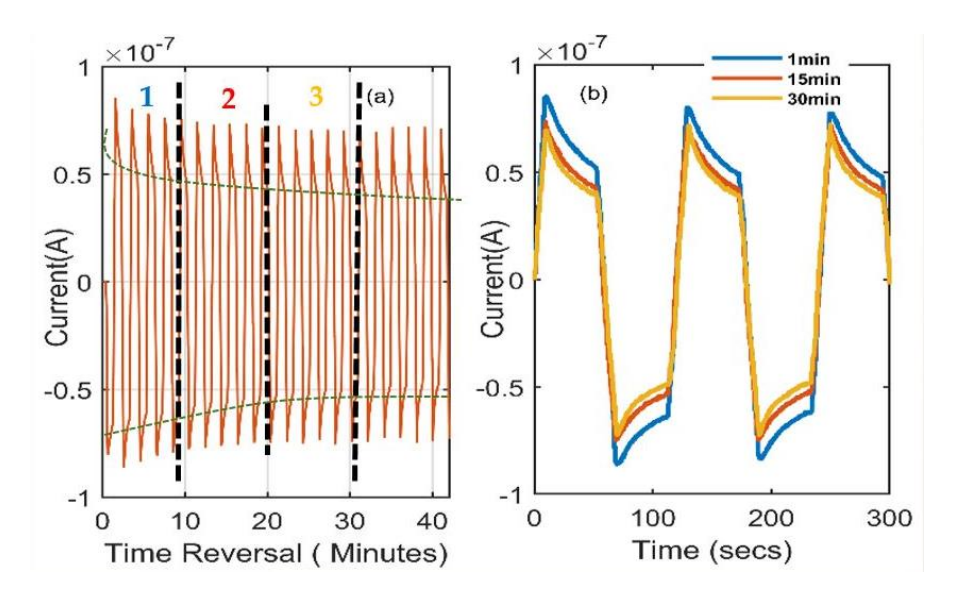


Figure 5.3 The 1-minute time interval leakage current (a) continuous (b) different period compared.

Similarly, the current is measured for 10-minute time intervals until breakdown. The 10-minute PR leakage current trend is split into three subsections, i.e., 0-160 minutes, 160-300 minutes and 300-450 minutes and comparison is shown in Figure 5.4. The polarization and the dielectric relaxation current profiles vary for different subsections and the sample breakdown has occurred at $\sim 500^{th}$ minute.

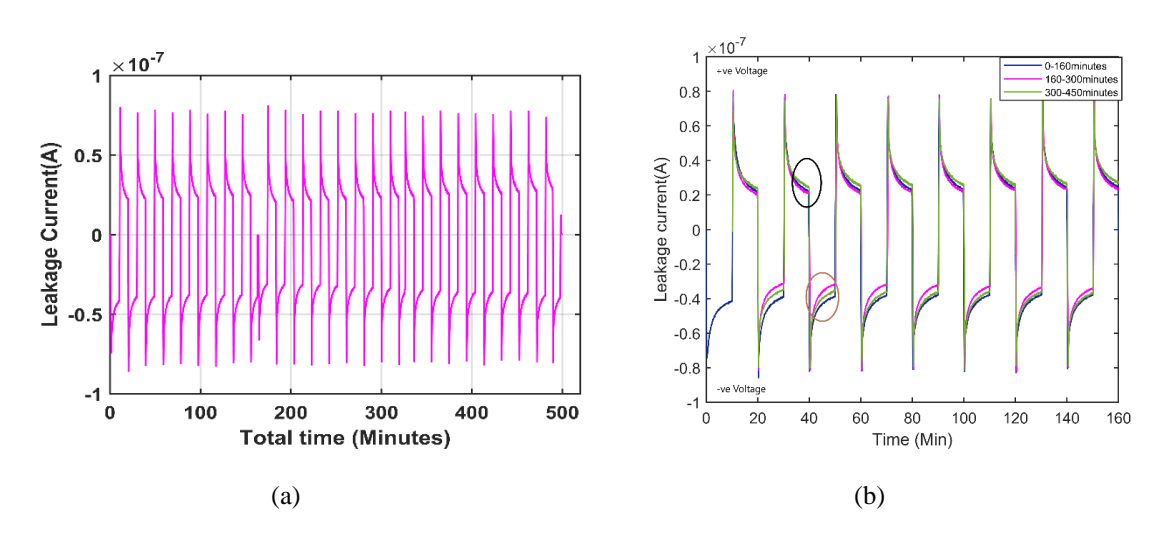


Figure 5.4 The different time period comparison of 10-minute reversal leakage current(a) continuous (b) different period compared.

5.4 Results and Discussions

Instantaneous polarization, slow polarization and conduction are the three major current components that flow in an insulator when subjected to an electric field. However, under PR due to shorter time interval voltages, the measured current is observed between the initial polarization and steady state conduction current. That difference in 1 minute and 10-minute interval PR current characteristics is shown in this section. The sequential current differences are compared within 10-minute interval until breakdown and against 1 minute interval reversal current.

5.4.1. Difference in 1 and 10 minute current characteristics

Figure 5.4 shows the leakage current characteristics for a 10-minute interval, where the transient effect of the three sections' current are compared.

The current trend was.

- Increased initially-The high currents flow up to 160 minutes in 10 minute first sub section.
- Decreased after a few PR cycles- After 160 minutes the current reduced to a level and the same trend is maintained till 300 minutes.
- Increased further in the last subsection- After 300 minutes the current increased once again.

The current trend is similar in both positive and negative voltages, but the difference is observed in the reduction of current magnitude, which is more in negative voltage as compared to positive voltage as shown in Figure 5.5 (a) and (b).

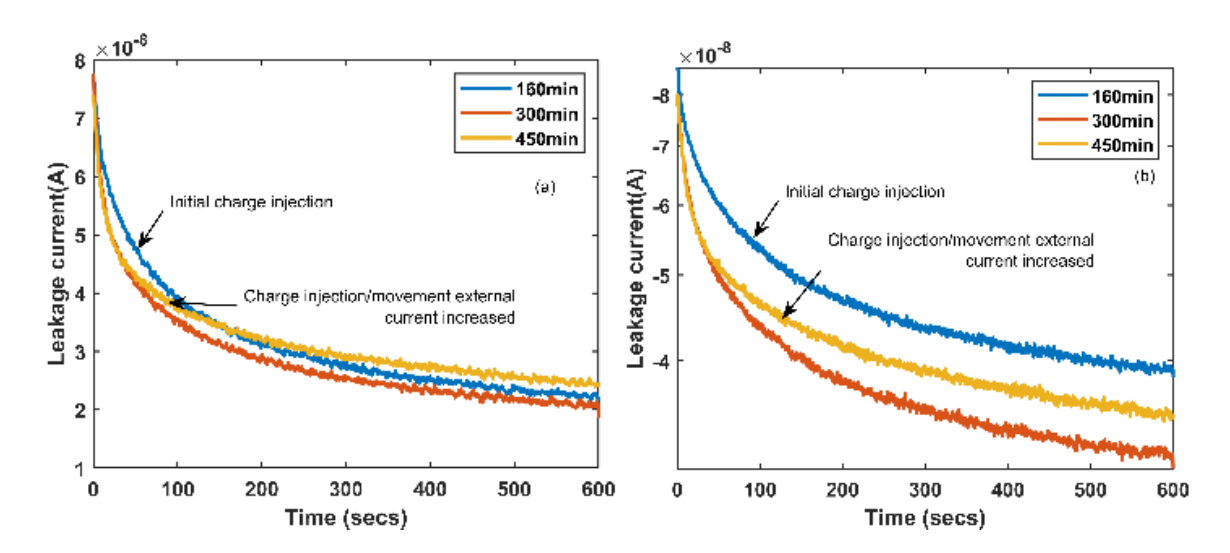


Figure 5.5 The 10 minute current characteristics under (a) positive (b) negative voltage

A similar analysis was conducted for 1-minute results too, in which the current characteristics show a continuous decreasing trend in all subsequent PR until the breakdown as shown in Figure 5.6 (a) and (b). The first subsection was detected with a high current flow and subsequently, the current magnitude decreased. The trend was similar under both positive and negative polarities

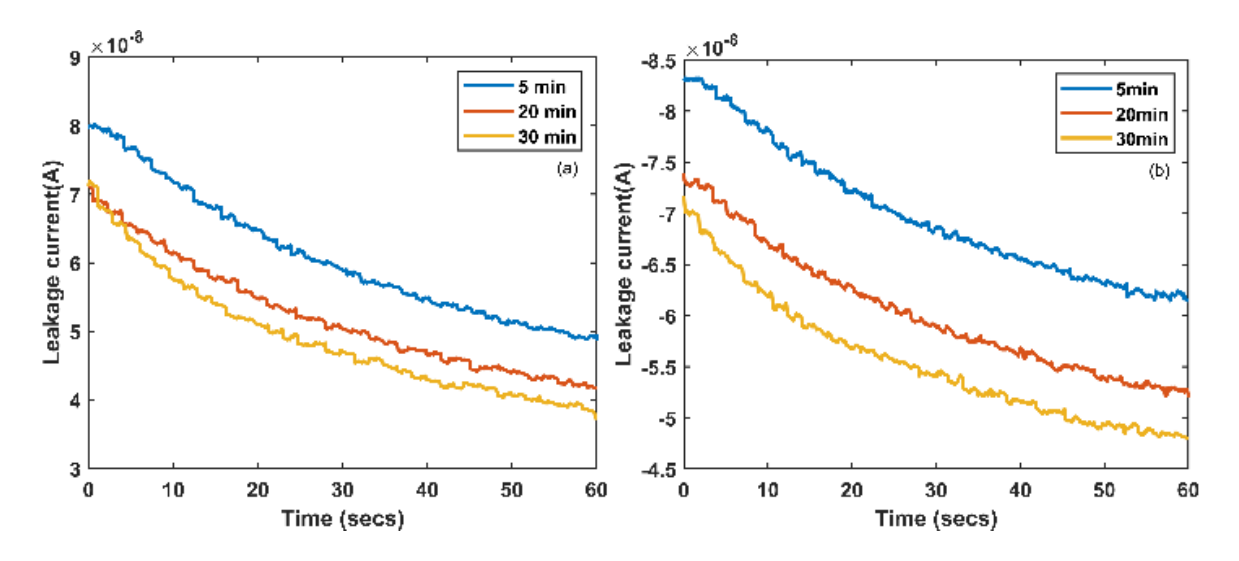


Figure 5.6 The 1 minute current characteristics under (a) positive and (b) negative voltage.

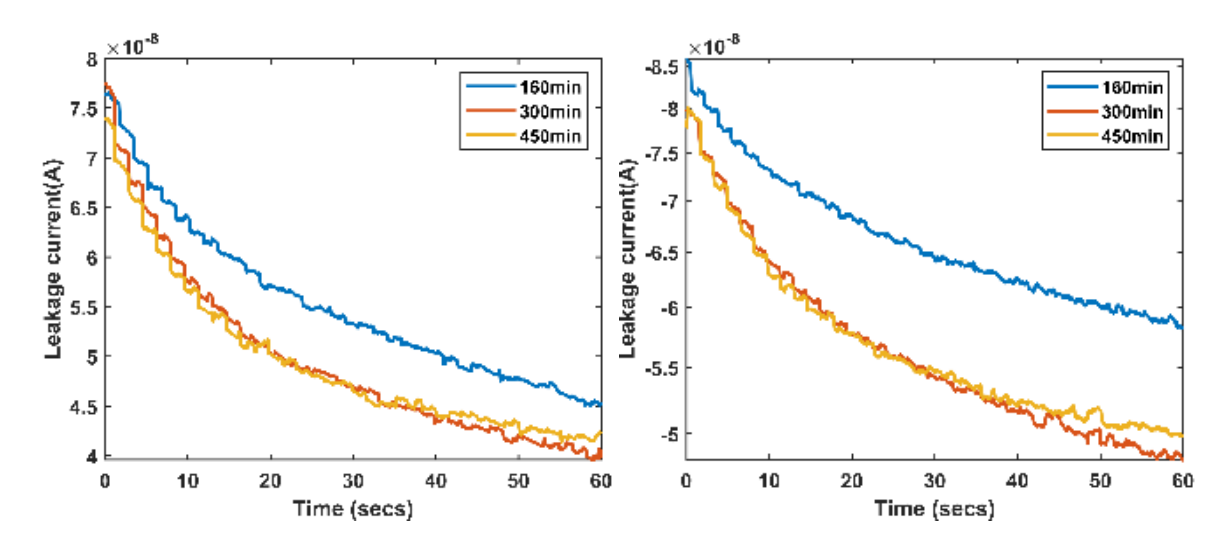


Figure 5.7 The 10 minute leakage current characteristics limited to 60 seconds for comparison, (a) positive (b) negative voltage.

Figure 5.7 shows the 10-minute interval current, limited up to 60 second range, to compare the difference observed w.r.t to 1 minute results. Significant differences in the trend in the 10-minute interval are observed even in a very short time, however, the overall trend (in the 60-second range) is quite similar to the 1-minute current trend.

5.4.2. Correlation of breakdown and current characteristics

Many literature [32] [33] related the leakage current with LDPE charge dynamics and reported that the increase in leakage current is due to charge injection [35] and the decrease in external current is due to dipole relaxation inside the LDPE. The changes in charge dynamics of LDPE reflect the change in external current measurement. Therefore, the increase in current in an early subsection of PR confirms the charge injection, and later continuous decrement represents no further possible injection due to the short time interval of PR. Eventually, this leads to charge accumulation (homo or hetero) in LDPE (either in electrode interface or bulk) and results in electrical field enhancement.

Whereas in 10-minute interval of PR, the current increment is observed in the first and third subsections. The increment in the first subsection is due to the charge injection and in the third subsection due to charge movement inside the LDPE. This charge movement inside the LDPE mitigates the local field enhancement temporarily and delays the time to breakdown of LDPE as compared to 1-minute PR. The inferred explanation is based on a correlation between the experimental breakdown data and the reported charge dynamics in response to the external current in the literature.

Comparing the 1 minute and 10-minute PR, the rate of change of charge injection and charge movement is restricted in 1-minute interval due to the inherent morphology of LDPE. Therefore, it is inferred that breakdown behavior in relation to voltage transients and alternate polarities, does not present any significant damage to the LDPE, but increased number of reversals within the stipulated time has a strong relation with the breakdown behavior of LDPE. Therefore, in an HVDC application, frequent power reversal in a short time interval possesses a severe damage impact on insulation than a reversal having a longer time. This understanding validates the conclusion established in Chapter 3. Thus the duration of time between reversals has a greater impact on the time of occurrence of breakdowns than voltage transients and polarity.

5.4.3. Equivalent circuit-based analysis

Furthermore, the current data were fitted using the proposed dielectric model to identify specific changes in circuit parameters, which were then associated with changes in material qualities. The equivalent circuit shown in Figure 5.8 is used.

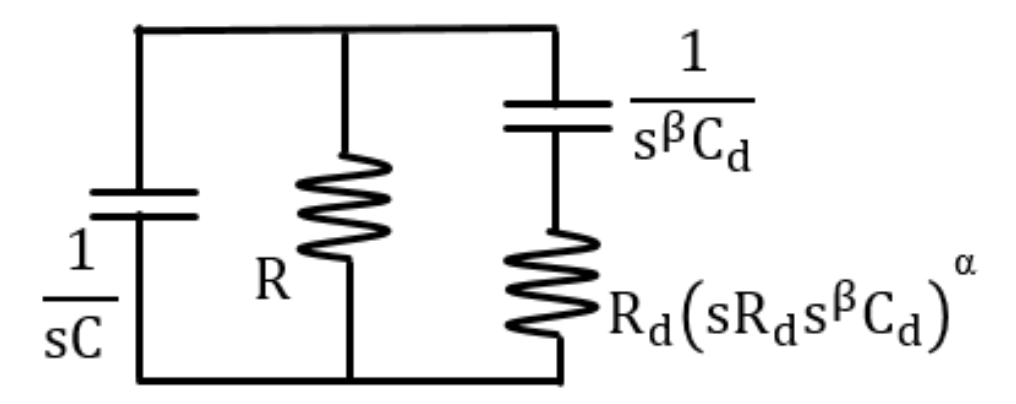


Figure 5.8 The dielectric equivalent circuit

Here the currents are measured at higher electric fields and are exponential in nature. As already stated in Chapter 4 at higher electric fields the α approaches zero and β pproaches to one, thus approaching exponential characteristics. Hence, with the α assumed to be zero, the current characteristics fitted for Equation (5.3) and the total amount of charge (Q) estimated using Equation (5.4).

$$I = At^{-\beta} \tag{5.3}$$

$$Q = A \int_0^t t^{-\beta} dt \tag{5.4}$$

Current (I) and Charge (Q) for 10-minute PR current characteristics of Figure 5.5 are estimated by fitting the equations (5.3) and (5.4). The estimated values are given in Table 5.1.

Table 5. 1. Parameter estimated from fitting 10-minute experimental data

Time		A	,	β	Q	
(min)	Positive cycle	Negative cycle	Positive cycle	Negative cycle	Positive cycle	Negative cycle
160	1.26e-07	1.07e-07	0.26	0.15	1.87e-5	2.8e-5
300	1.09e-07	9.69e-08	0.25	0.17	1.72e-5	2.3e-5
450	9.4e-08	8.94e-08	0.20	0.14	1.91e-5	2.5e-5

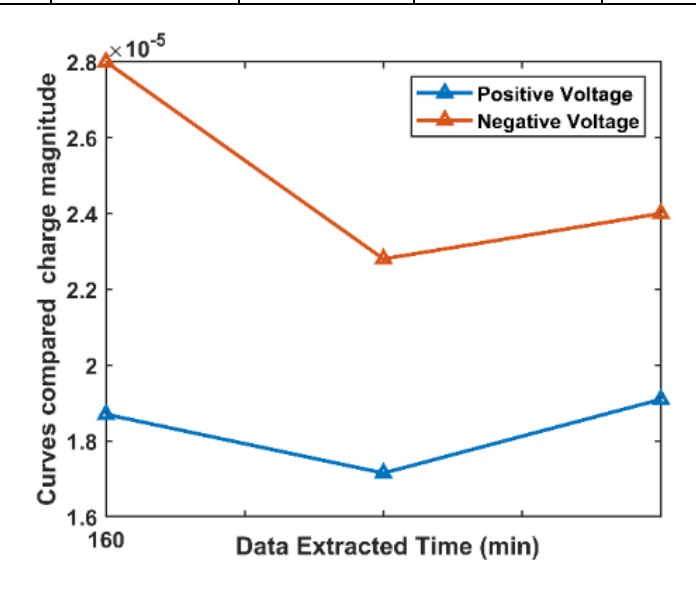


Figure 5.9 The current characteristics integrated value for 10-minute time interval.

Figure 5.9 shows the difference in the total amount of charge until breakdown at different time instants of the experiment. Compared to positive voltage, under negative voltage, the amount of charge transferred was observed to be more. The amount of charge varied at different time intervals is clearly understandable from Figure 5.9. Similarly, the estimated β value in Table 5.1 shows that the values are close to zero in negative voltage, and it increases and decreases after a certain number of reversals. But at a positive voltage, the β values keep on decreasing until the breakdown. Hence, is understandable that the charge injection and diffusion depend on the history of voltage application.

The charge distributes throughout the bulk of the sample and maintains partially uniform electric field distribution in 10-minute interval, thus delaying the breakdown. In 1-minute interval, however, there is no time for the charge to penetrate through the bulk, which results in disproportionate field distribution, thus causing accelerated breakdown. However, the inferences are still needed to be validated with space charge measurements to solidify the conclusion. Thus the current work extended with space charge measurement will be communicated as a future scope of this thesis work.

Chapter 6 Conclusions

6.1 Life estimation model

- 6.1.1 The conclusion, proposes a generalized inverse power law model based on rigorous experimental observations. The proposed model is found to closely predict the DC parameters, solely from PR data fitted to it.
- 6.1.2 The application of generalized inverse power law for PRs is justified by the experimental results and analysis. The model is considered useful and practical as the inverse power law has been practiced for a long time in life estimations.
- 6.1.3 The test can be conducted at any two different frequencies of reversals for estimating model parameters. The model also fits well for materials with space charge accumulation and predicts that such materials have a drastic reduction in life at a high frequency of reversals.
- 6.1.4 The percentage reduction in DC life with reversal frequency is of important consequence for deciding planned reversals in power systems as well as for deciding suitable materials for power equipment.
- 6.1.5 The percentage reduction in logarithmic life under PRs is shown to be a function of power law parameters and frequency of reversal, which is useful for designers.

6.2 Measurement Issues and Actual Current trend

- 6.2.1 The current dynamics observed in commercial electrometer are not actual LDPE current characteristics. The interaction of electrometer impedance and LDPE impedance alters the actual current characteristics of LDPE.
- 6.2.2 These anomalies/interactions are identified with the support of the new dielectric model proposed by the authors. The simulated results with the new dielectric model exactly matched the experimental results.
- 6.2.3 The real LDPE current characteristics were obtained and its trend was found to be uniform for different sets of voltages and temperatures.
- 6.2.4 The current observed in commercial electrometers is merely a representation of

voltage across the measuring circuit, and the straight conversion of voltage characteristics into current (I_{IN}) is erroneous. Therefore, it is unseemly to directly compare the charge dynamics in LDPE with the anomalous current profile measured using a commercial electrometer.

6.2.5 The polymer current characteristics involve trapping, detrapping and polarization phenomenon. However, the linear dielectric model explains only the polarization phenomenon. Hence, the recommended model is considered to be effective in clarifying the trapping and detrapping mechanisms in polymers, which are necessary to comprehend the deterioration mechanisms of insulation materials utilized in HVDC applications.

6.3 Conduction Current Characteristics under HVDC PR

- 6.3.1 The shorter the interval period of PR, the early is the occurrence of breakdown. Therefore, in an HVDC application, frequent power reversal in a short time interval possesses a more severe damage impact on insulation than a reversal having a longer time.
- 6.3.2 The duration of time between reversals has a greater impact on the time of occurrence of breakdowns than voltage transients and polarity.

6.4 Future Scope of the Work

While conventional FEM/circuit models can be used to determine conductivity-based field distributions, they do not incorporate space charge dynamics. Hence, the proposed dielectric model (which considers conduction and space charge phenomena) can be incorporated into the simulations to study the ageing-related characteristics. It is also believed that the proposed dielectric model can bridge the gap between phenomenological and physical life estimation models.

References

- [1] Marc Jeroense (2023 September) LinkedIn ,"This is a post in a series that intends addressing questions of future cable development "Where are we?" (this post)". https://www.linkedin.com/posts/marc-jeroense-94410817_hvdc-cable-project-activity-7100558420298145793Un0?utm_source=share&utm_medium=member_desktop
- [2] Y. Murata, M. Sakamaki, K. Abe, Y. Inoue, S. Mashio, S. Kashiyama, O.Matsunaga, T. Igi, M. Watanabe, S. Asai, and S. Katakai, "Development of high voltage DC-XLPE cable system," SEI (Sumitomo Electric) Tech. Rev., no. 76, pp. 55–62, Apr. 2013.
- [3] CIGRE Session Paper B4-10, J P KJÆRGAARD, K SØGAARD, S D MIKKELSEN .et.al, "Bipolar operation of an HVDC VSC converter with an LCC converter"; CIGRE:2012 San Francisco Colloquium.
- [4] T. Hasegawa, M. Hatano, K. Yamaji, T. Kouan and N. Hosokawa, "Dielectric strength of transformer insulation at DC polarity reversal," in IEEE Transactions on Power Delivery, vol. 12, no. 4, pp. 1526-1531, Oct. 1997.
- [5] W. N. Kennedy et al, "Recommended dielectric tests and test procedures for converter transformers and smoothing reactors," IEEE Trans. Power Del., vol. 1, no. 3, pp. 161-166, July 1986.
- [6] A. Cavallini et al, "Life model based on space-charge quantities for HVDC polymeric cables subjected to voltage-polarity inversions," IEEE Trans. Dielectr. Electr. Insul., vol. 9, no. 4, pp. 514-523, Aug. 2002.
- [7] A. Cavallini et al, "Life estimation of DC insulation systems in the presence of voltage-polarity inversions," IEEE Int. Symp. Electr. Insul., (ISEI), 2000, pp. 473-476.
- [8] A. P. S. Tiwana and C. C. Reddy, "Life estimation using damage equalization method and step-stress breakdown tests," IEEE Trans. Dielectr. Electr. Insul., vol. 23, no. 4, pp. 2311-2318, Aug. 2016.
- [9] G. Mazzanti, M. Marzinotto. and A. Battaglia, "A first step towards predicting the life of HVDC cables subjected to load cycles and voltage polarity reversal," Annu. Rep Conf.. Electr. Insul. Dielectr. Phenom. (CEIDP), 2015, pp. 783-786.
- [10] X. Chen et al, "Effect of voltage reversal on space charge and transient field in LDPE films under temperature gradient," IEEE Trans. Dielectr. Electr. Insul., vol. 19, no. 1, pp. 140-149, Feb. 2012.
- [11] J. Y. Steven, T. T. N. Vu, G. Teyssedre and N. I. Sinisuka, "Conductivity measurements and space charge inference in polymeric-insulated HVDC model cables," 2014 ICHVE International Conference on High Voltage Engineering and Application, 2014, pp. 1-4.
- [12] General Requirements and Test Code for Oil-Immersed HVDC Converter Transformers, IEEE Std C57.129-2007, 2008-01-29.
- [13] Y. Isayama et al, "The polarity reversal properties of power cable," IEEE Int. Conf. Dielectr. Liquids (ICDL), 1999, pp. 408-413.
- [14] Himanshu et al, "Investigations on ageing of low-density polyethylene under polarity reversals," Annu. Rep. Conf. Electr. Insul. Dielectr. Phenom. (CEIDP), 2016, pp. 931-934.
- [15] S.Ogata, et al, "Study on the dielectric characteristics of DC XLPE cables," IEEE Trans. Power Del., vol. 5, no. 3, pp. 1239-1247, July 1990.

- [16] G. C. Montanari, I. Ghinello, A. Motori, S. Gubanski and D. Das Gupta, "Searching for short-term techniques for the inference of electrical threshold of PET. DC conductivity measurements," in *IEEE Transactions on Dielectrics and Electrical Insulation*, vol. 5, no. 1, pp. 148-153.
- [17] G. Chen, "Towards understanding of high electric field phenomena in polymeric dielectrics," Proceedings of 2011 International Symposium on Electrical Insulating Materials, 2011, pp. 156-160.
- [18] Z. Lv, Y. Ma, C. Zhang, J. Peng, K. Wu and L. A. Dissado, "The Simultaneous Evolution of Space Charge and Conduction Current in LDPE," in *IEEE Transactions on Dielectrics and Electrical Insulation*, vol. 28, no. 2, pp. 616-624, April 202.
- [19] A. T. Oganesyan and A. A. Oganesyan, "A new equivalent circuit of dielectrics with space charge," [1991] Proceedings of the 3rd International Conference on Properties and Applications of Dielectric Materials, 1991, pp. 1029-1031 vol.2.
- [20] Y. Sekiguchi and M. Fukuma, "Electrical charges and currents distribution analysis in plaque samples by the DCIC-Q(t) method," 2017 International Symposium on Electrical Insulating Materials (ISEIM), 2017, pp. 609-612.
- [21] K.S and R.H Cole, "Dispersion and Absorption in Dielectrics I. AC Characteristics", J. Chem. Phys. 10, 98-105 (1942).
- [22] K.S and R.H Cole, "Dispersion and Absorption in Dielectrics II. Direct Current Characteristics", J. Chem. Phys. 10, 98-105 (1942).
- [23] Keithley Company, "Low Level Measurements Handbook" Precision DC current, Voltage and Resistance Measurements,7th Edition.
- [24] E. Occhini and G. Maschio, "Electrical Characteristics of Oil-Impregnated Paper as Insulation for HV DC Cables," in IEEE Transactions on Power Apparatus and Systems, vol. PAS-86, no. 3, pp. 312-326, March 1967.
- [25] S. Westerlund and L. Ekstam, "Capacitor theory," in IEEE Transactions on Dielectrics and Electrical Insulation, vol. 1, no. 5, pp. 826-839, Oct. 1994.
- [26] Shantanu Das, "A New Theory of Capacitor," in Lecture notes August 2017, Dept. of Power Electronics IIT-Bombay.
- [27] A. Teverovsky, "Absorption voltages and insulation resistance in ceramic capacitors with cracks," in IEEE Transactions on Dielectrics and Electrical Insulation, vol. 21, no. 5, pp. 2020-2027, Oct. 2014.
- [28] A. Many and G. Rakavy, "Theory of transient space-charge-limited currents in solids in the presence of trapping", Physical Rev., vol. 126, no. 6, pp. 1980-1988, 1962.
- [29] P. Fischer, P. Rohl, "Transient Currents in Oxydized Low Density Polyethylene", Prog. Coll. Polym. Sci., Vol. 62, pp. 149-153, 1977
- [30] P. Cambareri, C. de Falco, L. D. Rienzo, P. Seri and G. C. Montanari, "Electric Field Calculation During Voltage Transients in HVDC Cables: Contribution of Polarization Processes," in IEEE Transactions on Power Delivery, vol. 37, no. 6, pp. 5425-5432, Dec. 2022.
- [31] P. Ratheiser and U. Schichler, "DC Leakage Current Measurements: Contribution for the Qualification of extruded MVAC Cables for DC Operation," 2021 IEEE International

- Conference on the Properties and Applications of Dielectric Materials (ICPADM), 2021, pp. 450-453.
- [32] A. K. Upadhyay and C. C. Reddy, "Analytical model for homocharge accumulation in LDPE role of conduction, injection and diffusion," in IEEE Transactions on Dielectrics and Electrical Insulation, vol. 27, no. 2, pp. 565-573, April 2020.
- [33] C. C. Reddy, "Effect of diffusion on space charge formation in dielectrics under steady-state DC conditions," 2012 IEEE 10th International Conference on the Properties and Applications of Dielectric Materials, 2012, pp. 1-6,
- [34] C. Laurent, G. Teyssedre, S. L. Roy and F. Baudoin, "Charge dynamics and its energetic features in polymeric materials," in IEEE Transactions on Dielectrics and Electrical Insulation, vol. 20, no. 2, pp. 357-381, April 2013.
- [35] T. Mori, T. Kato, T. Koshimizu, H. Miyake, Y. Tanaka and T. Takada, "Relationship between packet-like space charge behavior and external current in polyethylene under dc high electric field," 2012 Annual Report Conference on Electrical Insulation and Dielectric Phenomena, 2012, pp. 637-640
- [36] K. Wen et al, "A calculation method and some features of transient field under polarity reversal voltage in HVDC insulation," IEEE Trans. Power Del. vol. 8, no. 1, pp. 223-230, Jan. 1993.
- [37] P. Cambareri, C. de Falco, L. Di Rienzo, P. Seri and G. C. Montanari, "Circuital Modeling of Polarization and Depolarization Currents in Polymeric Materials Under Low Electric Fields," in IEEE Transactions on Dielectrics and Electrical Insulation, vol. 30, no. 3, pp. 963-972, June 2023.
- [38] P. Cambareri, C. De Falco, L. Di Rienzo, P. Seri and G. C. Montanari, "Charging and Discharging Current Measurements and Impact of Polarization Dynamics on Electric Field Modeling in HVDC Paper-Insulated Cables," in IEEE Access, vol. 9, pp. 45155-45162, 2021, doi: 10.1109/ACCESS.2021.3066286.

Appendix

Chapter 2- DC current characteristics derivation

The detailed explanation to the equation (2.6) and (2.7) from the literatures [22] and [23] is provided in this section.

$$I(t) = At^{-\alpha} \tag{2.6}$$

$$I(t) = At^{-(2-\alpha)} (2.7)$$

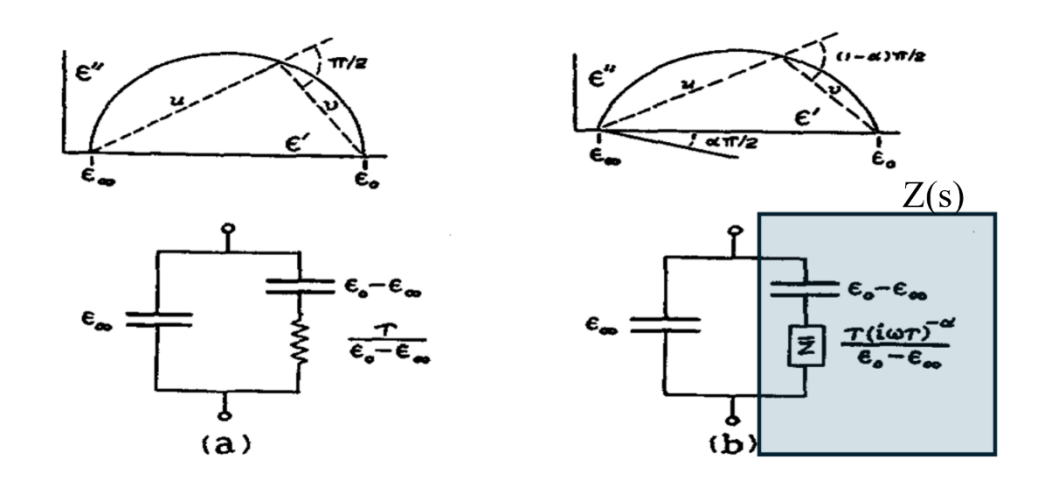


Figure A.1. Theoretical complex plane loci of the complex dielectric constant and equivalent circuits for dielectrics; (a) Debye theory, (b) as required by experimental evidence[22].

The circuit in Figure(a) modified as the circuit in Figure (b) to fit the measurement data.

$$\varepsilon^* = \varepsilon' - i\varepsilon''$$

Here $\varepsilon^* = Complex\ dielectric$, $\varepsilon' - real$, $\varepsilon'' - imaginary$

 ϵ_0 and ϵ_∞ are the static and infinite frequency dielectric constants.

 α assume the values between 0 and 1.

(a) Debye theory	(b)Modified circuit
$\varepsilon^* - \varepsilon_{\infty} = \frac{(\varepsilon_0 - \varepsilon_{\infty})}{(1 + i\omega\tau_0)}$	$\varepsilon^* - \varepsilon_{\infty} = \frac{(\varepsilon_0 - \varepsilon_{\infty})}{(1 + (i\omega\tau_0)^{1-\alpha})}$

The initial charging current due to ε_{∞} is negelected.

For a unit potential difference,the current characteristics are derived as follows

Derivation from [23]	Derived using laplace transform
$Y(i\omega) = i\omega\varepsilon^*$	$I(s) = \frac{V}{s} * Y(s); Y(s) = Y_1(s) + Y_2(s)$
$= i\omega \left[\varepsilon_{\infty} + \frac{(\varepsilon_0 - \varepsilon_{\infty})}{(1 + (i\omega\tau_0)^{1-\alpha})} \right]$	$Y_2(s) = \frac{(\varepsilon_0 - \varepsilon_\infty)}{(1 + (i\omega\tau_0)^{1-\alpha})}$
$I(t) = \frac{1}{\pi} \int_0^\infty i\omega \varepsilon^* e^{i\omega t} dt$	$I(s) = \frac{V}{s} * \frac{s * (\varepsilon_0 - \varepsilon_\infty)}{(1 + (i\omega\tau_0)^{1-\alpha})}$
	By expanding the series
	$I(s) = \frac{1 * (\varepsilon_0 - \varepsilon_\infty)}{(s * \tau_0)^{1 - \alpha}} * \left[1 + \frac{1}{(i\omega \tau_0)^{1 - \alpha}} \right]^{-1};$
	$k = \frac{1}{\tau_0^{1-\alpha}}; s = i\omega$
	$I(s) = k * \frac{(\varepsilon_0 - \varepsilon_\infty)}{(s * \tau_0)^{1-\alpha}} \left[1 - \frac{k}{s^{1-\alpha}} + \left(\frac{k}{s^{1-\alpha}}\right)^2 - \left(\frac{k}{s^{1-\alpha}}\right)^3 \dots \dots \right]$
For $\frac{t}{\tau_0} \ll 1$	Inverse Laplace transform
$I(t) = \frac{(\varepsilon_0 - \varepsilon_\infty)}{\tau_0} \cdot (1 - \alpha) \left(\frac{t}{\tau_0}\right)^{-\alpha} \times $	$I(t) = V(\varepsilon_0 - \varepsilon_\infty) k \left[\frac{t^{-\alpha}}{\Gamma(1 - \alpha)} - \frac{t^{1 - 2\alpha} * k}{\Gamma(2 - 2\alpha)} + \frac{t^{1 - 3\alpha} * k^2}{\Gamma(3 - 3\alpha)} + \dots \right]$
$\sum_{n=1}^{\infty} \frac{(-1)^{n-1}n}{\Gamma(1+n(1-\alpha))} \left(\frac{t}{\tau_0}\right)^{(n-1)(1-\alpha)}$ $I(t) = \frac{\varepsilon_0 - \varepsilon_\infty}{\tau_0} \left[\frac{1}{\Gamma(1-\alpha)}\right] \left(\frac{t}{\tau_0}\right)^{-\alpha}$	$I(t) = V(\varepsilon_0 - \varepsilon_\infty)k(1 - \alpha) \left[\frac{t^{-\alpha}}{\Gamma 1 + (1 - \alpha)} - \frac{2 * t^{1 - 2\alpha} * k}{\Gamma 1 + (2 - 2\alpha)} + \frac{3 * t^{1 - 3\alpha} * k^2}{\Gamma 1 + (3 - 3\alpha)} + \ldots \right]$
$I(t) = At^{-\alpha}$	$I(t) = \frac{V(\varepsilon_0 - \varepsilon_\infty)}{\tau_0} \cdot (1 - \alpha) \left(\frac{t}{\tau_0}\right)^{-\alpha}$
$\operatorname{For} \frac{t}{\tau_0} \gg 1$	$\times \sum_{n=1}^{\infty} \frac{(-1)^{n-1}n}{\Gamma(1+n(1-\alpha))} \left(\frac{t}{\tau_0}\right)^{(n-1)(1-\alpha)}$
$I(t) = \frac{(\varepsilon_0 - \varepsilon_\infty)}{\tau_0} \cdot (1 - \alpha) \left(\frac{t}{\tau_0}\right)^{-(2 - \alpha)} \times \sum_{n=1}^{\infty} \frac{(-1)^{n-1}n}{\Gamma(1 - n(1 - \alpha))} \left(\frac{t}{\tau_0}\right)^{-(n-1)(1 - \alpha)}$	For $\frac{t}{\tau_0} \ll 1$, with leading term of series th ecurrent is given as
$I(t) = \frac{\varepsilon_0 - \varepsilon_\infty}{\tau_0} \left[\frac{(1 - \alpha)}{\Gamma(\alpha)} \right] \left(\frac{t}{\tau_0} \right)^{-(2 - \alpha)}$	$I(t) = At^{-\alpha}$
$I(t) = At^{-(2-\alpha)}$	Similarly for $\frac{t}{\tau_0} \gg 1$,with leading term of series th ecurrent is given as
	$I(t) = At^{-(2-\alpha)}$

Chapter 4 section 4.9

The peak current characteristics derived taking into account the complex impedance branch

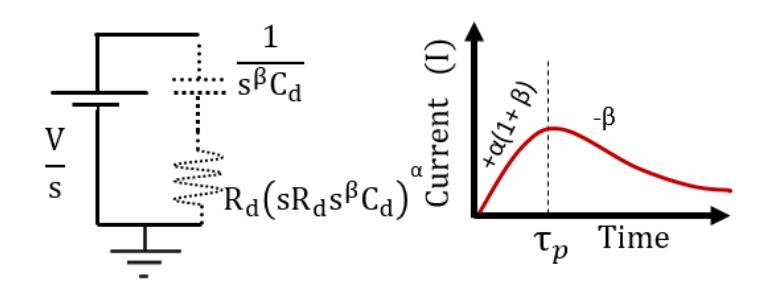


Figure 4.26 The proposed dielectric model circuit

I igure neo rue prop	osed dielectric model circuit
For $t \ll \tau_p$	$t\gg au_p$
$I(s) = \frac{V/s}{Z(s)}$ $Z(s) = \frac{1}{(s^{\beta} * C_d)} + R_d (R_d s^{\beta} C_d s)^{\alpha}$	$I(s) = \frac{V/s}{Z(s)}$ $Z(s) = \frac{1}{(s^{\beta} * C_d)} + R_d (R_d s^{\beta} C_d s)^{\alpha}$
$I(s) = \frac{V/s}{\frac{1}{(s^{\beta} * C_d)} + R_d (R_d s^{\beta} C_d s)^{\alpha}}$	$I(s) = \frac{V/s}{\frac{1}{(s^{\beta} * C_d)} + R_d (R_d s^{\beta} C_d s)^{\alpha}}$
$I(s) = \frac{\left(\frac{V}{s}\right) * (s^{\beta} * C_d)}{1 + R_d (R_d s^{\beta} C_d s)^{\alpha} * s^{\beta} * C_d}$	$I(s) = \frac{\left(\frac{V}{s}\right) * (s^{\beta} * C_d)}{1 + R_d (R_d s^{\beta} C_d s)^{\alpha} * s^{\beta} * C_d}$
$I(s) = \frac{V}{s * s^{\alpha+\beta+\alpha\beta} * (R_d C_d)^{1+\alpha}} \frac{(s^{\beta} C_d)}{\left[1 + \frac{1}{R_d (R_d s^{\beta} C_d s)^{\alpha} s^{\beta} C_d}\right]}$	$I(s) = \frac{V}{s} \frac{\left(s^{\beta} C_d\right)}{\left[1 + \frac{s^{\alpha + \beta + \alpha\beta}}{k}\right]}; k = \frac{1}{(R_d C_d)^{1 + \alpha}}$
$I(s) = \frac{V * k}{s * s^{\alpha + \alpha \beta}} \frac{(C_d)}{\left[1 + \frac{k}{s^{\alpha + \beta + \alpha \beta}}\right]}$	
$I(s) = \frac{V * k}{s^{1+\alpha+\alpha\beta}} \frac{C_d}{\left[1 + \frac{k}{s^{\alpha+\beta+\alpha\beta}}\right]}$	$I(s) = \frac{V}{s^{1-\beta}} \frac{C_d}{\left[1 + \frac{s^{\alpha+\beta+\alpha\beta}}{k}\right]}$ Binomial expansion
Binomial expansion	
$I(s) = \frac{V * C_d * k}{s^{1+\alpha+\alpha\beta}} \left[1 - \frac{k}{s^{\alpha+\beta+\alpha\beta}} + \frac{k^2}{s^{2(\alpha+\beta+\alpha\beta)}} - \frac{k^3}{s^{3(\alpha+\beta+\alpha\beta)}} \right]$	$I(s) = \frac{V * C_d}{s^{1-\beta}} \left[1 - \frac{s^{\alpha+\beta+\alpha\beta}}{k} + \frac{s^{2(\alpha+\beta+\alpha\beta)}}{k^2} - \frac{s^{3(\alpha+\beta+\alpha\beta)}}{k^3} \dots \dots \right]$

$$\begin{split} I(s) &= V * C_d * k \left[\frac{1}{s^{1+\alpha+\alpha\beta}} - \frac{k}{s^{1+\alpha+\alpha\beta} * s^{\alpha+\beta+\alpha\beta}} \right. \\ &+ \frac{k^2}{s^{1+\alpha+\alpha\beta} * s^{2(\alpha+\beta+\alpha\beta)}} \\ &- \frac{k^3}{s^{1+\alpha+\alpha\beta} * s^{3(\alpha+\beta+\alpha\beta)}} \dots \right] \end{split}$$

$$\begin{split} I(s) &= V * C_d * k \left[\frac{1}{s^{1+\alpha+\alpha\beta}} - \frac{k}{s^{1+\alpha+\alpha\beta} * s^{\alpha+\beta+\alpha\beta}} \right. \\ &+ \frac{k^2}{s^{1+\alpha+\alpha\beta} * s^{2(\alpha+\beta+\alpha\beta)}} \\ &- \frac{k^3}{s^{1+\alpha+\alpha\beta} * s^{3(\alpha+\beta+\alpha\beta)}} \cdots \right] \end{split}$$

$$I(s) = V * C_d * k \left[\frac{1}{s^{1+\alpha+\alpha\beta}} - \frac{k}{s^{2\alpha+\beta+1+2\alpha\beta}} + \frac{k^2}{s^{3\alpha+2\beta+1+3\alpha\beta}} - \frac{k^3}{s^{4\alpha+3\beta+1+4\alpha\beta}} \dots \right]$$

Inverse Laplace transform

$$\begin{split} I(t) &= V*C_d*k \left[\frac{t^{\alpha+\alpha\beta}}{\Gamma(1+\alpha+\alpha\beta)} \right. \\ &- \frac{t^{2\alpha+\beta+2\alpha\beta}*k}{\Gamma(2\alpha+\beta+1+2\alpha\beta)} \\ &+ \frac{t^{3\alpha+2\beta+3\alpha\beta}*k^2}{\Gamma(3\alpha+2\beta+1+3\alpha\beta)} \\ &- \frac{t^{4\alpha+3\beta+4\alpha\beta}*k^3}{\Gamma(4\alpha+3\beta+1+4\alpha\beta)} \dots . \right] \end{split}$$

Considering the dominant series the current derived as,

$$I(t) = \frac{VC_d}{(R_dC_d)^{1+\alpha}} \left[\frac{t^{\alpha(1+\beta)}}{\Gamma(1+\alpha+\alpha\beta)} \right]$$
$$I(t) = A * t^{\alpha(1+\beta)}$$

$$I(s) = V * C_d \left[\frac{1}{s^{1-\beta}} - \frac{s^{\alpha+\beta+\alpha\beta}}{s^{1-\beta} * k} + \frac{s^{2(\alpha+\beta+\alpha\beta)}}{s^{1-\beta} * k^2} - \frac{s^{3(\alpha+\beta+\alpha\beta)}}{s^{1-\beta} * k^3} \dots \dots \right]$$

Inverse transform

$$\begin{split} I(t) &= V * C_d \left[\frac{t^{-\beta}}{\Gamma(1-\beta)} - \frac{t^{-(2\beta+\alpha+\alpha\beta)}}{\Gamma(1-2\beta-\alpha-\alpha\beta)*k} \right. \\ &+ \frac{t^{-(3\beta+2\alpha+2\alpha\beta)}}{\Gamma(1-3\beta-2\alpha-2\alpha\beta)*k^2} \\ &- \frac{t^{-(4\beta+3\alpha+3\alpha\beta)}}{\Gamma(1-4\beta-3\alpha-3\alpha\beta)*k^3} \right] \end{split}$$

Considering the dominant series the current derived as,

$$I(t) = VC_d \left[\frac{t^{-\beta}}{\Gamma(1-\beta)} \right]$$

$$I(t) = A * t^{-\beta}$$